Analysis of high strength steels in a transmission gear

Dewi Emlyn Griffiths

Thesis submitted in 2018

Candidature for the degree of

Doctor of Philosophy at Cardiff University

Tribology and Contact Mechanics Group

Institute of Mechanics and Advanced Materials

Cardiff School of Engineering

Cardiff University

September 2018

Abstract

Within industry and research, engineers rely on computational simulation as it has become a day to day design tool, reducing the requirements for prototyping and extensive experimental testing. For the speed of results and cost savings compared to experimentation, the benefit of Finite Element (FE) modelling is clear. The modelling of transmission systems within FE is already established however very little attention is paid to the inclusion of the effects of heat treatment. A case layer provides resistance to high contact pressure, rolling and sliding forces but also contributes to the overall component strength. In terms of linear-elastic simulations, there is little to be gained by including specific material properties on near-surface elements to model the case layer. However, in applications where there is some plastic deformation occurring, such as those of interest to the industrial sponsor of this research, the inclusion of case properties becomes important. Through a literature review, the established methods of gear design based on experimental and computational methods within both industry and research were discussed. A summary of best practices in terms of modelling philosophy, element type, meshing, simplification and computational power was presented.

A test method for the extraction of mechanical properties through the case hardened layers of steel was developed and used to establish a relationship through the case. Through a series of look up charts, the elastic and plastic material properties can be determined for use in Finite Element (FE) analyses.

Such that FE models replicate the case layer in the most representative way possible, a Functionally Graded Material (FGM), based on the experimentally-measured case layer properties, is desirable. A *MATLAB* algorithm was developed which manipulates an *ABAQUS* input file, to identify near surface elements and apply the most appropriate material properties based on their depth into a case layer.

To demonstrate and validate the developed FGM-based modelling approach, finite element models of both simple tensile test coupons and a more complex gear were developed, using the experimentally obtained elastic-plastic case properties applied with the FGM. Their performance was compared directly to experimental test results, and areas for further improvement identified.

To summarise, this thesis contains the development of a modelling methodology for materials which have been case-hardened, using experimentally measured case properties, relevant to the design needs of the industrial sponsor, with levels of detail exceeding those found to date in the literature.

Declaration

This work has not been submitted in substance for any other degree or award at this or any other university or place of learning, nor is being submitted concurrently in candidature for any degree or other award.

Signed: ______________________________ (Candidate) Date: _________________

Statement 1

This thesis is being submitted in partial fulfilment of the requirements for the degree of PhD.

Signed: ______________________________ (Candidate) Date: _________________

Statement 2

This thesis is the result of my own independent work/investigation, except where otherwise stated, and the thesis has not been edited by a third party beyond what is permitted by Cardiff University's Policy on the Use of Third Party Editors by Research Degree Students. Other sources are acknowledged by explicit references. The views expressed are my own.

Signed: ______________________________ (Candidate) Date: _________________

Statement 3

I hereby give consent for my thesis, if accepted, to be available online in the University's Open Access repository and for inter-library loan, and for the title and summary to be made available to outside organisations.

Signed: ______________________________ (Candidate) Date: _________________

Statement 4: PREVIOUSLYAPPROVED BAR ON ACCESS

I hereby give consent for my thesis, if accepted, to be available online in the University's Open Access repository and for inter-library loans **after expiry of a bar on access previously approved by the Academic Standards & Quality Committee.**

Signed: ______________________________ (Candidate) Date: _________________

"Engineering is the art of modelling materials we do not wholly understand, into shapes we cannot precisely analyse so as to withstand forces we cannot properly assess, in such a way that the public has no reason to suspect the extent of our ignorance"

A.R. Dykes, Institution of Structural Engineers (1946)

Contents

Acknowledgements

As I write this section, it is the last part to write before submitting this complete document. They are the last words in a University Career of nine years. Because of this, I have a lot of people to thank.

Thanks to all the teachers at school who made me interested, enthused and motivated to pursue my love of Engineering. You are the ones that got the spark lit. Thanks to the model engineering societies that gave me my first taste of practical engineering. You are the ones that quite literally got the fires roaring (on coal), got me up to steam before heading to University.

To everyone at Cardiff Racing, you are the ones that gave me a means to apply the skills, knowledge and passion I have for Engineering. Not only did I learn more than I could possible imagine, but I achieved more also. Winning the competition outright in 2017 was an effort of not just a season, but many, and one of my proudest moments. To have shared it with lifelong friends made it even more memorable. A special mention to Lee Treherne for his support, advice and making me the person I am. Without his support, I would not be where I am. Thanks also to the staff (admin, academic and technical) at Cardiff University for their advice, time and support during my studies.

My academic supervisors I cannot thank you enough. To have guided me through this project in the way you have, I will always be thankful. The efforts of Alastair Clarke and Rhys Pullin are immeasurable to me. Without your supervision, I would not have completed my undergraduate degree, never mind a PhD. Thanks to Sam Evans for the support and guidance throughout, despite your overflowing calendar. Diolch enfawr I Pwt Evans am y cymorth, amser, a'r cyfle I gael gwneud rhan o'r PhD yn Gymraeg.

I must mention the group of friend and researchers and from the office and the wider group who made the PhD experience so enjoyable. It is also some of your fault that it took this long. Special mention to Aaron, Andy, Ben, Kostas, Mark, Paul, Ryan, Simon and Willis who were there from start to finish.

Massive thanks goes to my industrial sponsor for this opportunity. To work within the pinnacle of motorsport is one thing, but to work with this team has been an honour. A special thanks to Greg, James, Ryan and Simon for the advice and support throughout. Not only did you support, but went out of your way to care about the project when your attention was constantly being averted to the track.

Ignoring the chronological order, I need to thank my family. Without my parents, I would have amounted to nothing. They inspired me to work hard without pushing me, achieve huge amounts without expectation and hopefully they are proud of me and my achievements. Angharad, you're a tough act to follow, but at least I'm a proper Doctor. Lastly, massive thanks to my girlfriend, Manon. Thanks for being so understanding through my PhD. Now that it is finished, we can finally move on to the next part of our lives together. And a holiday.

List of Figures

List of Tables

List of Abbreviations

BC	-	Boundary Conditions
CAD	-	Computer Aided Design
CAE	-	Computer Aided Engineering
CD	-	Case Depth
CSA	-	Cross Sectional Area
EDM	-	Electron Discharge Machining
F1	-	Formula 1
FE	-	Finite Element
FEM	-	Finite Element Method
FGM	-	Functionally Graded Material
FIA	-	Federation Internationale de l'Automobile
FOV	-	Field of view
GUI	-	Graphical User Interface
HCR	-	High Contact Ratio
HPSTC	-	Highest Point of Single Tooth Contact
HRC	-	Hardness (Rockwell)
HV	-	Hardness (Vickers)
LCR	-	Low Contact Ratio
LHS	-	Left Hand Side
LPSTC	-	Lowest Point of Single Tooth Contact
NDT	-	Non-Destructive Testing
PSO	-	Particle Swarm Optimization
RPM	-	Revolutions Per Minute
SA	-	Simulated Annealing
WJC	-	Water Jet Cut

Nomenclature

Symbol	**Parameter**	**SI Units**
A	Area	m^2
A	Johnson Cook variable (Yield Stress)	N/mm^2
a	Thickness (Lewis Eqn)	m
B	Johnson Cook variable (Ultimate tensile stress – Yield Stress)	N/mm^2
C_φ	Helical Overlap	-
E	Elastic Modulus	N/mm^2
E_T	Tangent Modulus	
F	Normal load	N
F_t	Tangential component of load	N
F_{Total}	Total Force	N
k	Lewis non-dimensional factor	-
K_v	Velocity factor	-
k_f	Stress concentration factor	-
L	Length (Lewis Eqn)	m
M	Bending moment	-
M	Gear Module	m
m_n	Load sharing ratio	-
n	Johnson Cook variable (Exponent)	-
t	Width (Lewis Eqn)	m
W	Width	m
Y	Lewis form factor	-
y_{max}		mm
ϵ_{true}^{pl}	Plastic Strain	-
ϵ	Strain	-
ϵ_{nom}	Nominal Strain	-
ϵ_{true}	True Strain	-
σ	Stress	N/mm^2
σ_{true}	True Stress	N/mm^2
σ_{nom}	Nominal stress	N/mm^2

1. *Introduction*

1.1. Introduction

The research presented in this Thesis focuses on the development of a strategy for creating a Finite Element (FE) model that contains depth-dependent material properties as found in a component that has undergone a case hardening process. By understanding how material properties change through the case depth, representative properties can be applied to FE models. This can then allow greater understating of post-yield behaviour for these materials. Components can then be simulated more realistically, creating the potential for weight saving or a reduction in material. Case hardening is applied to a range of engineering components including gears and bearings, however this Thesis focuses on gears for Formula 1 gear boxes.

For the 2014 Formula 1 (F1) season, a new formula consisting of turbocharged V6 engines with a 1.6 litre displacement including kinetic and heat energy recovery systems was introduced. Compared to the predecessors of these 'power units', fuel consumption reduced by almost 30% and output torque doubled from 300Nm to 600Nm. Within the transmission system (Example in Figure 1-1) very little has changed.

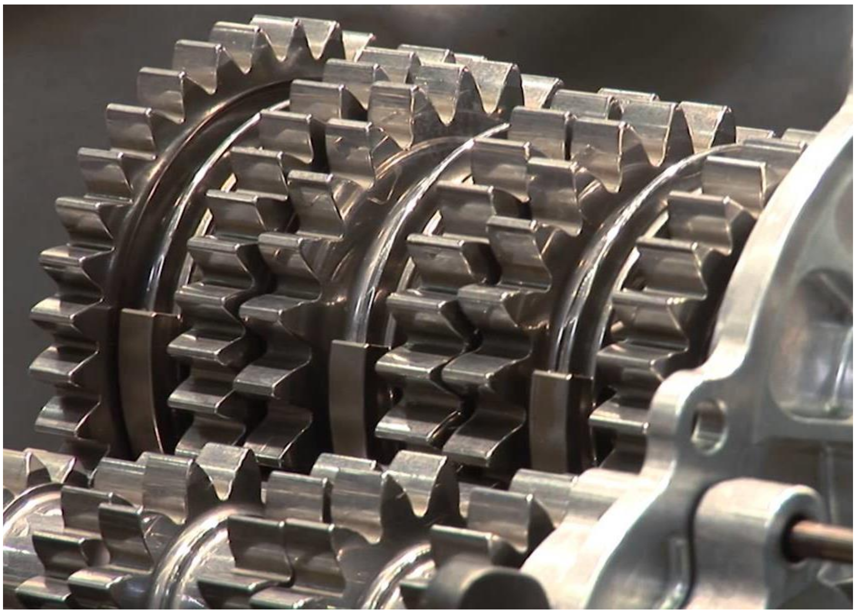

Figure 1-1: *A Formula 1 gear ratio cluster*

As with all motorsport of the highest level, the FIA (Federation Internationale de l'Automobile) rules (FIA Formula 1 Technical Regulations, 2014) dictate much of the architecture of a transmission system. The system may not drive more than two wheels, must not have any form of traction control, and is defined as 'all the parts in the drive line t

hat transfer torque from the engine crankshaft to the drive shafts'. Any component whose primary purpose is for the transmission of power or selection of gears together with the casing in which they are housed is included under this description.

In the current set of regulations, the transmission used must feature eight forward ratios and a single reverse with the following geometries; all components must be made from steel with a minimum face width of 12mm when measured at the root diameter; all chamfers or radii, not exceeding 2mm may be applied to the sides and tip of the teeth, with a maximum overall chamfer to the gear teeth of 10°; the centre distance between input and output shaft must not be less than 85mm, and no gear pair may have a mass lower than 600g.

At the beginning of the hybrid era of Formula 1, in 2014, the gear and final drive ratios were to be nominated prior to the season with a 'joker' available that would allow the team to change them at a single point during the season. All seasons since have not included a 'joker'. This limitation to gear ratios was introduced as a cost saving activity as previously teams were permitted to change their final drive (and gear ratios) to suit each race weekend. Changes would be made between practise sessions to optimise for each circuit, with some instances of changes between qualifying and the race being made in spite of this requiring the car to start from the pit lane, i.e. the back of the grid.

Therefore, the Industrial sponsor for this research instigated an investigation into the material properties of their transmission gears such that a better understanding can be attained, in particular, of behaviour when gear teeth yield due to momentary overloads, and used to ensure design is pushed to the limit of what is possible, which is the ethos of Formula 1 itself. Within the high-end motorsport of today, efficiency wins races and championships, therefore a lightweight, efficient and reliable transmission system is essential.

Considering the substantial increase in torque from the 3.5L V8 to the 1.6L V6 hybrid engines, the minimum gear geometric parameters listed above are unchanged. As the engine torque was increased by 100%, the minimum face width for the gears is unchanged. Therefore, the design of transmission components has become considerably more challenging as far as achieving the minimum parameters stipulated in the regulations is concerned. As gear overloads are the most common means of failure within these transmission systems, the combination of double the engine torque and the complexity of the transmission system means that the design of gears is of increased importance.

Gear design is often thought to be complex and is sometimes considered a black art (British Gear Association, 2015). With up to sixty-four parameters that make up gear geometry, their design can be seen as an art form. As parameters such as bending stress and module are inversely proportional to each other, the design of gears is often a balancing act. The traditional approach to gear design includes the Hertzian Contact Equations, the American Gear Manufacturers Association (AGMA) and ISO Standards, taking into consideration the geometry under a simplified loading. Furthermore, the stresses around the root of the involute teeth can be estimated using basic cantilever theory (Tran, 2015) and Lewis bending equations as demonstrated by Ciavarella & Demelio (1999). Tran (2015).

Ventakesh *et al.* (2014) stated that due to the advancement of computational power and design tools such as FE modelling since the year 2000, engineering analysis of structures and components has developed considerably. Combined with the increased power available in desktop, cluster and cloud based computing, FE has become an essential tool for the design engineer.

Within gear design, analysis of stresses in and around the involute gear geometry including features such as dog teeth and splines is possible. This allows for a more thorough analysis of a gear, therefore giving engineers the tools to make mass reductions and efficiency increases whilst maintaining performance and reliability.

These analyses are often completed using basic material properties only, with little or no consideration of any heat treatments used on the components. This is often logical if components operate in the elastic regime. High performance gears typically undergo processes to harden the outer layers of the material, making the components less susceptible to damage through rolling, sliding and contact forces (Ciavarella *et al.* ,1999). Case hardening is a process commonly associated with hardening of gears, and has been modelled in FEA for applications including bearing raceways, splines and rolling elements (Barsoum, 2013). When an analysis does include such varying material properties, it is normally included in a simplified form where properties corresponding to the fully hardened material are given to the case depth and the raw material properties are given to the remainder. Very few analyses consider a varying material property over the case depth, with none considering the geometry itself. This is particularly important for gears which, under extreme loadings, can experience plastic deformation or localised yielding.

Figure 1-2 shows how a case penetrates a gear tooth and Figure 1-3 show how the Vickers hardness (y axis) varies as it goes through the case depth (x axis). The case pattern of a sectioned gear in Figure 1-2 is determined using X, hence the different appearance. As demonstrated in Figure 1-2 and Figure 1-3 , the depth of the case is influenced by the geometry of the gear tooth. Figure 1-2 shows a sectioned gear tooth where the case layer is visible. Using the scale on the image, it is possible to see that the depth of the case varies over the involute geometry. The addendum (tip) of the gear has a thicker depth of case than at the root due to the increased surface area. The tip would be affected by the propagation of the heat treatment from each flank and the tip itself. The root would only have the case propagate from the root. Due to the geometry of the root, it has a lower surface area and therefore less propagation of the case. Figure 1-3 (taken from the work reported in this Thesis) demonstrates the difference in penetration of the case in various areas of the involute geometry. The root and the gear flank both share similar penetrations, with the addendum having a consistently higher hardness after a depth of 200µm. Below 200µm the edge effects of the coupon can affect the hardness measurement.

A larger penetration is expected at the tip due to the increased surface area at that point, however distortion during thermal processing would be at its maximum there and therefore more material removal would be required in the final manufacturing processes. At the root, the case penetration is less deep, but there is less distortion during heat treatment, therefore less material removal is required.

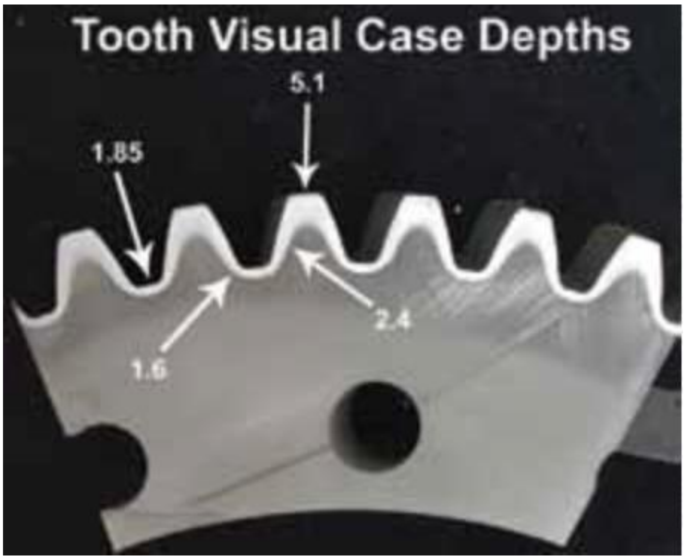

***Figure 1-2**: Demonstration of a case pattern in an involute gear (ERS Engineering Corp.2014)*

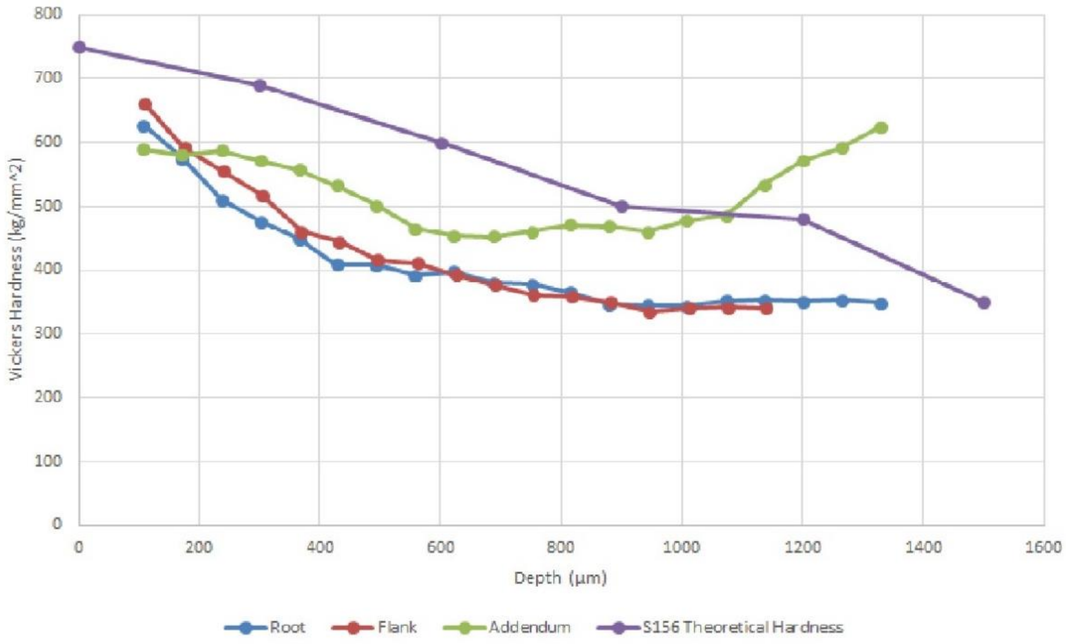

Figure 1-3*: Vickers hardness of gear tooth at various positions as a function of depth below the tooth surface*

For the industrial sponsor (and in other industries) the process of creating FE models is not as conventional as using a single software tool for all stages in the task. As an example, the industrial sponsor's gear design process is as follows:

1. Create the components within Catia (CAD software).
2. Create assemblies within Altair Hyperworks (FEA Pre-Processor).
3. Apply loads, boundary conditions and mesh the components within Altair Hypermesh (Meshing tool).
4. Output the input file for the analysis.
5. Run within the *ABAQUS* solver (FE solver).
6. Analyse results within Altair software (Post processing /visualisation).

Thus, to allow the findings of this research to be compatible with the current approach of the industrial sponsor and make it more industry relevant, the most suitable approach would be to apply custom material properties, representing the case hardened surface layers, to the model between stages 4 and 5, by manipulating the input file to include a variation of the material properties, without disrupting the other existing modelling methodologies. Within this investigation, *ABAQUS* will be used for steps 2-6 and consideration of the industrial sponsor's processes will be factored into the research.

1.2. *Motivation for the Study*

The motivations for this study are:

- Within both industry and research, very little attention is paid to the material property changes within a component's case depth. For gears this is no different. The maximum stresses found within gears are the contact stresses when teeth are in mesh, which are of the order of 1-2 GPa, typically. This is calculated using the Hertzian Contact equations which model concentrated contacts between semi-infinite elastic bodies. Bending stresses are also considered, particularly for high load situations, but are generally calculated through a combination of geometric parameters and derivations from cantilever bending theory, such as the Lewis Bending equation. Realistically, these bending stresses are considered the limiting factor within gear design. As the maximum bending stresses occur at the surface of the gear root fillet, for best results the material properties of the case depth should be included in the analysis.
- Within the academic literature, there are a range of approaches reported concerning gear Finite Element Analysis (FEA). Some approaches consider computational efficiency as the most important parameter in gear analysis and therefore model a single pair of meshing teeth alone. Where accuracy is the focus, models will include all gear features such as dog teeth, splines or keyways. Additionally, there is a mid-ground where three or five tooth models of a gear are included, with the remainder of the teeth simulated using a cylindrical surface, thus replicating the bulk stiffness of the gear whilst minimising the requirements to model the complex geometry of the involutes for all teeth. Despite this, there are historical trends which point to researchers aligning on FE parameters such as software, element type, meshing conditions, loading and boundary conditions that are used.
- For multiple sectors of engineering, data sheets alone are not satisfactory in the stress analysis of components. Aerospace and high-end motorsport companies commonly manufacture multiple test components for fatigue testing to generate S-N curves such that geometry and heat treatments are included. However there is little emphasis on the material properties within the case depth and how these contribute to the overall performance of the component. A clear understanding, quantification and application of these properties through the case depth would be of great benefit at the design stage, and this challenge is the subject of this Thesis.

1.3. *Objectives*

The main objectives of the project are as follows;

- Derive, produce and develop a method for determining the material properties and their variation over the case depth of a case carburised component. Develop material models and data for sponsor's use.
- Develop a method for the application of material data to an FE model that takes the form of a Functionally Graded Material (FGM).
- Provide a set of validated design rules for the modelling of transmission gears to the industrial sponsor.

1.4. *Novelty Statement*

The following areas demonstrate the novelty of this Thesis:

- A method was developed for testing multiple heat-treated dogbone test coupons such that the case could be quantifiably removed for a range of thicknesses. These samples were then tested to failure to generate stress-strain curves for each thickness. A method was then developed and applied to calculate the stress-strain curves for the case-hardened material as a function of depth within the carburized layers.
- A means for the depth dependent material properties of the case to be applied to an FE model, so as to take the functionally graded nature of the material into account, was developed. This was based around a novel *MATLAB* algorithm that reads an *ABAQUS* input file and manipulates it such that elements can be assigned material properties in a user defined number of groups corresponding to their centroidal depth below the surface of the component.
- The *MATLAB* algorithm is generally applicable to other FE systems with adjustments to input and output formatting.
- A FE model that is validated through the use of non-contact measurement systems, with a set of design rules for the modelling of gears within FE.

1.5. Thesis Structure

Chapter 2 contains a literature review of the current methods in gear design accepted by industry and the research community. An overview of the parameters that contribute to the modelling of gears in FE modelling, material used and validation methods is also presented.

Chapter 3 explains the most common experimental methods used through this Thesis. This includes details on micro-hardness measurements, tensile tests, Digital Image Correlation (DIC) and Video Strain Gauge (VSG) as full field non-contact validation methods. Specific applications of the approaches are discussed in the relevant Chapters.

Chapter 4 explains how material data was extracted for use in this Thesis. This includes details on the test setup, fixtures and test procedure, data analysis and processing to obtain properties for the case, and comparison to theoretical material models.

Chapter 5 outlines how the material properties from Chapter 4 are used to create a FGM model and how it is applied to an FE model. Input files from FE are manipulated using a *MATLAB* algorithm such that material properties can be allocated to elements on a depth-dependent basis. The *MATLAB* algorithm is thoroughly explained and includes case studies to show and prove its effectiveness.

Chapter 6 describes a physical gear test including the use of full field non-contact measurement devices to validate the accuracy of the FE model.

Chapter 7 applies the FGM codes from Chapter 5 to FE models of tensile coupons and the physical gear test used in Chapter 4 and 6 respectively. Sensitivity of the results obtained to mesh density and the number of different material properties used is assessed and the capabilities of the FGM code are investigated

Chapter 8 contains a discussion of this Thesis, followed by conclusions and suggestions for further work.

2. Literature Review

2.1. Introduction

This chapter presents a literature review on the FE analysis of numerous aspects of gears, gear teeth, case hardening, case depth and strain hardening, together with some validation techniques.

With increased access to FEA packages in recent decades, their use is widespread for gear analysis. When used correctly and validated, they can give accurate results to assist design and understanding. Also, more complex analyses can be performed where geometry, mesh and loads can be changed to account for crowning, addendum modifications, asymmetric tooth profiles or even incorporating a layered analysis where steps in case hardness are considered.

2.2. Gear Analysis

The analysis of stresses in gear teeth generally falls into two categories – the evaluation of bending stress at the root of the tooth where it joins the main body of the gear, and the calculation of contact stresses on the tooth flank where it makes contact with a tooth on the meshing gear. Both bending and contact stresses may be evaluated analytically or by FE analysis. In this section, the analytic approaches for the calculation of stresses induced by gear bending are first outlined, followed by more detailed consideration of the various approaches to FE analysis of gears presented in the literature.

2.2.1. Contact Mechanics (Hertzian Contact)

Hertzian contact mechanics is a theoretical means of calculating the contact stress between two non-conformal contacting bodies. It involves taking into consideration the geometry of both contacting surfaces together with the load case involved, and determines the stresses based on the contact semi-dimension that quantifies the contact area when the surface elastically deforms. In practice, lubrication conditions and surface roughness may affect the contact stress however this is not relevant to the research in this Thesis.

It is important to consider the surface stresses of a contact because these give an indication of the likelihood of surface failure, typically through micro pitting or scuffing. Although the Hertzian approach assumes frictionless dry contact, whilst most gear tooth contacts are lubricated, because the lubricant film thickness is much smaller than the elastic deflection it is a reasonable approximation to the problem and allows the relatively straightforward evaluation of contact stresses for proposed gear designs, concepts and geometries. As

Hertzian theory is only necessary for surface contacts and not in bending calculation for gears, further detail is not necessary in the scope of this Thesis.

2.2.2. Gear Bending Theory - Lewis Bending

It is essential at the sizing stage to understand the bending stresses in contacting gear teeth. The first approach to this was to approximate the gear teeth as simple cantilever beams. On this basis of this approach, a formula was derived by Lewis (1892) and remains a starting point in the design process in the present day.

Figure 2-1 shows a cantilever of length L, thickness *a* and width *t.* The load F_t is a uniformly distributed load across the face width.

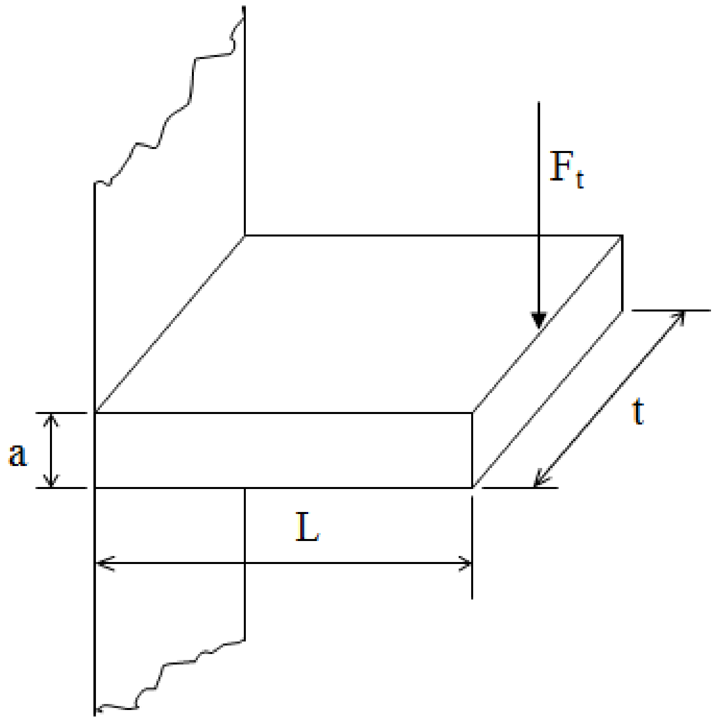

Figure 2-1*: Cantilever theory*

The bending stress at the simulated root of the cantilever are shown by Equation (1).

$$\sigma = \frac{My_{max}}{I} = \frac{F_t L(a/2)}{\frac{1}{12}(ta^3)} = \frac{6F_t L}{ta^3} \tag{1}$$

This approach is simplified and cannot be directly applied to the geometry of a gear tooth, and was modified to take into account more accurately the gear tooth geometry. This is shown in Figure 2-2. This geometry takes into account the worst load case: when the Force F is acting on the tip of the simulated cantilever, with its tangential component Ft contributing to the bending stress calculation. There is the assumption therefore that the maximum bending stress occurs at the root fillet (point c) at the radius r_f when the line from the centre line at the loaded point is tangent to the root fillet of the tooth.

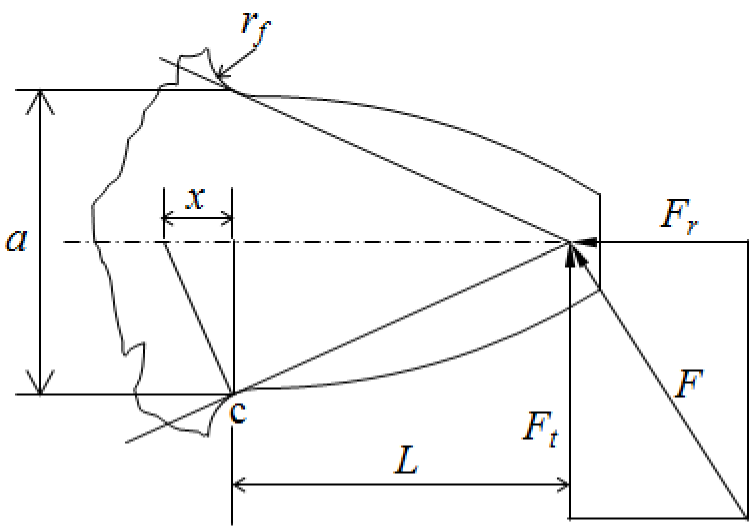

***Figure 2-2**: Cantilever theory applied to a gear involute*

Considering the geometry x = $a^2/4L$ and therefore $a^2 = 4Lx$

Combining this with Equation (1) gives Equation (2)

$$\sigma = \frac{6F_tL}{4tLx} = \frac{3F_t}{2tx} \tag{2}$$

Due to the dimensions of the tooth and their near proportionality with respect to the module (m) of the gear, *x* may be replaced by *k.m* where k is a non-dimensional factor. Therefore,

$$\sigma = \frac{3F_t}{2tkm} \tag{3}$$

By replacing 2k/3 with another notional parameter, *Y*, this becomes Equation (4).

$$\sigma = \frac{F_t}{tYm} \tag{4}$$

The non-dimensional factor Y is known as the Lewis form factor and is a value which depends solely on tooth shape (given by the number of teeth). The Lewis form factor can be determined using Figure 2-2 on a layout drawing of the tooth profile. Example values are included in Table 2-1. Note, all pressure angles are taken as 20°.

Table 2-1: *Lewis form factor for a given number of teeth*

Number of teeth	**Form Factor *Y***	**Number of teeth**	**Form Factor *Y***	**Number of teeth**	**Form Factor *Y***
12	0.230	20	0.308	38	0.377
13	0.243	21	0.314	45	0.391
14	0.255	22	0.320	50	0.399
15	0.266	24	0.331	60	0.410
16	0.276	26	0.340	75	0.423
17	0.285	28	0.348	100	0.436
18	0.293	30	0.355	150	0.449
19	0.301	34	0.367	300	0.464

It can be deduced from Equation (4) that the bending stress is inversely proportional to the module, therefore for a stronger gear a larger module must be used. However, the level of sliding increases proportionally with the module. Therefore, the engineer has to balance strength with sliding (frictional dissipation, wear, likelihood of scuffing etc.) when designing a gear tooth.

The Lewis bending equation can also be extended to take into account dynamic loading effects. At moderate or high speeds the effective maximum loading on the gear tooth increases. For this reason, the velocity factor (K_v) in Equation (*5*) and (*6*) is introduced to create Equation (*7*).

Equation (*5*) is typically used for a hobbed or shaped profile, thus represents most types of stock gears.

$$K_v = \frac{3.56 + [V]^{0.5}}{3.56} \tag{5}$$

Equation *(6)* represents ground gears, thus a higher quality than the former.

$$K_v = \left[\frac{5.56 + [V]^{0.5}}{5.56}\right]^{0.5} \tag{6}$$

Following the inclusion of the velocity factor, the bending stress equation becomes,

$$\sigma = \frac{K_v\, F_t}{W\, Y\, m} \tag{7}$$

The Lewis bending formulation however makes some assumptions about the situation. There is no load sharing assumed, i.e. there is a single pair of teeth in contact. There is also no consideration of the root geometry, and therefore the stress concentration effects. Although this method gives engineers a means to estimate the bending stresses so that approximate gear dimensions can be determined, it is not completely accurate.

For further accuracy, it is generally accepted that FE analysis is required to produce accurate stress estimations. This Thesis therefore strives to increase the knowledge in this area for the research and engineering community.

2.2.3. American Gear Manufacturers Association (AGMA)

Even though the Lewis bending method is an accepted means of estimating gear sizes for external spur gears, it does not apply to all types of gear teeth, and is subject to the previously discussed limitations. Due to the geometric assumptions (the cantilever being a slender beam), it is not applicable to internal gears which are wider at their base. The AGMA method introduces a geometry factor, J, which takes into account the following:

1. Shape of the tooth
2. Worst load position
3. Stress concentration
4. Load sharing between oblique lines of contact in helical gears

Taking consideration of points 1 to 4, it is apparent that the AGMA method is a considerable improvement over the Lewis bending method. In light of the motorsport application of this research, helical gears are not investigated due to the unimportance of transmission noise therefore, point 4 is not applicable. Equation (8) introduces the AGMA equation and lists each parameter.

$$J = \frac{Y\, C_\varphi}{k_f m_n} \tag{8}$$

$Y =$ Tooth form factor

$C_\varphi =$Helical overlap

$k_f =$ Stress correction factor

$m_n =$ Load sharing ratio

The AGMA method of gear design is primarily based upon strength calculations performed within the AGMA (2004) standard. The data in this standard determines the bending strength and pitting strength based on empirical formulas, and all validated through field experimentation. Unlike the Lewis approach which does not consider the stress concentration effects of the root geometry, the AGMA method does. However, the AGMA standard does not include the calculations to determine the contact band, therefore contact stresses cannot be calculated accurately. It is stated that the AGMA predictions include a 25% scatter therefore should be combined/checked/validated using at least one other method.

The AGMA (2004) published a study comparing the AGMA and FE calculations of gears and gearbox components. It demonstrates that with an appropriate model both FE and AGMA analyses are comparable. Results are shown below in Table 2-2. Although it is mentioned that mesh refinement is essential in producing meaningful and accurate results from FE, at no point is it stated how the mesh was formed at the contact or the root.

Table 2-2: *Comparison of AGMA and FE results (extracted from AGMA(2004)).*

Gearbox element	Calculation type	AGMA	FE
Gear teeth	Pitting (Pinion)	815MPa	800MPa
	Bending (Pinion)	137MPa	116MPa
Shaft	Stress	134MPa	100MPa
	Deflections (Bending)	8μm	10 μm
	Deflection (Torsion)	0.0026rad	0.0011rad
Splines	Stress (Shear)	27MPa	23MPa

The AGMA calculations have a specific location where the bending stress is at its maximum. This position is in between the Lewis Parabola and the tooth root, thus the position changes based on the position of the tooth in its mesh.

2.2.4. ISO 6336:2006

When calculating maximum contact stress, the ISO standard assumes that the loading is shared over the average number of teeth in contact. Therefore, the highest load case for a pair of gears where the contact ratio < 2, which is at the highest point of single tooth contact (HPSTC) is not the one used in the standard. Thus, ISO 6336 (2006) underestimates the contact and bending stresses significantly. AGMA 2001-D04 (2004) does not share load, thus giving more accurate and realistic Figures for contact stresses.

The ISO 6336 standard assumes a location for the highest bending stress that is at the 30° tangent point. This does not change with the position of the tooth in mesh. The standard also ignores the compressive stresses within root bending. This is due to the most likely form of failure of the tooth being from the tensile stresses, where cracks can propagate through the tooth during high loading cycles or gear overloads.

Lisle, (2017) completed a comparison between ISO 6336:2006, AGMA 2010-D04 and ANSYS FE analysis. The former two methods of gear design are the most accepted by industry, and both are derived from physical data. Unlike other comparisons within literature, Lisle conducted a physical test to validate the results, thus providing a thorough investigation into which approaches are most accurate.

As described, the location of the maximum bending stress differs between the AGMA and ISO methods, so a direct comparison is not possible. However, the value for the maximum can be compared. Figure 2-3 shows the difference between the two approaches. For the highest loaded condition, the AGMA and ISO get a maximum bending stress of 132MPa and 117MPa respectively, representing an overall difference of 11%.

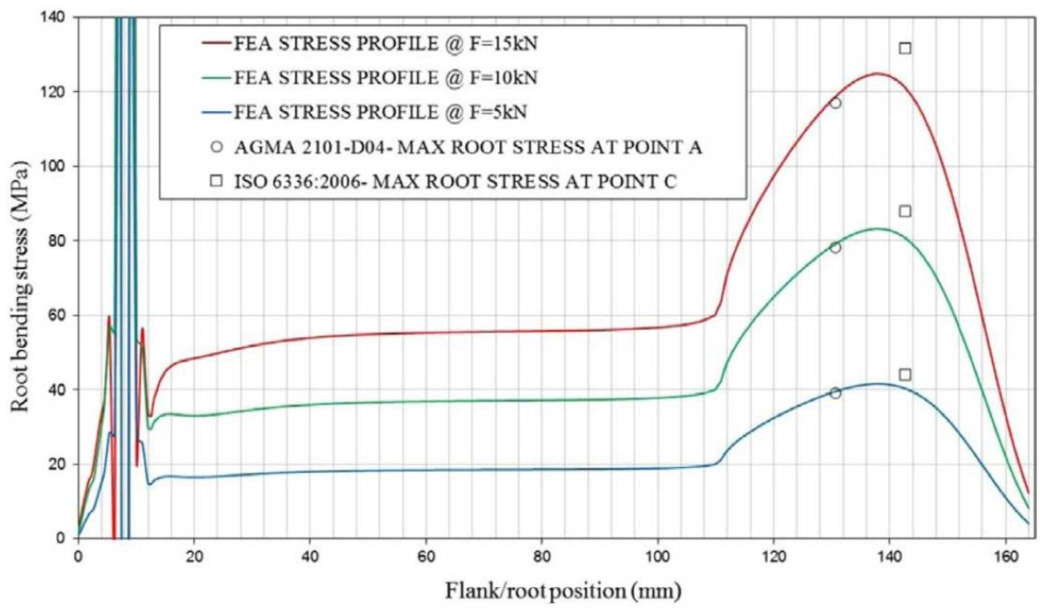

Figure 2-3: *Comparison of AGMA vs ISO on a validation model.*

The physical validation results of the Lisle research is discussed in the validation section of this Thesis, in Section 2.3.

2.2.5. Modelling Approach

For the FE analysis of any component it is beneficial to include all features that will influence the results of an analysis, whilst neglecting features which do not influence the results in order to simplify the computational problem. In practice, it is computationally much more efficient to analyse a simplified component especially if there are complex geometries or areas of low stress. The next section outlines the various approaches to the modelling of gears as found within current literature, in particular single tooth, multiple tooth, and complete gear models, with varying degrees of simplification.

Single tooth models are the simplest form of FE analysis for gears. Andrews (1991) established that one complete loaded tooth with two adjacent half-teeth was sufficient for the modelling of root bending stresses. In comparison with a three tooth model, it could generate stresses that were within 1% of the larger, more complex model. Naturally, there are limitations to a single tooth model, the main one being the limitation of the contact ratios that can be simulated. A single tooth model would only be applicable to gears with a contact ratio of less than two, and can only simulate single tooth contact.

Other researchers such as Tsay (1988), Bray *et al.* (1998), and Tran (2015) have compared the root bending stresses from single tooth models to those obtained through analysis with the AGMA code for a full gear. It was proven that the stresses at the root were within 2% of those calculated using the AGMA code, which was considered to be of an acceptable order. It was stated that significant increases in the error were apparent when the correct boundary conditions were not used (along the bore and radial faces). The boundary conditions for gear modelling are discussed in more detail later in this chapter. The same investigation stated that the contact stresses had differences of 15% compared to those calculated using the AGMA code. As described previously, an error of up to 25% can be expected on AGMA calculated contact stresses due to the method's inability to calculate the size of the contact strip. Due to these investigations focusing on the root bending stresses, it is unlikely that the mesh density along the flanks of the gear teeth was optimised for the analysis of contact stresses.

A summary of literature including single tooth gear analysis is shown in Table 2-3.

Table 2-3: *Literature including analysis of a single pair of teeth in contact*

Author (Single Teeth)	Year	2D/3D	Software	Elements
Andrews (1991)	1991	2D	Not Stated	Not Stated
Tsay, (2001)	2001	3D	TCA*	Quadrilateral
Bray *et al.* (1998)	1998	3D	Not Stated	Not Stated
Tsay (1988)	1988	3D	Not stated	Not Stated
Tran (2015)	2015	3D	Not Stated	Triangular
Kramberger *et al.* (2004)	2004	2D	Not Stated	Triangular/Quadrilateral
(Ding *et al. (*1995)	1995	2D	Not Stated	Quadrilateral
(Ahamed *et al. (*2014)	2013	2D	FRANC**	Quadrilateral

****Tooth Contact Analysis*** *****FRacture ANalysis Code***

To increase complexity, many researchers have investigated three tooth models. Çelik (1999) compared three tooth gear models and full gear models to find a 2% difference in the root bending stresses. Further investigation by Kawalec (2006), and Kawalec and Wiktor (2008) supported this conclusion. As noted in the previous section there is a limitation with a three tooth model which can only model gears with a contact ratio of less than 2. Although in this instance, loading conditions outside of the range of single tooth contact can be considered.

Çelik stated that a minimum of two teeth in contact should be considered due to the substantial tensile stress at the root fillet of the adjacent tooth. Adding a tooth either side of the loaded tooth would therefore include the tensile and compressive bending loads and will reduce the bending load error compared to a full gear analysis and represent the structure more accurately. This is under the assumption that the contact ratio is between one and two and the highest load-case would be for the highest point of single tooth contact (HPSTC). Therefore, a three tooth model is preferable to a single tooth approach.

In a comparison between a single and three tooth approach by Dabnichki and Crocombe (1999), the stresses in the adjacent teeth of the three tooth model were found to be minimal, thus justifying the use of a single tooth model for gear analysis. Although the stresses were minimal in the adjacent teeth, it is generally accepted that their structural support to the loaded tooth influences maximum bending stresses.

In addition to conventional gears, Andrews (1991), von Eiff (1990) and Kawalec and Wiktor (2004) applied the three tooth approach to internal gears. The application was found to be accurate provided that the gear rim depth is at least five times the module.

A summary of three tooth gear models is included in Table 2-4.

Table 2-4: *Literature including analysis of three pairs of teeth in contact*

Author (Three Teeth)	**Year**	**2D/3D**	**Software**	**Elements**
Çelik (1999)	1998	2D	Not Stated	Not Stated
von Eiff (1990)	1990	2D	TCA	Not Stated
Sfakiotakis (2002)	2002	3D	Not Stated	Hexahedral
Kawalec (2006)	2006	3D	Not Stated	Hexahedral-20 Node
Kawalec (2008)	2008	2D	TCA	Quadrilateral
Ciavarella (1999)	1998	2D	ANSYS	Quadrilateral
Patil *et al.* (2014)	2014	3D	ANSYS	CONTA 174/TARGE170
Woods (1999)	1999	2D	ANSYS/GEARBEMM	Not Stated

Typically the literature includes only the minimum number of teeth in contact, to simulate the worst load case. Conversely, Li *et al.* (2006) used a simplified four tooth model of a gear with a contact ratio of 1.5 but included the analysis of two pairs of teeth in contact also. Figure 2-4 includes an illustration explaining the sections of the tooth flank and when each will be in contact, dependant on the number of pairs of teeth in mesh.

For high contact ratio gears (> 2), simplified models with more teeth are common, and typically analyse the case where contact occurs at the highest point of the region where the load is carried by the minimum number of tooth pairs.

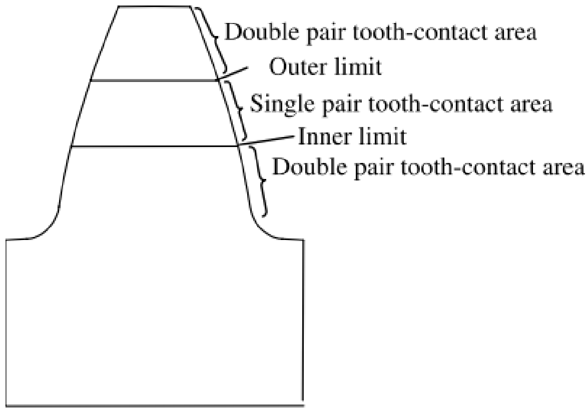

Figure 2-4*: Tooth contact areas and limits, Li et al (2006)*

Park, (2004) used a five tooth model in an analysis of deformation overlaps of spur and helical teeth, shown in Figure 2-5. Stating a contact ratio of the meshing pair as 2.87 however indicates that a five tooth model is an applicable simplification for modelling since there is a leading and trailing pair of teeth in addition to a maximum of three pairs of teeth in mesh. The literature follows this trend of basing the model size on the contact ratio of the meshing pair. The number of teeth in these models are equal to the maximum number of teeth in contact, plus two.

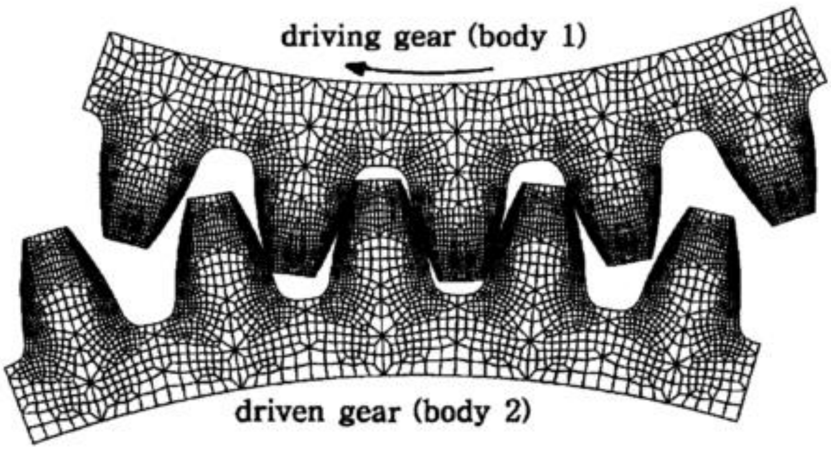

Figure 2-5*: FE model of a five-tooth spur gear, Park et al. (2004)*

A summary of literature with four or more teeth is included in Table 2-5.

Table 2-5: *Literature including analysis of four or more pairs of teeth in contact*

Author (Four+ Teeth)	**Year**	**2D/3D**	**Software**	**Elements**
Li (2007)	2007	3D	Not Stated	Hexahedral
Park (2004)	2004	2D	Not Stated	Quadrilateral
Fuentes (2014)	2014	3D	*ABAQUS*	Hexahedral

Ma (2015) demonstrates an alternative method of modelling a substantial amount of a gear whilst minimising the computing power necessary. The complex geometry around the teeth in contact is included, similar to previous examples in this literature review, however the remainder of the gear is included as a cylinder. In this instance, the meshing strategy would allow the number of elements to be reduced and their geometry simplified. Where section models are restrained on both bore and radial faces, this cylinder method requires restraint in the bore only, and thus is a closer representation of a full gear model. An investigation into this method could yield the best compromise between a simplified and complete model.

Further investigation by Çelik (1999) compared a three tooth model with a cylinder/whole body model. The whole body model featured three teeth, identical to the section model, however the rest of the gear was a constant radius cylinder at the pitch diameter. This also included the root stresses between the teeth and the cylinder, thus more realistically representing the gear. A comparison of the components used in the two models is shown in Figure 2-6. The study found that the cylinder/whole body approach yielded more representative results as the boundary conditions are able to better represent the restraint of a gear. The section approach with its encastre boundary condition on the bore and radial faces is not representative. Additionally, a section gear approach does not have adjacent teeth/material to distribute the stress into, thus not providing representative conditions.

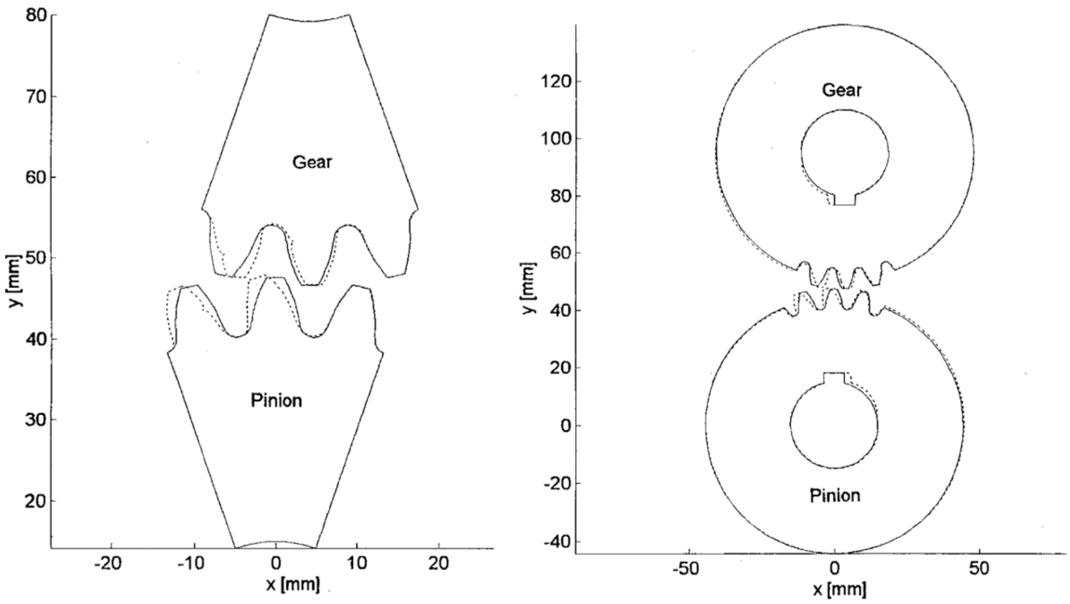

Figure 2-6: *Three tooth segment and three tooth barrel analysis by Çelik (1999)*

The results included a comparison to existing NASA experimental data. The compressive strains for the three tooth segment was approximately 2% lower than the whole body model. Çelik concludes that the full body model gives more realistic results, however the segment performs well. If the user requires the model for iterative analysis (multiple analyses with slight changes), a segment model would suffice. For the more accurate results where computational efficiency is not an important factor, a full body model is recommended.

A summary of literature featuring gears modelled as a cylinder (whole body) is presented in Table 2-6.

Table 2-6: *Literature including gears modelled as a Cylinder (Whole body)*

Author (Cylinder Model)	Year	2D/3D	Software	Elements
Ma *et al.* (2015)	2015	2D	ANSYS	Not Stated
Çelik (1999)	1999	3D	BEM	Not Stated
Kumar (2008)	2008	3D	Not stated	Not stated
Brauer (2005)	2005	3D	Not stated	Not stated

As previously mentioned, analysis using a validated complete model is the most desirable. Despite substantial literature pointing towards simplified models, many analyses have been completed using full gears. Most often full gear analyses are single comparisons that do not require multiple iterations, therefore computational efficiency is not often considered.

Baragetti (2007) used a full gear model for the analysis of fatigue resistance of various coatings. It was stated that the mesh around the root/crack tip was not refined to a sufficient degree to yield definitive results, stating computational efficiency as the reason, and confirming that a simplified analysis with a refined mesh is a sensible direction when investigating multiple iterations. A summary of approaches to a full model approach can be found in Table 2-7.

Table 2-7: *Literature including a full model approach to gear analysis*

Author (Full Model)	Year	2D/3D	Software	Elements
Baragetti (2007)	2007	3D	*ABAQUS*	Tetrahedral and and Hexahedral
Barbieri (2014)	2014	3D	“Helical Pair”	Hexahedral
Liao *et al.* (2008)	2008	3D	Not Stated	Not Stated

Sub-structuring is a method where large sections of the FE model are represented as a single elements with multiple nodes. These nodes are placed all along the outer layer of the sub-structured area. A comparison with and without this sub-structuring would be essential in quantifying the difference. This could be applied to substantial areas of the body of the analysed gear, thus speeding up the computational process when multiple models are being analysed for comparative data/results.

Woods (1999) used sub-structuring in the analysis of a gear model being used to investigate the effect of pre-setting on the bending fatigue strength of carburised gear teeth, shown in Figure 2-7. These modelling techniques were verified by producing an elastic FEA model in ANSYS and comparing results for the root bending stress to results obtained from GEARBEMM (a boundary element modelling program from Ohio State University). The comparison resulted in a 1.5% difference between stresses and therefore the approach was deemed acceptable by the author. In addition to this, further validation was completed in an elastic-plastic condition where the permanent tooth tip deflection was measured using a

Coordinate Measuring Machine (CMM) and compared to an equivalent elastic-plastic FE model.

Woods stated that this method maximised the output of the analysis with the computational power that was available, whilst allowing the use of sufficient mesh complexity in key areas of the model. Similar to the work of Çelik, the three tooth model also features encastre boundary conditions along the bore and radial faces which, can be seen clearly in Figure 2-7.

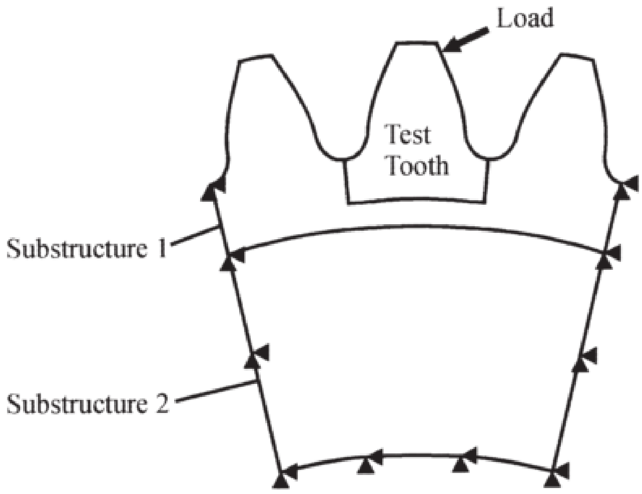

Figure 2-7*: Sub structuring of a gear tooth (Woods, 1999)*

The boundary conditions applied within an FE model will affect the accuracy of the results achieved from the analysis. They should restrain the modelled part in such a way that best recreates the real life problem. With a full model, representative restraints can be applied along the inner bore, spline, dogteeth or keyway.

When analysing a simplified or sectioned model, this is not always possible. For any of the sections of gears previously mentioned in this review, there is further restraint (resisting circumfrential and radial motion) required on the radial face of the gear as shown by Tsay (1988), Tran (2015) and Chabert *et al.* (1974). The encastre boundary condition along both bore and radial faces constrains both circumferential and radial motion. A visual comparison of the boundary conditions for a sectioned and full model is shown in Figure 2-8. Results from a single tooth analysis were compared to a three tooth analysis completed by Çelik (1998) and found to be comparable (within 2% of bending stresses).

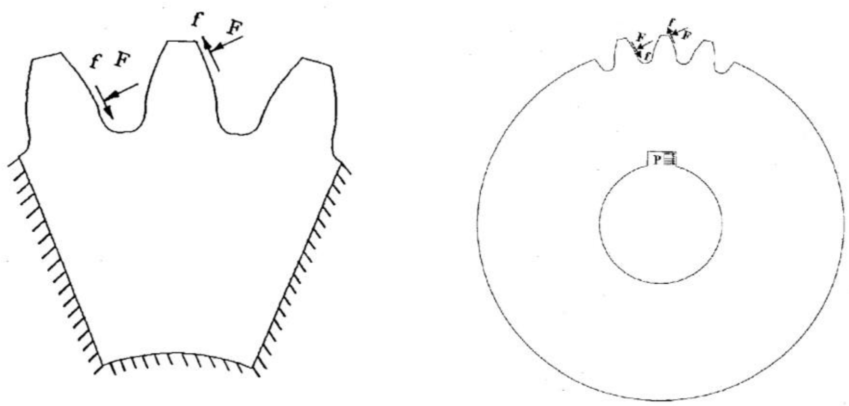

Figure 2-8*: Çelik (1998) three tooth and three tooth full body model*

Above, Çelik included a comparison of BEM (Boundary Element Modelling) and strain gauge testing. Through comparative modelling between a three tooth model and a full gear, the former presented bending stresses at the root that were 2% lower than the latter.

2.2.7. Mesh Size

Within FE analysis, Lisle *et al.* (2017) embarked on an investigation for an unnamed industrial sponsor to compare both AGMA and ISO approaches to that of FE. The investigation stated that FE analysis has the capability of being more accurate than both AGMA and ISO, providing the mesh refinement is sufficient. Lisle did not elaborate on the exact type of 3D meshing used within the investigation, and stated that the mesh used in the Figures was for demonstration purposes only as shown in Figure 2-9.

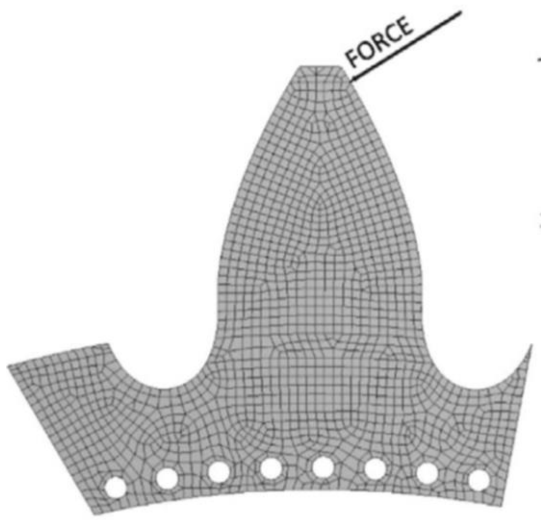

Figure 2-9: *Lisle (2017) demonstration of meshing.*

(Coy and Chao, 1981) and Woods *et al.* (1999) (Pasta and Mariotti, 2007) used the radius of relative curvature of the involute, and the root fillet radius as the basis of a relationship for mesh size calculation. In the interest of a set of design rules, using a relationship such as this is ideal. The mesh density within FE analysis will have a direct influence on the quality of the results obtained. As previously stated, computational power is proportional to the mesh density. With the vast improvements in computational power over the years as represented by Moore's law, running fine meshes in FE analysis is no longer perhaps the substantial issue that it once was. Moore's law generally states that computational power doubles every two years.

The objective of the analysis will determine the mesh density. For instance, if micro-pitting is included in the analysis the mesh would be required so be in the order of 0.1mm on the tooth flanks (Personal Communication, 2017). For analysis of contact stresses between gear flanks a mesh density in the order of 0.2mm is required at the contact, (Personal Communication, 2018). For the evaluation of bending stresses in a gear tooth, mesh density in the order of 0.5mm is required in the region of the tooth root. For the remainder of the model, where stresses (and stress gradients) are considerably smaller, the mesh density can be reduced. Typically, the mesh size and structuring is subject to the opinion and experience of the engineer creating the models. Typically, these areas will be subject to a mesh refinement study to ensure that the meshing is of an acceptable standard.

Further results on mesh sizing can be found in the work of (Fuentes, Ruiz-Orzaez and Gonzalez-Perez, 2014) who were interested in stress distributions in curvilinear gears, and (Barbieri, Zippo and Pellicano, 2014) who developed an adaptive meshing strategy to automatically optimise the mesh density.

In literature, the mesh density at critical areas has been varied based on a trial and error means. Filiz and Eyercioglu (1995), Sfakiotakis and Anifantis (2002) and Kawalec *et al.* (2006) are examples of this, where the mesh density was varied until the mesh converged on results from Hertzian contact analysis, and maintained through numerous iterations. As this was a 'one off' analysis it was reasonably time effective. Coy and Chao (1981) and Pasta and Mariotti, (2007) both consider mesh density requirements for accurate representation of contact stresses within the flanks of gear teeth. However, within literature, numerous researchers have not stated how or if their mesh was refined. As previously discussed, may workers have investigated the relationship between mesh size and contact semidimensions, but have included insufficient detail to allow independent verification of their results.

Some authors do not state a minimum mesh size, but do state and graphically represent how it is proportionately different in key areas. The work of Brauer (2004) shows the gear model and the mesh density in key areas. Global–local FE meshing is adopted, which yields a dense FE mesh in the contact region. Despite considerable work on the contact meshing, these analyses do not consider the appropriate meshes for root bending. Figure 2-10 however shows a disregard for the meshing at other areas of the gear. The mesh density and skewness in the body, tooth core and roots are less than ideal for an analysis of a gear tooth as a whole.

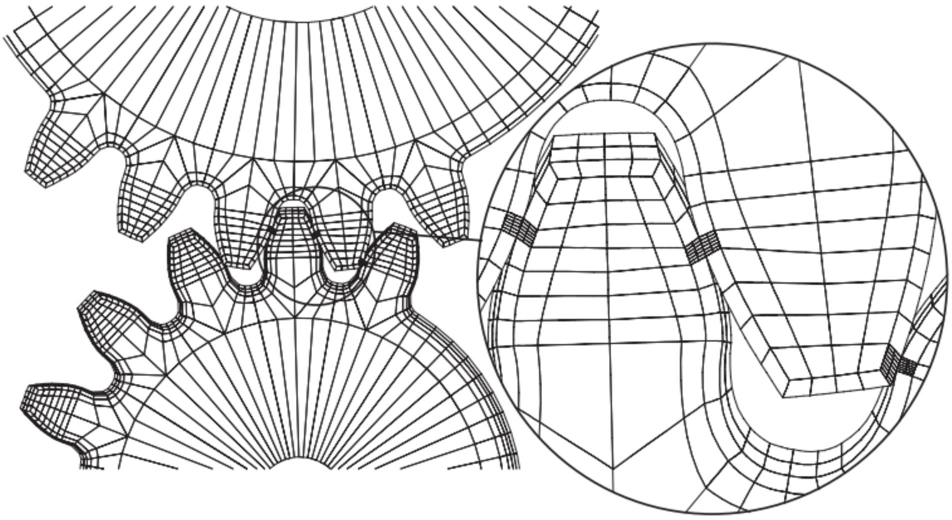

Figure 2-10*: Demonstrating the varying mesh across the analysed gear,* (Brauer, 2004)

Brauer (2004) also stated that automatic meshing was possible on areas of the model. (Bryant, 2013) stated that the “Adaptive Meshing” tool within *ABAQUS* should be considered if significant iterations are modelled, and the meshing can be proven to be producing realistic and appropriate results. Adaptive meshing (also known as Arbitrary Lagrangian Eularian meshing (ALE meshing)) allows for a high quality of mesh to be maintained through an analysis where large deformations occur, by allowing the mesh to adapt to the deformed shape of the body whilst maintaining mesh quality. The initial objective of the technique is to re-mesh areas that have radical shape changed due to plastic deformation. Thus, this technique could be applied to a partitioned section around a Hertzian contact point. It must be noted that this technique is only suitable for static analysis of a Hertzian contact point.

2.2.8. Element Types

The majority of literature discussed in this chapter uses quadrilateral or hexahedral elements. This is most likely for the reasons of computational efficiency and to more accurately represent the tooth surface.

Other element types are also used in literature. Quadrilateral, hexahedral and tetrahedral are used in a combination of 2D and 3D variations. Pyrakos, (1996) states that "a combination of tetrahedral and hexahedral elements provides the optimum mesh" however states that hexahedral alone are preferable due to their improved geometric accuracy. It can be deduced from literature that in recent years many researchers have converged on *ABAQUS* and ANSYS solvers with models consisting of quadrilateral and hexahedral element types.

2.2.9. Heat Treatments

As previously stated, components that are exposed to high contact stresses, sliding and rolling are often case hardened to increase resistance to failure, pitting and to extend their fatigue life. Within the scope of this investigation, it is necessary to understand the manufacturing processes that are used to create the finished component. Within the media, motorsport transmission systems have been compared to Swiss watches, with the levels of accuracy and the elegant nature of the mechanisms. During discussions with the industrial sponsor (Personal Communication, 2014), it was stated that gears are manufactured with a tolerance at the tooth tip of no less than 0.25µm. It was also stated that no gear will enter a Grand Prix with a tooth bend of more than 10µm. To achieve this level of tolerance, the distortion effects of the heat treatment processes must be considered carefully.

The case carburisation process is conducted in a carbon rich environment at +800°C temperatures thus metallic components could be susceptible to heat distortion. As the transmission components are oil quenched, distortion once again becomes a factor. To produce undistorted components at the end of their manufacture, an additional grinding process is completed after the heat treatment which gives the gears their high surface finish and dimensional accuracy. However, to achieve this accuracy, some of the hardened material will inevitably be removed.

A hardened surface is usually specified with a surface hardness and then a hardness at a specific depth. For high-end motorsport gears, it is typically 750HV at the surface and 550HV at 1.0mm depth. Considering that an additional grinding process is completed, is this specification achieving its objective? The area of highest material removal, in the grinding phase is along the tooth flanks where rolling/sliding will take place, as these areas are most sensitive to distortion during the heat treatment. This is caused by the rate of heating and cooling (quenching) due to the increased surface area (for a given volume) when compared to the gear body Quantifying the material removal and incorporating it into FE models would give the designer greater knowledge as to where the least case thickness occurs within the finished gear teeth.

2.2.10. Modelling layers in FE

Within a large proportion of the literature previously mentioned, no consideration is given to the material properties of case layer. This is only of any importance if the model considers elastic-plastic behaviour as hardening treatments will not significantly affect elastic properties. Any examples that do consider the properties of layers of the case depth tend to concern bearings as opposed to gears.

The simplest form of modelling hardened layers was reported by Lai *et al.* (2009) where induction hardened components were modelled. The model was sectioned into three areas, shown in Figure 2-11. The Figure shows two bodies a cylinder in grey, a raceway in blue and the case depth represented by the red section (labelled CD).

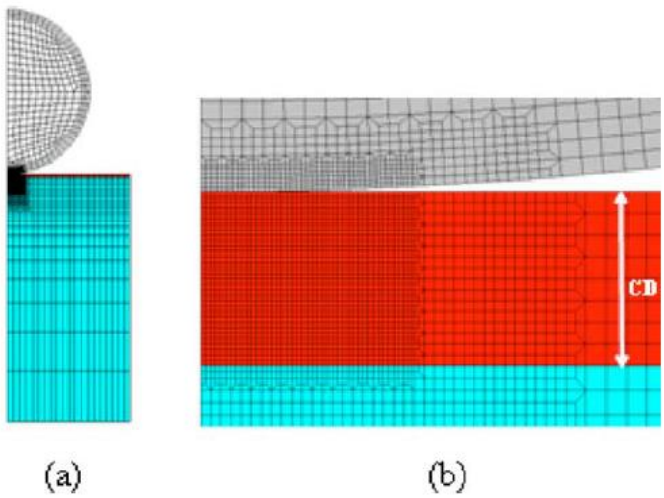

***Figure 2-11**: Model and mesh of a case depth (CD) from Lai et al. (2009) Note – the quality of this Figure is representative of that in the original publication.*

Each layer was assigned a stress-strain curve based on the data produced from compression tests on raw material and on a fully hardened sample. Figure 2-12 shows how the stress-strain curve for the transition area was produced from interpolating between the case and core properties.

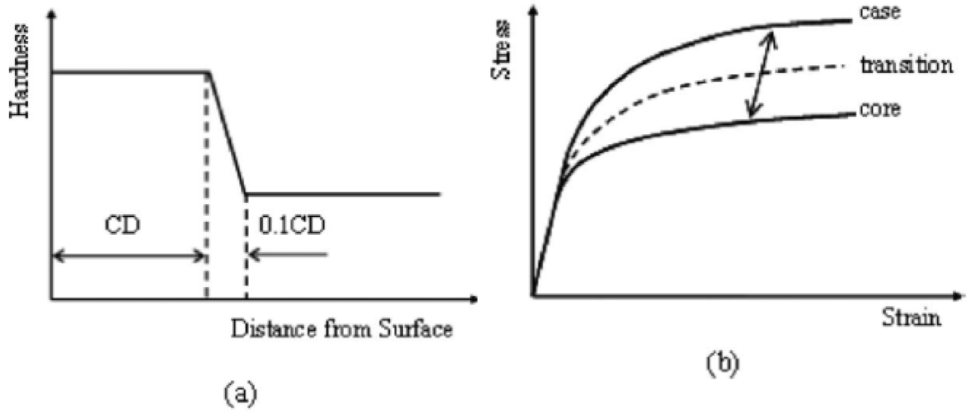

Figure 2-12: *Material properties from Lai et al. (2009)*

Once again a three layer representation of the case depth was produced by Kunc *et al.* (2007) where the core, case and intermediate case layer were given separate properties. These properties consisted of fatigue damage and strain hardening models.

Barsoum *et al.* (2014) produced an investigation into the torsional stiffness of hardened splines having gone through an induction hardening process. From this process the yield stress and strain-hardening behaviour was considered. For a relationship between hardness, strain behaviour and depth, JMATpro software was used. This software combines the thermodynamic modelling of the induction hardening process with a material models database to produce the desired models for the application. This analysis produced the mechanical properties shown in Figure 2-13.

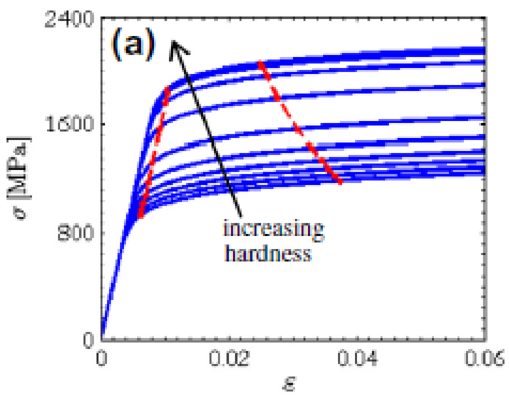

Figure 2-13: *Material properties used by Barsoum et al. (2014)*

The resulting analysis produced by Barsoum *et al.* created a FE model shown in Figure 2-14. The model consists of a single spline in contact with a mating hub. As shown in the Figure, each colour coded layer of the spline represents a single material property applied to it. The 13 layers that make up the spline are split into depth dependant sections. The 'Case' which includes the spline tooth is 2.5mm thick, with all resulting layers having a thickness of 1mm.

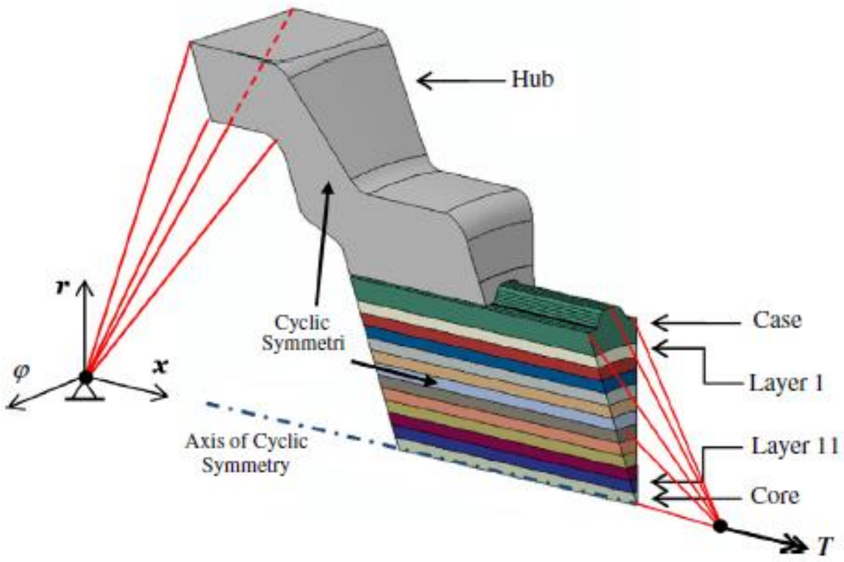

Figure 2-14: *Spline model created by Barsoum et al. (2014)*

Despite the inclusion of varying material properties being uncommon in comparison to other works of literature, the way in which the materials are stepped still does not truly represent the penetration of a real heat treatment.

Kirov (1996) produced an investigation comparing the AGMA method of gear design to that of FE analysis. Despite stating that the analysis was applied to a carburized and ground pair of gears, no mention is given as to surface properties, core properties or depth of the case.

In the little literature that does attempt to replicate the hardened layers, it is completed in one of two ways. One method involves a partition that is applied to the external face of the modelled components where a different material property is applied to the whole section. In this case, the material property of the case is not specified and is likely derived from an approximate relationship between hardness and yield stress. The other method is to partition the case into several layers and apply material properties to each of these layers. This method generally uses material properties based on a hardness measurement and is not outlined in great detail within the literature. This consideration is likely to be rare due to the additional time, effort and increase in mesh density that is required. In the event that the engineer desires four different layers to represent the case, it requires the case to be a minimum of four elements deep. With a typical case for a case carburisation process being in the order of 1mm, a mesh size of 0.25mm would be required. This is smaller than the mesh sizes previously reported in the literature. Figure 2-15 demonstrates an ideal application of material properties for an involute.

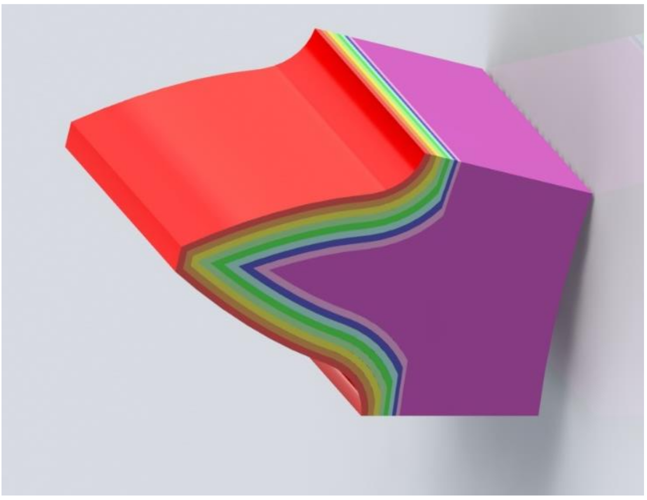

***Figure 2-15**: Demonstration of a layered material structure in a single gear tooth*

Jing *et al.* (2015) undertook a study to optimise the mass of a gear through use of a FGM. The research is very much focused on reducing mass of gear trains by selecting varying elastic moduli and has no focus on replicating a case layer or similar. As can be seen in Figure 2-16, the direction of material change is not representative of a case layer as the material change should follow the surface profile over the root geometry and not be a closed area of material application through the dedendum of the gear. There is no explanation as to why this approach was taken and in the opinion of the Author, is not the correct approach for the simulation of surface treatments. Material properties are applied in 0.125mm sections, therefore 9 layers up to a depth of 1mm, and analyses conducted in ANSYS Workbench

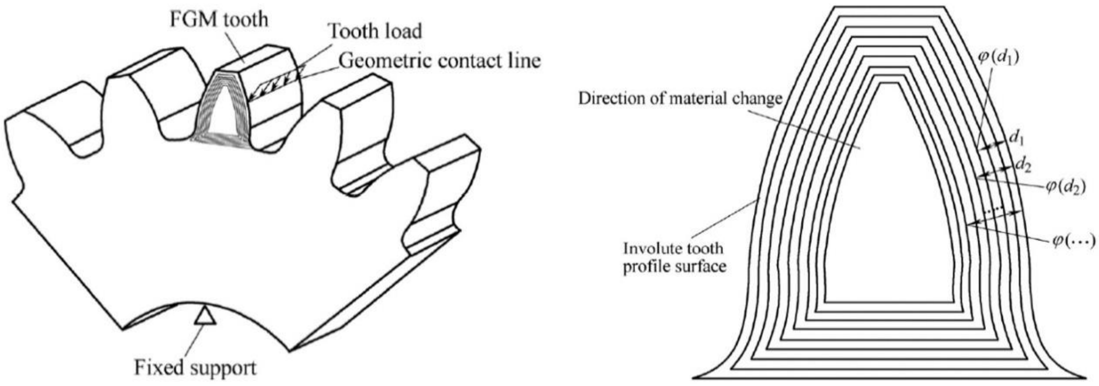

Figure 2-16: *Schematic of material distribution of a FGM gear (Jing et al, 2015)*

As previously stated, the application of multiple material layers is based on a relationship between hardness and yield strength. Some of these data are provided in Table 2-8. The table outlines the general material properties applied to each layer (layer 1 nearest to surface and layer 6 represents the core) in an analysis completed by the industrial sponsor, prior to the Author commencing the research contained in this Thesis.

Table 2-8*: Table of material parameters by layer used by the industrial sponsor*

Parameter	Layer 1	Layer 2	Layer 3	Layer 4	Layer 5	Layer 6
E	1.8E+11	1.8E+11	1.8E+11	1.8E+11	1.8E+11	1.8E+11
Yield (MPa)	1807	1748	1603	1515	1399	1030
UTS (MPa)	2144	2069	1834	1724	1551	1500
N (Strain Hardening Component)	26	26	26	26	26	26
HV	750	690	600	550	480	350

2.2. Validation

To obtain truly accurate simulations in which the engineer can have confidence, the results require validation. This section of the literature review includes validation methods that have been used to strengthen the understanding of gear analyses.

2.3.1. Validation: Comparison to Theory and Calculations

Only a minor amount of literature exists which compares the results of FE analysis against traditional gear calculation methods such as AGMA 2101-D04 software, ISO 6336:2006 and Hertzian theory. To further establish FE as an accurate, repeatable and representative method of design justification, further work is required to compare results to the traditional means of gear design.

Within much of the literature available, there is mostly comparative validation; i.e. an original 'simplified' model will be used as a benchmark and compared to a more advanced or novel modelling technique. FE modelling is commonly compared to an accepted measurement technique or an accepted means of gear analysis however other validation methods are rarely mentioned. Due to the complexity and time consuming nature of these comparisons, perhaps, it is often neglected.

2.3.2. Validation: Comparison to Accepted Means

As previously mentioned, the AGMA and ISO approaches to gear analysis are often compared to that of FE analysis. As the AGMA and ISO are both based on physical data, it is generally the most common means of validation. Chen and Tsay, (2005) published data where the AGMA 2101-C95 code was shown to be within 2% of the root bending stresses found in the FE analysis. Despite this relatively accurate comparison, the contact stresses produced by the FE model were found to vary by 15% when compared to the AGMA Figures. With little information regarding the mesh density, it is assumed that the contact stresses were not the foremost priority of the work.

Similar research conducted by Yothirmai *et al.* (2014) found comparable results (2% difference in root bending stress) when comparing FE models to the same AGMA code. Vajayarangan and Ganesan (1994) obtained a 4.5% difference in using a 2D model constructed of triangular elements. The most promising results for FE validations came from Pasta and Mariotti (2007) where root bending stress was within 1.5% and contact stresses within 2.3%. However, this analysis was between FE models and ISO 6336:2006.

2.3.1. Validation: Experimental

An alternative to computational validation, physical validation methods are also possible where data from sensors on a component can be analysed. Traditionally, measurement of stress/strain in a physical component uses strain gauges. In recent decades, the National Aeronautic and Space Administration (NASA) have completed investigations into the measurement of root bending stresses in transmission components, including numerous gear types; spur, helical, bevel and epicyclic (Krantz, 1992). As highlighted in the paper, only the surface strains can be measured. The greatest challenge with strain gauges is that their positioning and orientation can be challenging to allow comparison to values attained through FE analysis. Also, a strain gauge will average over its length, thus providing an inaccuracy in the measurement, especially for a small gear such as that shown in Figure 2-17. Highlighting the point being made, Corder and Gautier (1999) stated that strain gauging is a well understood and reliable technique but it is limited to a few discrete points, an achieving reliable positioning and hence dimensional accuracy can be challenging.

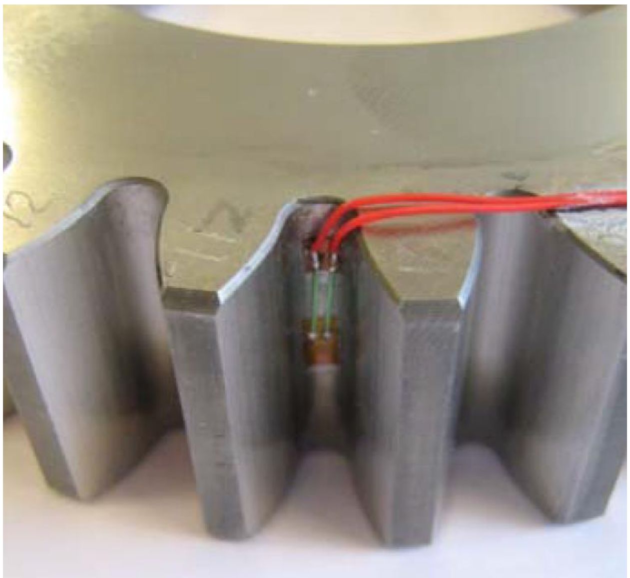

Figure 2-17: *A strain gauge positioned on the root of a typical automotive gear (Lisle, 2017)*

Lisle (2017) used strain gauges as a validation method to compare between AGMA and ISO values. Due to the aforementioned positional inaccuracies, a large gear of module 50mm was used to minimise positional error. As a strain gauge is relatively large in comparison to a typical gear for automotive transmissions, therefore there is a substantial area over which strains. Lisle confirms the positional and orientation inaccuracies of placing the strain gauges on the test component. Although, it is possible to use multiple strain gauges on areas of interest such as those shown in Figure 2-18. For reference, the strain gauges shown in Figure 2-17 and Figure 2-18 are Vishay type EA-06-031EC-350 (1.07mm x 3.56mm).

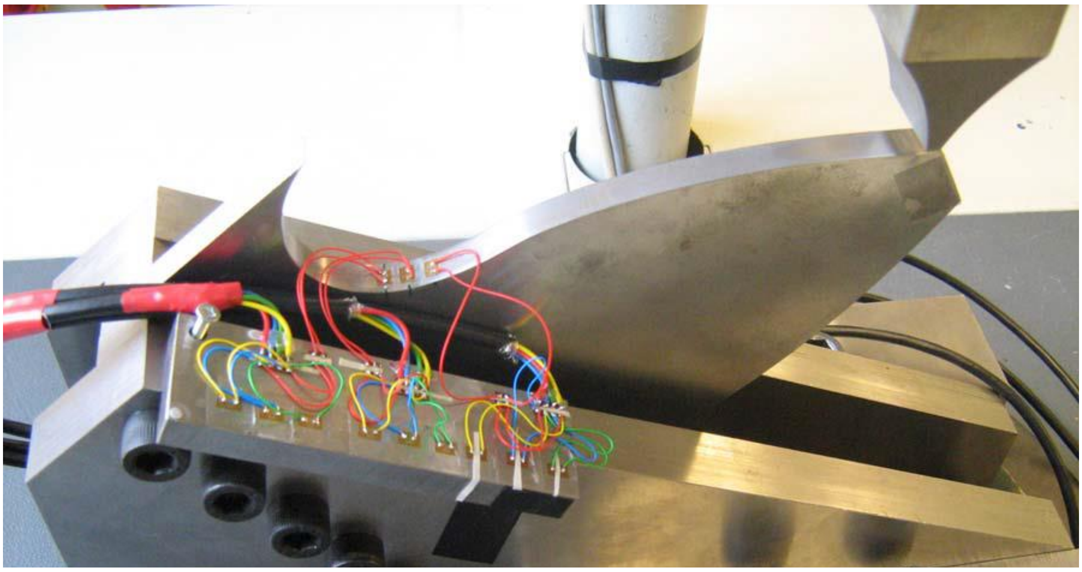

Figure 2-18: *Strain gauges applied to a 50mm module gear tooth (Lisle, 2017)*

Linear Variable Differential Transformers (LVDT's) typically would be used as an additional data collection method during a test for use as an additional validation method. The LVDT data covers only deflection in one axis, so there are assumptions that there is no out of plane movement as a test is in progress and that the LVDT is perfectly parallel to the plane of machine crosshead movement. However, this can be useful to compare with the crosshead deflection of a load machine so quantify the stiffness and measure any deflection in test fixtures.

However, fewer investigations have compared FE results to physical measurements of a gear. Naturally, it is highly challenging to measure the contact stresses using physical measurement due to the proximity of the meshing gear teeth. The root, flank and tip stresses are possible to measure however. The major difficulty in measuring using strain gauges in this application is the averaging effect of the strain gauge over its installed position and the accuracy of the position of gauge in comparison to the FE model. Handschuh and Lev (1999) found a difference of 10% in root bending stresses between FE and a strain gauge. In comparison to the ISO and AGMA literature results of the previous section, this is a relatively high error.

Photoelasticity measurements are also a means of gear measurement from literature. The results of Allison and Hearn (1980) were compared with numerical simulations in the works of Andrews (1991) and produced errors of 7%. This relatively high error has been put down to the low mesh density that was inevitable considering the computational power that was available at the time of the investigation. Photoelasticity also requires large strains to produce fringes in measurement therefore is not an accurate means to determine stress in low strain elastic loading.

2.3.2. Validation: Non-Contact Measurement

Preferably, a non-contact method should be used as it means that surface instrumentation cannot affect the surface stresses or component loading. Digital Image Correlation (DIC) is a full-field displacement measuring tool used for the measurement of displacement and strain for materials/component testing (LIMESS, 2015). Using multiple cameras, a stereoscopic analysis is undertaken where images throughout the loading and unloading of a component are compared, with displacements tracked to an accuracy of a micrometre; although dependant on camera resolution, quality and magnification. DIC involves the area of interest being marked with a speckle pattern. A white background is commonly used with an additional 'random' layer of black speckles, typically at a 50/50 distribution. The speckle pattern or indeed the natural texture of the material is tracked by the manufacturers' software throughout the loading cycle to provide a map of displacements/deformation, and therefore generate strain maps (Gillard *et al*., 2014). The speckled pattern is considered to be physically attached to surface.

In 2010, DIC was used as part of an investigation into Structural Health Monitoring (SHM) of gears within Cardiff University (Figure 2-19). Although this method was used in parallel with Acoustic Emission analysis to correlate energy release and crack mouth opening displacement, it was seen to be a viable option in non-contact strain monitoring. Over thousands of cycles, it demonstrates that some comparisons could be drawn between DIC and FE analysis of a gear tooth also. The results of this investigation are somewhat immature and would require further work in the test setup, test coupons and analysis packages used to attain useful results. The report quoted 10% errors between the bending strains produced by the DIC results when compared to those of an FE model. This error can be explained by the difficulty in capturing stresses and strains at a close enough proximity to the edge of the gear.

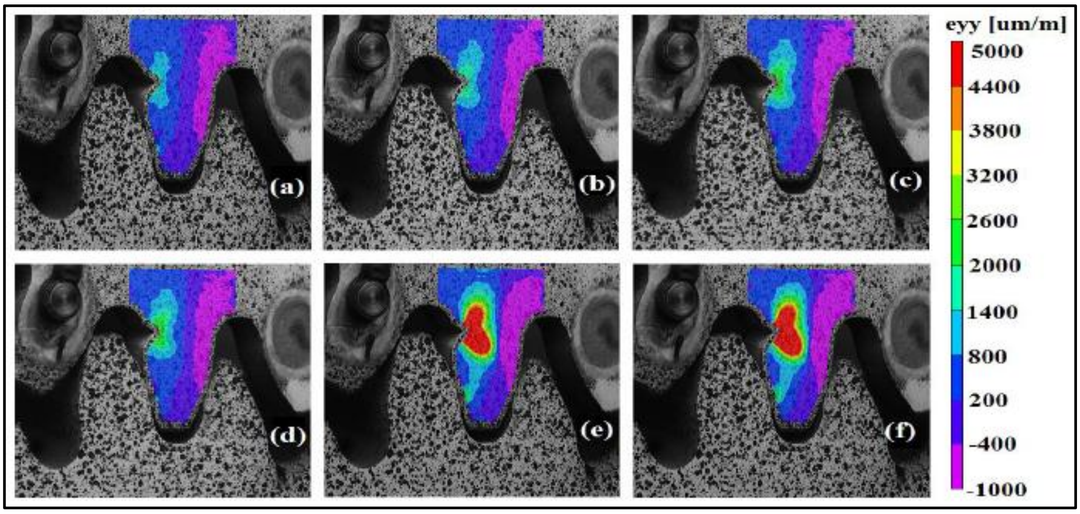

Figure 2-19*: DIC analysis of gear tooth strain (McCrory, 2010)*

It was noted by Pullin *et al.* (2010) that due to the large speckle pattern relative to the small gear teeth, the accuracy of the method is compromised. Ideally, a finer speckle pattern combined with a higher resolution camera would improve the resolution and therefore the data gathered. Additionally, analysis of a larger gear tooth could give improved resolution of data for validation of an FE model. It would allow a greater resolution from non-contact measurement solutions and the incorporation of more accurately positioned strain gauges over several areas of an involute. Scaling up the involute requires substantially larger loads to achieve the bending and contact stresses that can be modelled in FE, however the model can be validated at lower loads.

2.3.3. Comparison between physical and practical data

In the literature that actively attempts to validate the FE models, a means of comparison is required. For studies that include strain gauges on physical test coupons, the strain is compared to that of a corresponding position on the computational model. For those that use non-contact measurement systems such as DIC or VSG the comparison is done simply by the visual similarities of stress or strain plots with the colour plots matched.

A far more scientific method would be to computationally compare stress or strain plots from each data source. The works of Patterson *et al*. (2014) have used and developed the Chevychev method which required two image files of equal size and colour plot. From these images, an additional colour plot is produced which highlights areas of highest and lowest conformity.

2.4. Material data in FE Analysis

This section of the literature review outlines the current state of material analysis within literature.

In all the literature previously mentioned in this chapter that investigates the optimisation of FE models for gears, very little consideration to the material properties has been given. When using FE models the inclusion of an accurate material model will be essential if plastic deformation occurs and accurate results are desired. It can be seen from the papers reviewed that the majority of analyses are conducted in the linear region with a purely elastic material model. This is a perfectly reasonable assumption providing the analysis does not include a load case close to the yield of the material. Very few analyses range into elastic-plastic behaviour, let alone material models that consider replicating a heat treatment such as case carburisation or similar.

In reality, no materials have elastic-perfectly plastic properties, which considers that material is elastic until the point of yield, beyond which is develops the yield stress for any strain. It is also the case that elastic-perfectly plastic contact analyses are more difficult to converge than ones that contain strain hardening behaviour. The simplest way to consider some form of strain-hardening model is to assume the material will be linearly elastic up to the yield point, and use a tangent modulus to describe the stress-strain relationship post yield. An example of this is shown in Figure 2-20. Although this analysis seems very basic it is extensively used in research and industry.

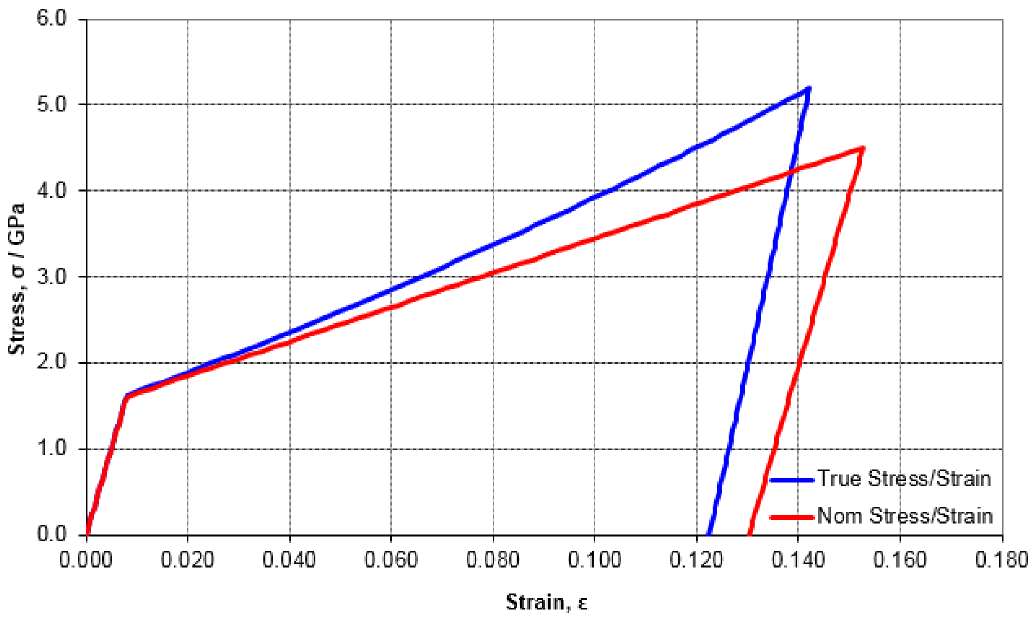

***Figure 2-20**: Stress/Strain characteristics (Simplified for ABAQUS)*

Researchers have created their own spreadsheets to outline the stress-strain relationships of materials. These also produce the material properties required for inputting to FE. As can be seen from Figure 2-20, the required parameters for plastic behaviour are yield stress and plastic strain (Eq. 4). Equations 9 to 13 outline the calculations for obtaining the plastic strain.

$$\epsilon = E\,\sigma \tag{9}$$

$$\sigma_{true} = \sigma_{nom}\,(1 + \sigma_{nom}) \tag{10}$$

$$\epsilon_{true} = \ln(1 + \epsilon_{nom}) \tag{11}$$

$$\epsilon_{true}^{pl} = \epsilon_{true} - \frac{\sigma_{true}}{E} \quad \text{True plastic strain} \tag{12}$$

$$\frac{E_T}{E} = 0.1 \text{ Tangential Modulus} \tag{13}$$

The generated material properties can then be input to the desired software as shown in Figure 2-21.

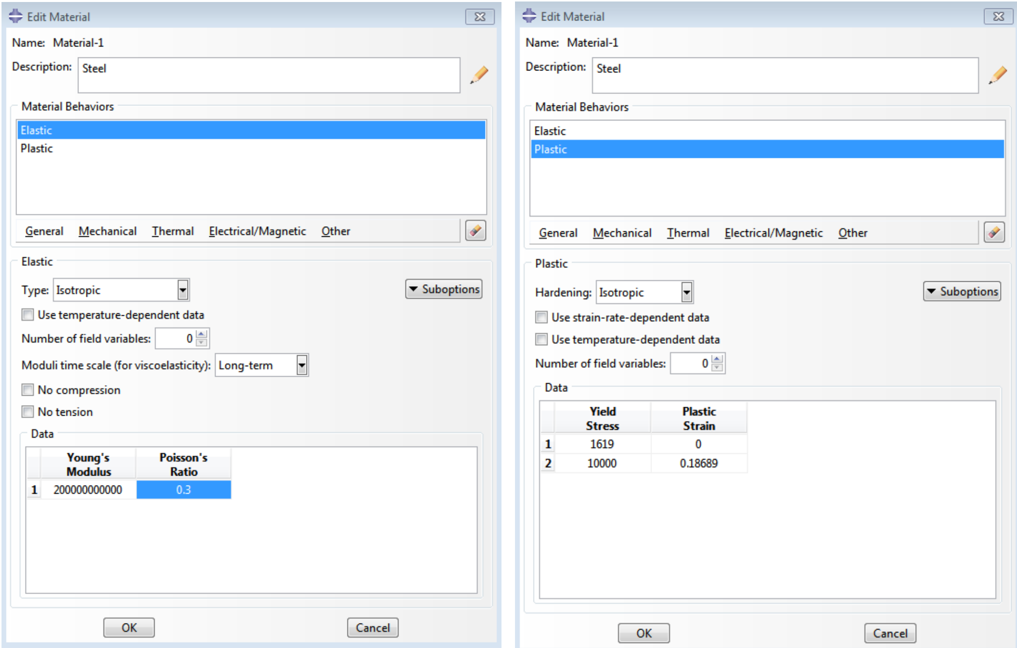

***Figure 2-21**: Material inputs in ABAQUS*

As for analyses that require more complex control of the behaviour around the yield point, more data points are required for the plastic region. It must be understood that *ABAQUS* linearly-interpolates between data points on a user-defined stress-strain curve. Therefore, if the user desires sufficient accuracy in the material model, then the number of points that make up the stress-strain curve for the material must be sufficiently high to replicate a realistic strain-hardening material curve with reasonable fidelity.

For some analyses, yield behaviour may be critical to the research. In the case of the industrial sponsor, initial modelling consisted of 13 data points to replicate a stress-strain curve. The first two points represent the elastic region up to the yield point, with the 11 remaining points describing the yield characteristics and becoming asymptotic up to the UTS of the material. The engineering strain is converted to a logarithmic plastic strain using Equation (12) and this is shown in Figure 2-22. The removal of the scale on the X axis is for commercial confidentiality reasons at the request of the industrial sponsor.

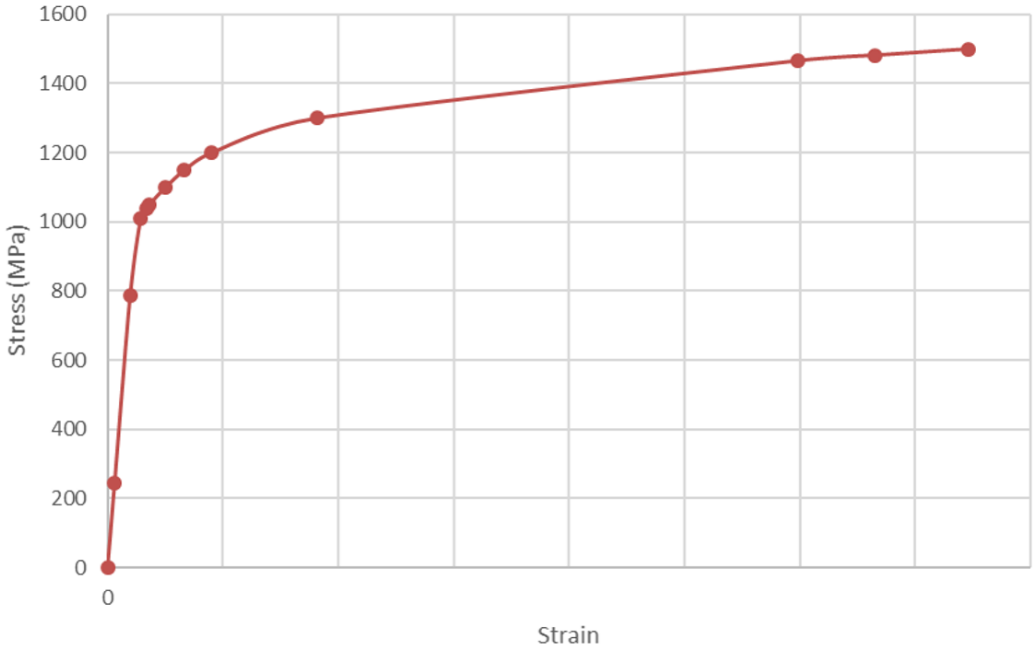

Figure 2-22: *Material property as used by the industrial sponsor*

This material data was created in a spreadsheet using a combination of material data from physical testing (Microhardness) and data sheets which provided expected yield, UTS and strain hardening exponents (explained in Chapter 4). In addition, these properties were applied for a single layer of material in a single gear model that consisted of multiple layers.

2.5. Determination of case properties.

Thus far, it is apparent that very little literature has accurately represented heat treatments in gears or bearings. Of those that do include an accurate representation of a case layer (or other heat treatments), even fewer include the application of material properties determined from experimentation.

A method to achieve this objective would be to include sacrificial components in the batch manufacture of heat-treated components. These would receive the same heat treatment as the machine components and would be sectioned for the material properties to be checked prior to final machining or releasing components to a customer. The sectioned components would have a series of hardness tests through the case layer to ensure the desired properties are present. From these measurements, it would be possible to estimate the yield stress of a material. (Branch *et al.*, 2010) and (Bepari, Haque and Md. Shorowordi, 2010) are two contributions which have discussed this approach.

To accurately model the post yield behaviour of a material, stress-strain curves are required. Traditionally the determination of mechanical material properties is completed using a tensile test. A coupon of a pre-defined geometry is loaded through its elastic and plastic region until failure. These material properties describe the behaviour of a single material, thus the assumption is usually made that the sample is completely homogenous. Heat treated components can also be tested, however the stress-strain curve generated in such tests describe the behaviour of a material that is a composite of raw and heat treated material.

Additionally (Chen *et al.*, 2018) investigated the difference in mechanical properties between various steels heat treated at varying temperatures. The resulting phase changes and the mechanical properties were both compared along with parameters such as corrosion resistance. The mechanical properties were measured and analysed as a set of stress-strain curves shown in Figure 2-23. No further investigation into the case properties was made, thus the whole tensile sample was treated as a composite.

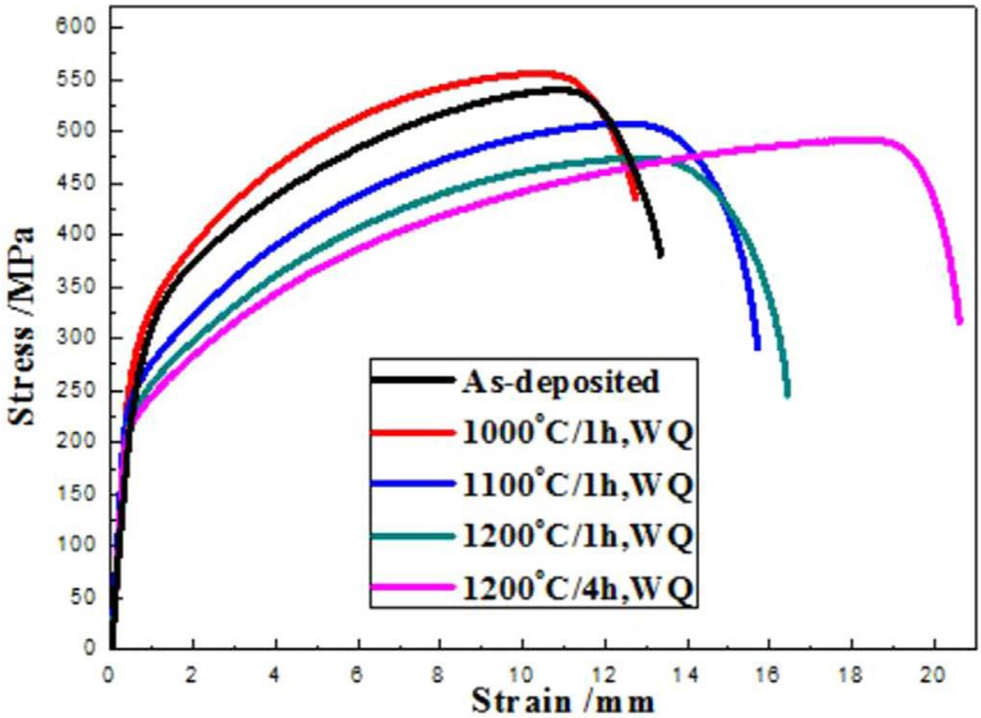

Figure 2-23: *Stress-strain curves of GMA-AM 316L*

During a series of tests conducted by Woods, Daniewicz and Nellums, (1999), thin carburised tensile samples were produced with material properties comparable to that of a case hardened gear. From tensile test results, the through case variation of flow stress and elastic modulus was determined for an elastic-perfectly plastic model. A similar experimental setup by (Chaouch, Guessasma and Sadok, 2012) compared physical data to an FE simulation.

Using a bilinear elastic-plastic model, the yield stress, elastic modulus and tangent modulus were tuned to minimise errors between the physical and computational results.

Abudaia, Evans and Shaw (2005) used compression tests to generate physical data from through hardened steels, the properties of which were comparable to those of case hardened layers. A Ramberg Osgood relationship was then fitted to the experimental data set.

Nobre *et al. (*2010) presented detail of a "XRDABM" method for determining the stress-strain behaviour in the surface layers of a material using X-ray diffraction for the measurement during a four point bend test. Combined with a strain gauge for surface measurement, the X-ray diffraction method was used to measure stress-strain curves throughout the sample. A shot-peened sample was measured, however the author states that the method could be used for any material with depth-dependent material properties. Figure 2-24 shows the experimental setup with typical results shown in Figure 2-25.

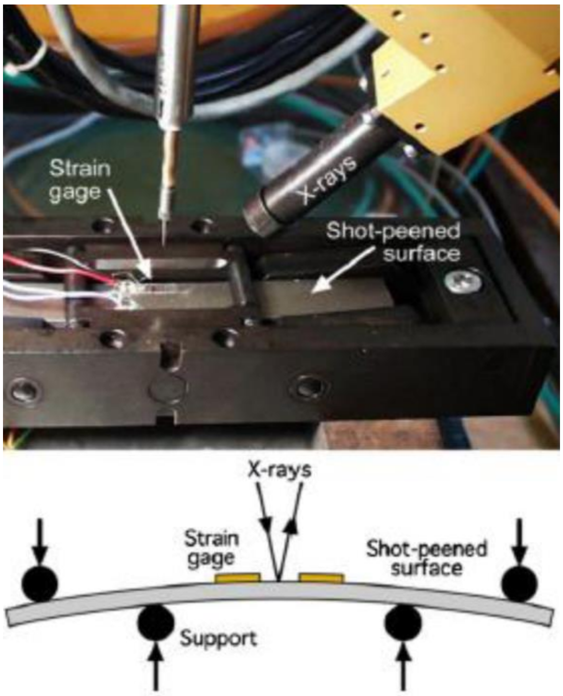

Figure 2-24: *XRDABM setup of Nobre et al. (2010)*

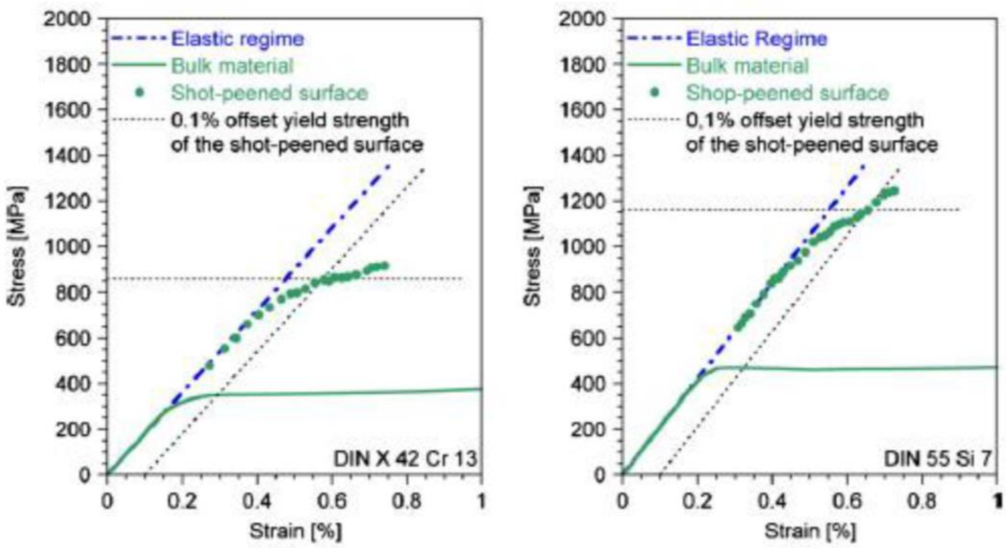

Figure 2-25: *Elastic-plastic behaviour of a shot-peened surface by Nobre et al. (2010)*

The final method for the measurement of elastic-plastic properties is via depth-sensing nano or micro indentation. As an indenter (similar to industry standard hardness indenters) is forced into the surface of a sample, its load as a function of penetration depth is measured. The resulting data can be used to infer the elastic-plastic material properties. Similar to hardness measurement, multiple measurements could be made at a range of positions through a case depth. From force and depth data, the strain-hardening law can be obtained by solution of an inverse problem using FE models of the indentation process. The works of (Elghazal *et al.*, 2001), (Antunes *et al.*, 2007), (Luo and Lin, 2007) and (Branch *et al.*, 2011) all include variations of approach for inferring material properties from the force and indentation depth data.

2.6. Literature Conclusion

This section summarises the conclusions from the literature review and outlines the parameters that are used in this Thesis.

2.6.1. Gear Analysis (Modelling Approach)

The most accurate results from FE analysis in literature were obtained when modelling a complete gear with the trade-off of processing time and computational power. A cylindrical body provides a most efficient means of modelling the majority of a gear however reducing the complexity of geometry in areas of low stress. A minimum of two adjacent teeth should be present either side of the loaded tooth to ensure sufficient support.

2.6.2. Gear Analysis (Element Types)

Hexahedral elements are most common within current literature where gears are modelled. Additionally, the industrial sponsor requested the use of hexahedral elements in modelling work based on their previous experience with FE models.

2.6.3. Gear Analysis (Mesh)

The literature of Lisle, Brauer and Lai outlined the use of a wide variety of mesh densities over an involute depending on the area of interest within the analysis. As this Thesis strives to apply the most appropriate material data to the case layer in the root, the mesh density will be dependent on the number of material layers the engineer desired to include in the simulations.

2.6.4. Gear Analysis (Boundary Conditions)

For a full gear analysis, boundary conditions typically restrain gears along the inner bore to simulate the gears' restraint on a shaft thus representing splines as demonstrated by Çelik (1999) and Woods (1999). Where possible, the FE model should be simplified by reducing the number of teeth included in the simulation and symmetrical boundary conditions applied to reduce model size. These concepts as supported by the literature of Barsoum (2014) and Çelik (1999).

2.6.5. Validation

For the scale of gears in this research, a non-contact measurement system is most appropriate for the validation of an FE model. Without scaling up the size of the gears being analysed, more traditional means of instrumentation such as strain gauges cannot be positioned accurately or repeatably as described by Lisle (2017). In light of the instrumentation available to the Author, a VSG system is most appropriate.

3. Experimental Methods

3.1. Introduction

Within this Thesis, methods for the measurement, testing and validation of material and gear samples are used. This chapter outlines the potential methods available within Cardiff University's School of Engineering, their benefits and drawbacks, and explains how the selected methods were implemented.

3.2. Material Sectioning in preparation for Microhardness Measurements

The analysis of case carburised materials using FE analysis requires knowledge of material properties. In gear analysis, one of the most important properties is the hardness of the material and its variation through the component. The datasheet for the gear steel was provided by the industrial sponsor (Albert & Duval, 2015) and outlines the material properties for the material in its supplied condition and following typical heat treatment processes. The parameters are presented in Table 3-1.

Table 3-1: *Table of S156 material parameters.*

Parameter	Value
0.2% Yield Strength	1030 $\mathrm{N/mm^2}$
UTS	1320-1520 $\mathrm{N/mm^2}$
Hardness (Core)	350-390 HV
Hardness (Surface)	700-750 HV
Case Depth	550 HV @ 1.00 mm

The industry standard for measuring material hardness is to section components such that hardness measurements can be made to evaluate the variation of hardness with depth below the gear surface. Within these standards no specific method of sectioning is stated, and so three were investigated. The most common sectioning methods are disc cutting, Electrical Discharge Machining (EDM) and Water Jet Cutting (WJC). In order to evaluate the thermal effects of the sectioning process on the measured hardness, a range of hardness samples were prepared (Figure 3-1) with each technique and their hardness evaluated.

Disc cutting is the fastest and most readily available option however, due to the nature of the abrasive discs and unpredictable lubrication/cooling, substantial heat is transferred to the components, regardless of rotational speed and feed rate of the cutter. The process leaves a discoloured surface that suggests a degree of tempering has occurred and can be seen in the left hand side of Figure 3-1.

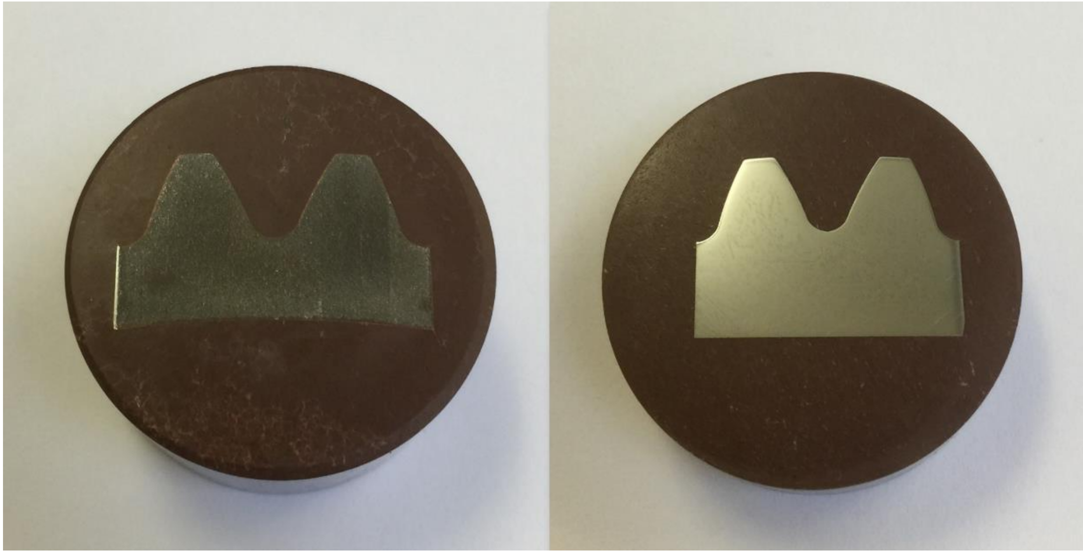

Figure 3-1: *Hardness sample surfaces post sectioning (Disc cut on left, and WJC on right)*

WJC provides a process that lends itself to the sectioning of heat treated components for material clarification perfectly. During the WJC process temperatures will not exceed 50°C (Precision Waterjet, 2014), therefore lower than the typical operating temperatures of 130°C of a motorsport transmission system. Due to the low temperatures involved in the process, there is no risk of tempering the material's surface. The downside of this process is the difficulty in clamping/fixing the component to be sectioned. This is alleviated by creating a custom fixture for the gear that is positioned inside the WJC tank. A secondary precaution is bonding the section to be removed to the fixture, such that it is not lost into the WJC tank.

Within Cardiff University, EDM is freely available, convenient and cost effective. The Author provided a detailed set of instructions to the operator to minimise temperature exposure, and to reduce tank time. Both of these features of the process have a secondary benefit of avoiding oxidisation of the steel components. During EDM, the temperature surrounding the electrode can exceed 8000°C locally, therefore tempering is a concern. The work piece is continually fed with a coolant to ensure a consistent temperature throughout the process.

The gear in Figure 3-2 was sectioned to provide three samples, one produced by disk cutting, one using WJC and one using EDM. The disk cut sample is not included in the Figure.

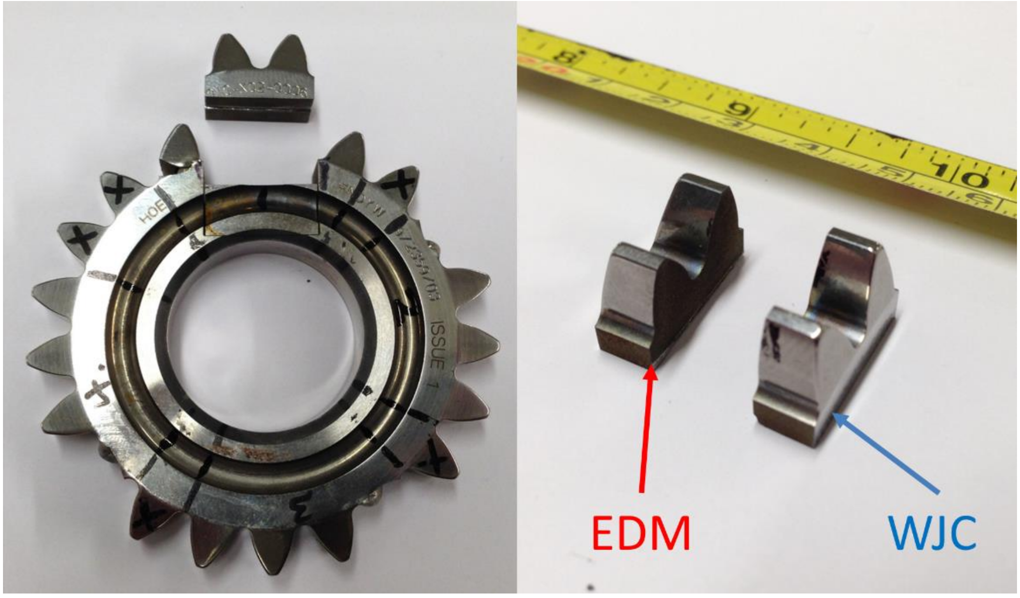

Figure 3-2: *Sectioned Gears*

3.3. *Microhardness Indentation*

Following the sectioning of each sample, hardness measurements are required at specific points over the involute. Due to the natural convex nature of the gear involute and the concave geometry of the root fillet, there will be a difference in the case depth from the root to the tooth tip. The red lines in Figure 3-3 show the positions where the hardness measurements were taken. Twenty indentations were made along each line, up to a distance of 2mm from the surface, ensuring that the line through the measurements was nominally perpendicular to the surface, therefore obtaining detailed measurements of the variation of hardness with respect to depth. Due to the size of indents and the positioning of the X, Y table on the Microhardness indenter, post measurement adjustments to the depth were made based on the angle (Θ) to account for any error in the alignment of the indents relative to the edge (tangent) of the gear surface.

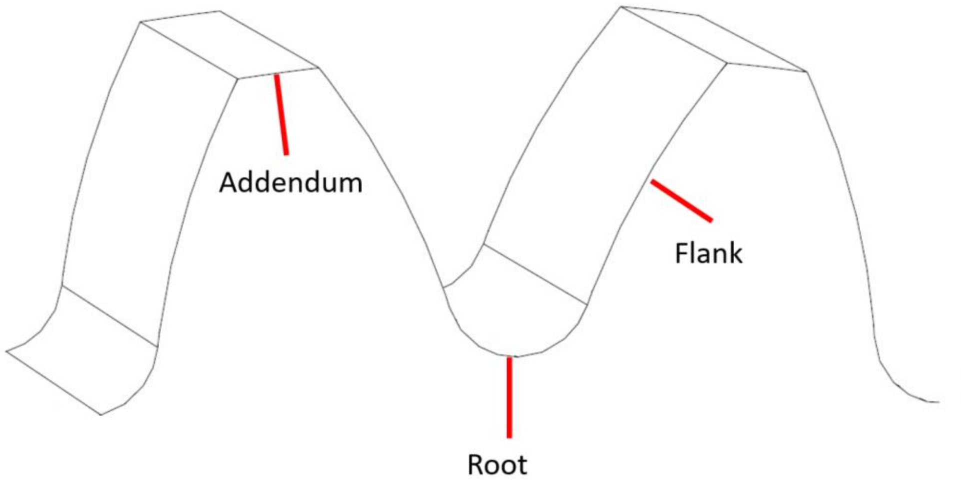

Figure 3-3: *Positions of Microhardness indentations along the involute.*

As per the ASTM E92-17, indentations should not be positioned within three times the indent diameter of each other. Indentations at a mass of 0.2 kg with a 10 s dwell time are specified in the standard. For a material hardness of 750 HV an indent of 22.2 µm across points is created. For a hardness of 350 HV an indent of 32.6 µm across points is created. Therefore a distance between each indent of 100 µm is suitable, allowing 15 measurements over a typical 1.5 mm case depth. Measurements were made to a depth of 2.0 mm to ensure that the entire case depth was covered. Figure 3-4 shows the spacing between indents at the root of the gear.

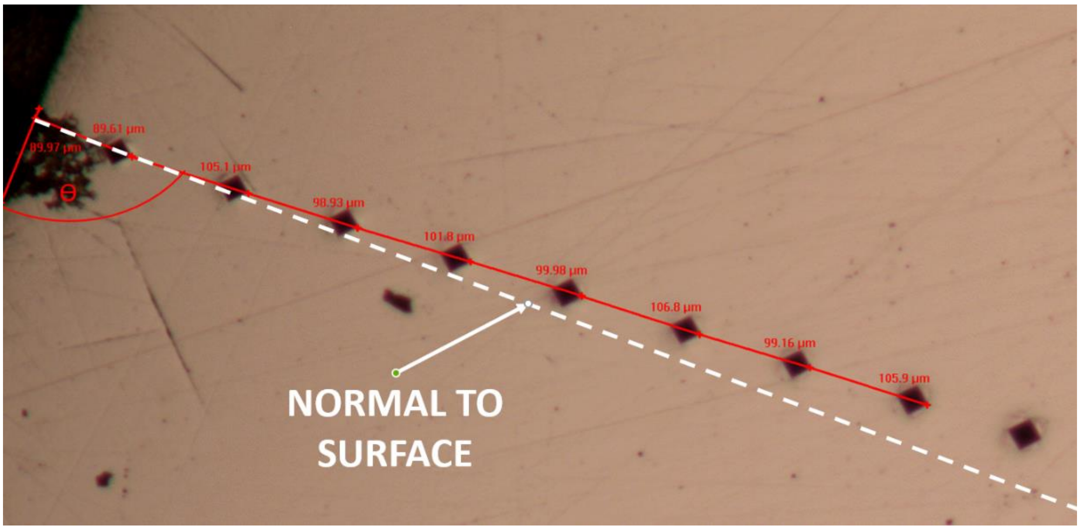

Figure 3-4: *Indent spacing (100µm) through the surface of a gear*

3.4. Digital Image Correlation (DIC) – Non-Contact Validation of Strain

Within Cardiff University's School of Engineering, a Dantec Q400 DIC system is used as an experimental tool in a wide range of research projects. Combined with XUP2.0/28 Compact Lenses, it produces a field of view (FOV) of 4.5mmx6.0mm, and is thus suitable for the non-contact measurement of the gear shown in Figure 3-5. A dual camera setup (stereoscopic) allows for any out of plane movement to be accounted for.

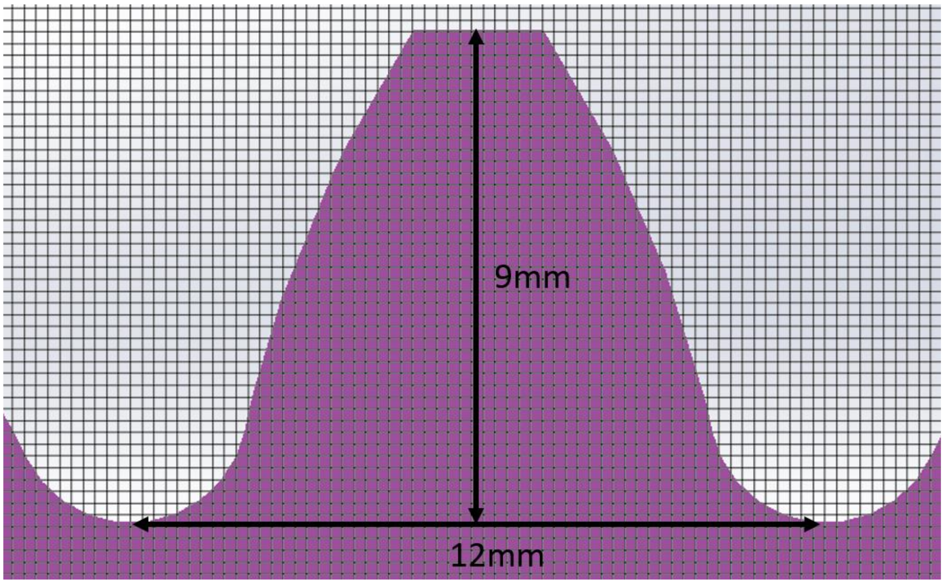

Figure 3-5: *Dimensions of a gear for analysis*

An initial setup was positioned to monitor the test of a tensile coupon (Figure 3-6) of 6mm thickness, thus the camera and lens combination selected. The stereoscopic test setup (two cameras) was mounted on a single tripod with an angle of 30 degrees between the camera axes, the minimum angle stated by the manufacturer.

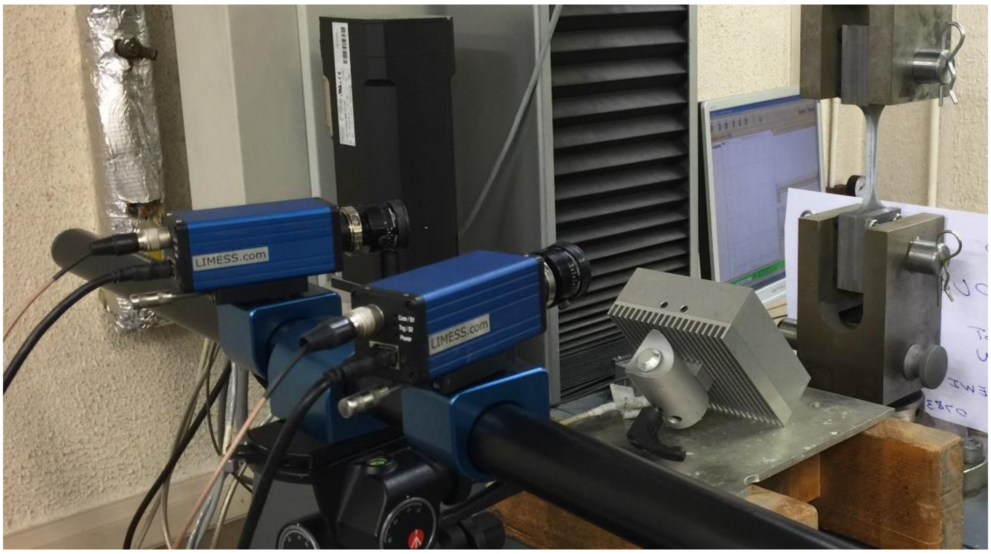

Figure 3-6: *Stereoscopic DIC setup for tensile test*

Some difficulties were encountered during this test, and the main issues that arose with the use of this system were as follows.

1. The mounting of the cameras. The setup time for a non-contact measurement system is generally underestimated. With such a small FOV, the slightest movement from one camera influences the other. To provide the largest area for analysis and therefore the greatest accuracy, both cameras must have the same section of the object in their FOV. Custom fixtures to mount the cameras separately are recommended by the DIC system manufacturer to reduce the test set up time and increase the adjustability in the system.
2. Focussing the cameras. Due to the small FOV required for this research, there is an inherently small focal length. The focal length is defined as the distance between the centre of the lens and the point of interest. Due to the stereoscopic setup, each camera is mounted at an angle to the normal direction of the surface being measured. This causes a variation in distance to the centre of the lens for points at the centre and the extremities of the FOV, thus creating a shift in focus that can be seen in Figure 3-7. For reference, the FOV of the camera is 4.5mm x 6.0mm.
3. For a stereoscopic DIC system, a calibration is required such that the cameras and software are able to detect out of plane motion. With the desired lens, a calibration tile is supplied that is specific to the FOV. The tile is typically glass square with a QR code or chequer pattern printed on it. During calibration, the test component remains in place and the tile positioned in the view of the camera. Through tilting the tile a few degrees in each direction, the software characterises the out of plane motion of the tile from the images on the cameras. At this stage to achieve the best calibration, it is important to

keep the tile as close to the component as possible. Due to the small FOV necessary in this research, and therefore the small focal length, positioning of the tile in front of the component is not possible. Despite the slender tile used for a FOV of this size, its additional thickness goes beyond the focal length of the camera and lens combination. Therefore to calibrate the DIC system, it is necessary to remove the component from the test fixture and calibrate in free space. It is now possible to obtain an adequate calibration, however upon reintroducing the test component, it becomes essential that it is positioned in the exact same position as previously. If it is not, then the calibration is of little use since the component will have fallen out of the focal length becoming blurry. To complicate the process once again, some gear tests require a preload to ensure the cameras are entrained on the correct test area. Therefore there is an additional stack of errors involved including any compliance in the test fixtures during the preload and test loading.

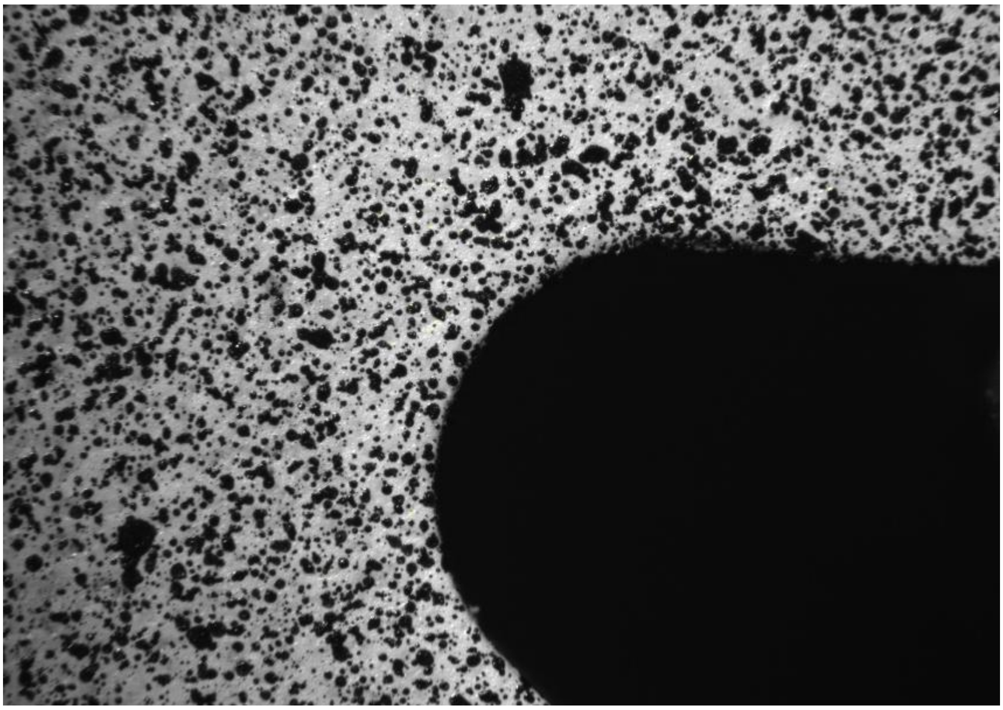

Figure 3-7: *Image from DIC camera. Note the change in focus across the FOV.*

4. Due to the stereoscopic setup causing an inconsistency of focus, the DIC analysis software cannot track the speckles on the surface of the loaded object. A clear, in-focus boundary is required for the algorithms to accurately track the speckles and thus establish displacement and strain data between unloaded and loaded images.

In summary, the stereoscopic DIC system available to the Author was not applicable as a validation method for this thesis.

3.5. Video Strain Gauge - Non-Contact Validation

Video Strain Gauge (VSG) is another non-contact validation method akin to that of DIC. It supersedes DIC by taking images as a video throughout the loading of a component and has the capability of providing strain maps and data from virtual strain gauges in real time. As the video feed is analysed in real time, it is also possible to move the strain gauges in the post-processing software if the user desired. Therefore, a VSG system is the next generation in strain measurement technology. During the period of the research an Imetrum VSG system with capabilities of 2D and 3D measurement was acquired by the University. The initial brief of this research project included DIC as a method to validate computational models. With an up to date VSG system with a higher specification than the existing DIC system, the opportunity arose for a comparison with DIC.

To provide a FOV appropriate to the research and comparable to the DIC system an Imetrum MTM28 lens was fitted. This provides a FOV of 7x8mm and a fixed focal length of 186mm.

Figure 3-8 shows a side by side FOV of both DIC (left) and VSG (right). Both cameras are focussed on a single root fillet of a loaded gear tooth with displacement in the Y axis being shown in the colour plot. In comparison of both measurement methods, it is clear that there is far greater coverage from the VSG system with greater clarity along the boundary of root and flank of the gear tooth. Note the black dot on the VSG screenshot. This is a single large speckle which results in the black region of missing measurement which can be seen. Care should be taken to ensure that speckles are applied as evenly distributed as possible, as described in Section 3.6.

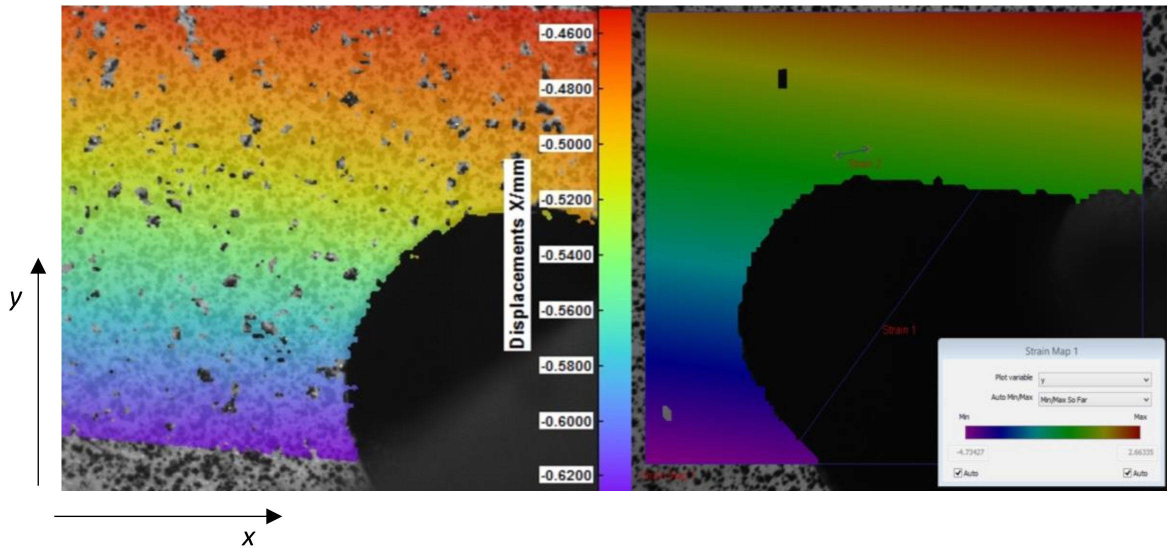

Figure 3-8: *Image of the vertical axis displacement from DIC and VSG respectively*

As previously mentioned, the VSG system records the video footage of the loaded component. For all sections of this thesis where VSG has been used to collect data/monitor a component, the following settings have been used.

- Calibration magnitude = 1. As the lens has a fixed focal length of 186mm, the system is calibrated using this value. With an alternative lens, the calibration can be completed through specifying a known value in the GUI of the Software, or by moving the load machine crosshead through the a known displacement through the FOV.
- Frame rate of 25fps. This is the maximum capability of the system whilst retaining all data for the full 1600x1200 resolution.

A brief comparison outlining the differences between the DIC and VSG systems is shown in Table 3-2.

Table 3-2: *Differences between the Dantec DIC system and the Imetrum VSG system.*

DIC – Dantec	**VSG - Imetrum**
Stereoscopic system	Single camera system
Calibration required via tile	Calibration not required with some lenses
User triggered image capture	Video Rate - 30fps maximum. Higher possible if FOV can be narrowed.
Results only viewed following post processing	Real time plotting of results
Displacement and strain maps	Displacement, strain maps, multiple strain gauges
Fov of 4.5mm x 6.0mm with most appropriate lense	Fov of 7.0mm x 8.0mm with most appropriate lense
1200 x 800 pixels	1600 x 1200 pixels

3.6. *Application of Speckle Pattern*

A non-contact method of monitoring a gear is an ideal solution to validate FE models. For both DIC and VSG techniques, the application and quality of a speckle pattern is essential as it can influence the accuracy of the results. Each manufacturer specifies various parameters for the size and distribution of the speckles. The dimensions must be above or below a specific number of pixels, and the ideal distribution is generally an equal split between the area of black speckles and a white background area.

Dantec recommend that each speckle be between 5 and 8 pixels in size. Thus for a FOV with a 6.5mm width resolved into 1200 pixels, each pixel represents some 0.005mm. Thus, each speckle should be between 0.025 and 0.040mm in diameter. Imetrum provide a stamp kit with its system such that speckle application is standardised. As the MTM28 lens is not part of the standard system, it requires an alternative method for speckling. During training with the manufacturer the rule of thumb of 5 to 8 pixels per speckle was again recommended (Personal Communication, 2016).

To achieve such small speckles, spray painting was considered a realistic approach. Prior to spraying, components are cleaned to eradicate any dust or swarf that would affect the smoothness of the surface. To ensure sufficient adhesion of the paint, acetone (or similar) should be used to clean the surface. The component is first sprayed with a layer of matt white paint. Matt paint is used to minimise the reflection of any light into the DIC/VSG cameras. DIC and VSG assume that the paint applied to the component displaces with the same direction and magnitude as the component's surface, therefore careful consideration is made to ensure that the thinnest layer of paint is applied.

Prior to this white layer drying completely, the black speckles can be applied. To ensure the smallest speckles, the component was placed on the bed of a spray booth with a can of black spray paint (also matt) approximately 1m above. The can is sprayed horizontally above the component allowing full atomisation of the spray. This is continued with periodic inspection of the speckle pattern until an approximate balance of 50% white and 50% black areas is achieved as shown in Figure 3-9.

Figure 3-9: *Image of speckle pattern applied to gear sample*

The percentage of area that is black/white is measured using the public domain software, 'Image J', a Java-based image processing programme. Using the threshold function, the percentage area of black/white is calculated and displayed as shown in Figure 3-10 where the Figure 49.5% is shown.

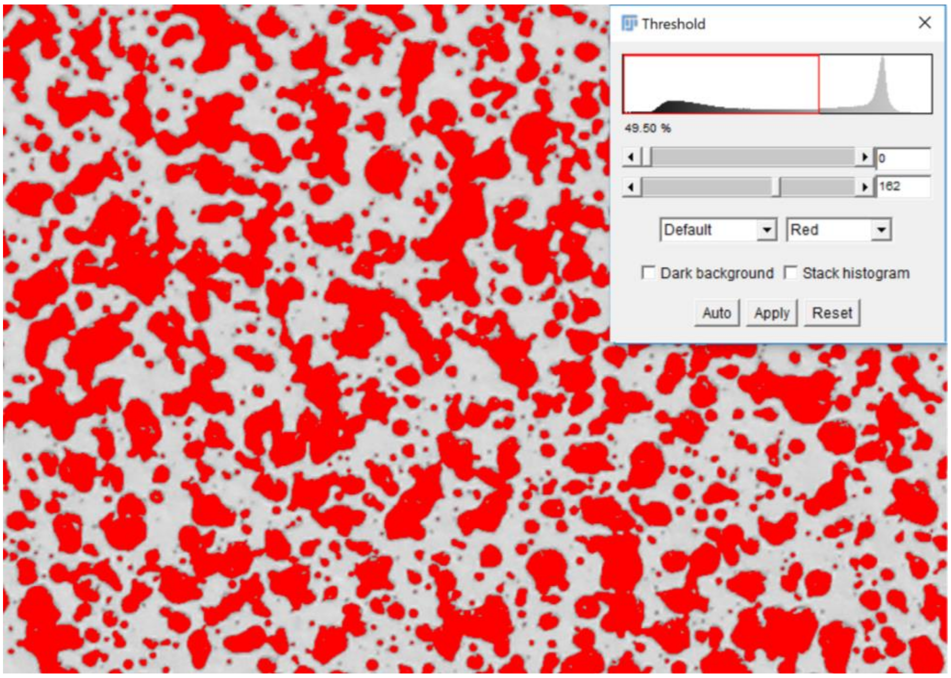

Figure 3-10: *Analysis of the speckle pattern in 'Image J'*

3.7. *Summary of Experimental Methods*

3.7.1. *Material measurements*

All hardness measurements were completed with 200g force, 10s dwell times and a minimum separation between indents of three times the diameter to avoid measurements affecting each other.

3.7.2. Validation

The non-contact strain measurement systems available to the Author, an Imetrum Video Strain Gauge system was deemed the most appropriate for measurement of displacement/strain on the gears being analysed. Due to the minimal/negligible out of plane motion, the advantages of a stereoscopic Digital Image Correlation measurement is negated. The VSG unit available was used as it has a better resolution in comparison to the DIC alternative.

3.7.3. *Tensile Test*

All tensile testing was completed in conformance to ISO:6892. For testing at high temperature, ASTM E21 was adhered to for temperature conformity. A displacement rate of 1mm/minute is used with all tests. For room temperature testing and extensometer was used for strain measurement. Due to the capability of the instrumentation, high temperature testing is completed with a VSG system monitoring the strain.

4. *Material Data*

4.1. *Hardness of Case Layer*

Prior to measuring the material properties of a case hardened layer, an initial investigation was conducted into the hardness variation throughout a case. These data were then used to outline the application of material properties. Microhardness measurements at intervals throughout the involute were made to investigate penetration of the heat treatment. All measurements were in accordance to the methods described in Section 3.2 and 3.3.

4.1.1. *Hardness measurements*

There was a concern that temperature effects, after EDM of the gear samples, would affect the hardness measurements. Hardness measurements for both EDM cut and WJC samples were made such that any tempering or hardening of the material from wire EDM could be identified. Both samples were from an identical gear with the same heat treatment, from the same batch. Measurements at the same position on the root radius were made on both samples, with the results shown in Figure 4-1. It is clear that once the surface is polished that there is no change in material property from apparent surface tempering on the EDM sample compared to that of the WJC sample. The reader will notice a 70HV difference between the first measurements. This is due to the close proximity to the edge of the gear sample. The aforementioned standard for Vickers hardness states that measurements made within three times the indent diameter of each other, or the edge of a sample are subject to an error due to the localised plastic deformation caused during the indent. Further measurements of this section of the gear yielded closer results however the error is included to highlight this phenomenon to the reader.

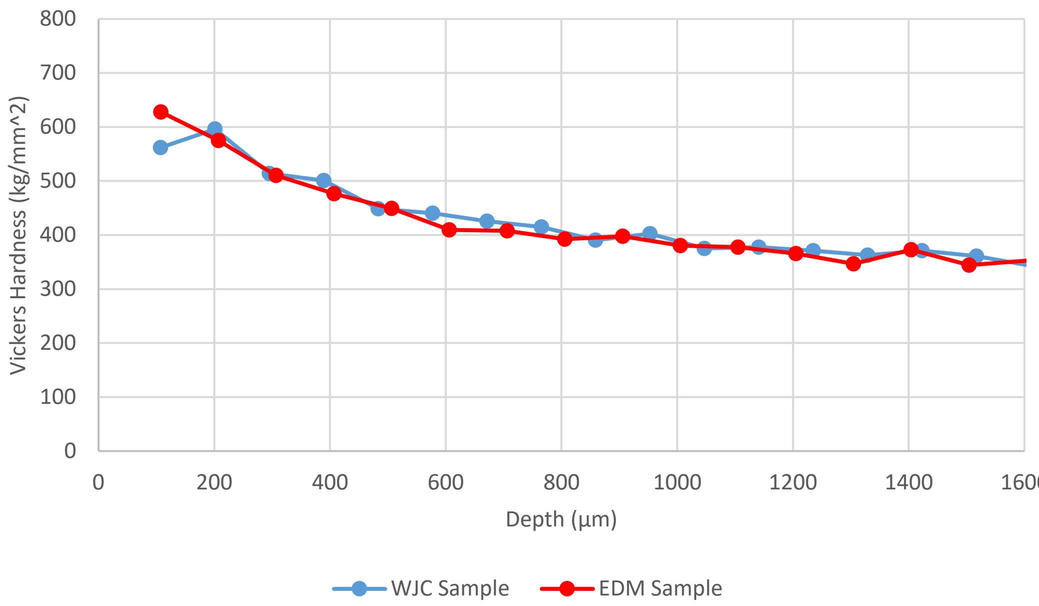

Figure 4-1: *Variation of hardness with depth below surface of WJC and EDM samples of a gear*

Measurements were made at different positions around the involute to investigate the penetration of the case on varying geometries. The convex geometry of the addendum tip should in theory promote penetration of the heat treatment due to its higher surface area. Areas within the addendum could be affected by the case from two or more surfaces – i.e. the flank(s) and tip of the gear tooth. The concave geometry in the root can be seen as vice-versa, and an example is shown in Figure 4-2.

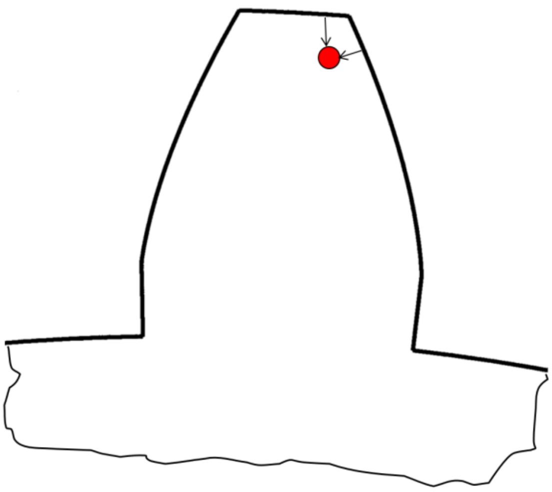

Figure 4-2: *Demonstration of how a single point can be affected by heat treatment penetration from multiple surfaces*

Data from the micro hardness measurements for various positions over the involute are shown in Figure 4-3. The Figure shows experimental data that was collected as part of this Thesis alongside the purple line which shows the hardness through the depth. This data is supplied by the sponsor's gear supplier. Note the variation of the hardness between the root and the addendum. The addendum is consistently 75-100 HV harder than the root. This is caused by their surface geometry and how it influences the penetration of the heat treatment. It may also be seen that the measurement in the addendum is clearly influenced by heat treatment effects from more than one surface, as the hardness falls then increases again with increasing depth. The measurements at the root and flank of the gear are in good agreement and are typical of what one might expect.

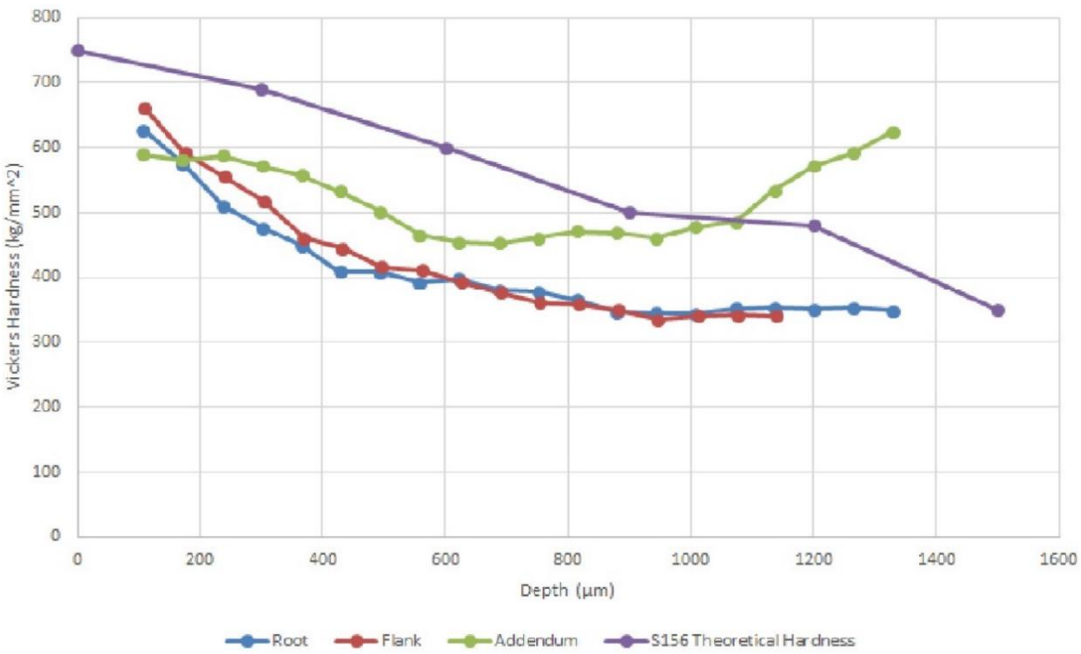

Figure 4-3: *Vickers hardness of a gear tooth at various positions as a function of depth below the tooth surface*

Each of the above positions were chosen due to their ease of positioning using a manual micro hardness indenter. Multiple measurements were made to ensure the results were representative. The set shown in Figure 4-3 includes a single data (single line of measurements) as each position change over the gear results in a slightly different depth from the surface. In future investigations an automated indenter is recommended such that consistency in depth, indent spacing, dwell time and indent measurement is ensured.

4.2. *Hardness Penetration through Involute Geometry*

Figure 4-3 demonstrated varying penetration for the heat treatments over various points of the involute geometry. To further understand this, an Indentec µHV hardness indenter was used to measure multiple points around the root of a gear in a Cartesian coordinate format.

To ensure repeatability of measurements between the CNC indenter and those completed at Cardiff University, the same 200g indentations, 10s dwell time and spacing of 100 µm (3 x the indent diameter) was adopted to satisfy the standard. The colour plot of Figure 4-4 demonstrates the differing penetration of the heat treatment over the root of the gear tooth. Figure 4-4 includes a mosaicked image which outlines where the measurements were made. The colour plot was created using the *surfaceplot* function of *MATLAB* where a matrix includes the magnitude of the hardness and each row/column represents a 0.1mm spacing.

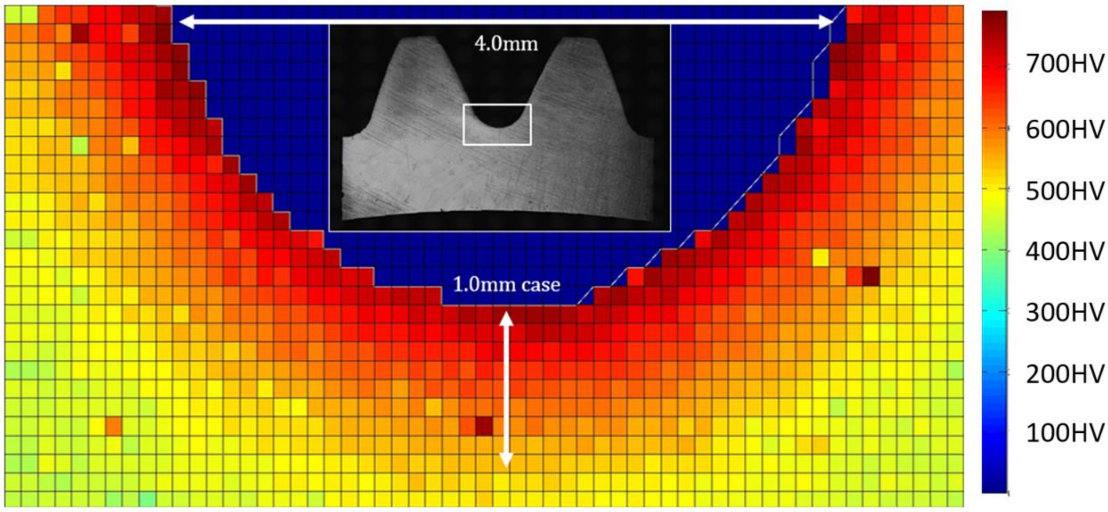

Figure 4-4: *Colour map of hardness from an Indentec hardness tester*

The Indentec indenter includes a CNC bed that allows the user to specify the working area of the sample. The indenter will then take a series of images over the surface and stitch them together to create a mosaicked image. The measured area is shown at the top of Figure 4-4. The user can then specify the mass, dwell and indent spacing over the mosaic thus allowing the user superior accuracy when compared to an indenter with a manual X-Y stage. Once specified, the option is available to automatically measure the indent diameter and calculate the hardness. The reader may notice a discrepancy between the hardness between Figure 4-3 and Figure 4-4 when measured at 1mm case depth at the root. This is due to the hardest measurements being very close to the gears edge, thus the plastic deformation at the surface being affected by the edge, and appearing harder.

Following each indent, the machine switches to a lens (used to create the mosaicked image) and uses a light-based system to measure the indent diameter. Due to the length of time to make each indent, the measurement was made out of office hours; therefore switching lights on/off within the room can cause an error to the measurement. Figure 4-4 includes some hardness measurements that appear as outliers. This was put down to the laboratory lights being switched on/off by security/cleaning staff.

4.3. *Tensile Testing Introduction*

To produce the best possible material data for a computational model, physical data is preferred to that of a material manufacturer's data sheet. Despite the data sheets using experimental data to inform them, additional testing should be completed to ensure defects and batch conformity to expected values. Additionally, data sheets typically do not include a complete stress-strain curve for the raw material or any heat treatments. For heat treated components, developing stress-strain curves which represent mechanical property variations over the case depth requires extensive testing.

The aim of this section of analysis is to produce an experimental procedure to extract material data for a case carburised layer. Material testing is extensively used throughout industry to find the properties of a new material and also to ensure consistency between batches. The most common method is a tensile test, using either a round or flat coupon. There are benefits to both depending on the type of material properties that are being measured. Figure 4-5 shows the general form of a round tensile coupon typically used for fatigue testing to generate data for S-N curves.

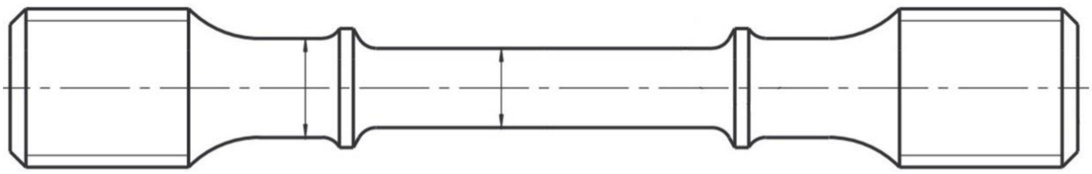

Figure 4-5: *Industrial sponsor Tensile Coupon (Round section – dimensions removed at sponsor request)*

Due to the focus of this research on the properties and contribution to overall material strength of the case layer, a round coupon similar to that in the Figure was not deemed the most suitable. A flat dogbone coupon cut from a heat treated sheet of material would create a component with only two faces of heat treatment, thus a two dimensional problem. Therefore, case hardened layers should only exist on the largest flat faces of the coupon, as demonstrated in Figure 4-6.

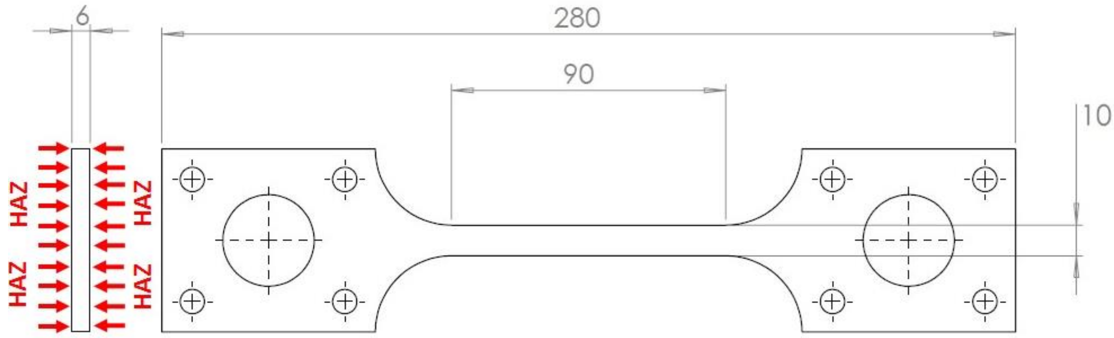

***Figure 4-6**: Final machining of heat treated coupons*

The design of the tensile coupon is in accordance with ISO:6892. All testing is also in accordance with this standard. The coupon has a parallel length and a width of 10mm, respectively. The coupon is 6mm thick. This was recommended by the industrial sponsor and the heat treatment provider. They stated that any component that is case hardened be at least three times thicker than the case itself. The case depth applied to S156 steel is nominally 1.5mm therefore a 6.0mm thickness provides a coupon with sufficient material that, when the case layer is ground away, it can be tested on the same machine as an unground sample and provide data within a comparable load range. Additionally, a 6mm coupon was calculated to be sufficiently thin that the expected loads would not exceed the 100kN tensile capability of the Zwick Z100 tensile test machines chosen to conduct the testing. The complete drawing can be seen in Figure 4-7.

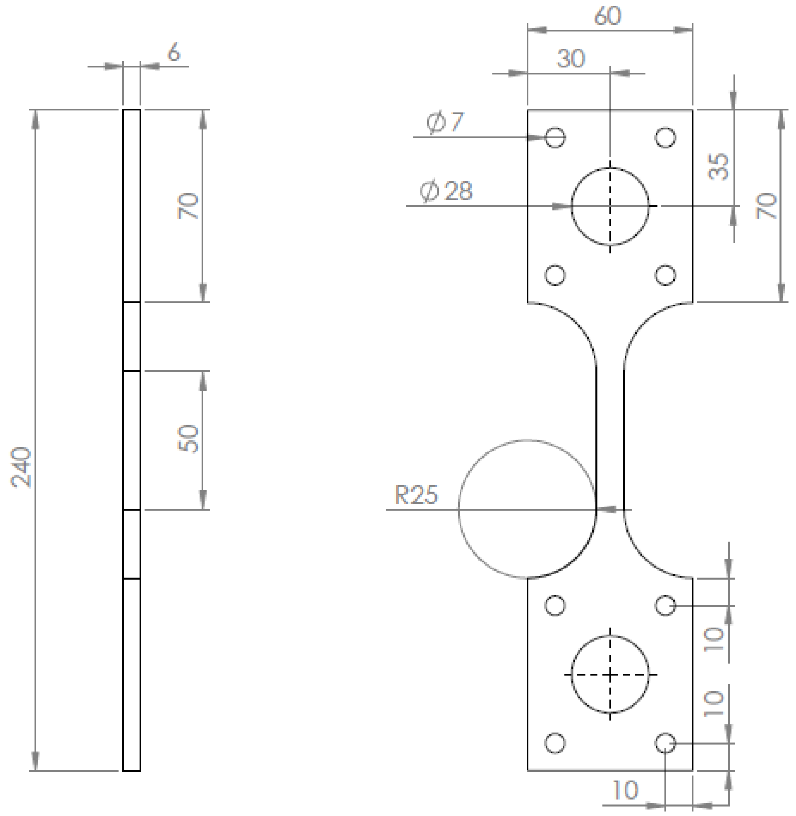

Figure 4-7*: Final machining drawing of tensile test coupon*

The concept of the tensile test is as follows. 50 flat dogbone tensile coupons were produced with the necessary heat treatment. To negate the end effects as previously mentioned, 'blanks' were heat treated first and the dogbone geometry machined afterwards. The coupons were then ground to different thicknesses, thus removing quantifiable amounts of the case layer equally from both flat faces. Testing these coupons to failure then generates stress v strain curves for coupons with varying amounts of case layer remaining. Using a novel analysis of the data the material data for each layer was estimated.

Coupon grinding was completed on a CNC grinder at Cardiff University where material was removed from each side in 0.25 increments prior to the coupon being turned over, in order to ensure minimal distortion and residual stresses. Coolant was constantly fed onto the coupons to ensure there were no temperature effects that would impact the heat treatment that is at the focus of the research. In addition to these rules for grinding, the same technician was assigned to all grinding operations to ensure consistency.

4.3.1. *Tensile Test Specification*

From the raw material datasheet (Albert & Duval, 2015) for the specification of gear steel, the UTS for the core material beneath the carburised layer is quoted as 1400MPa. With the determined cross sectional area of 60mm (10mm parallel width and 6mm thickness), the predicted load at the UTS therefore is 84kN as shown in Equation (14)

$$P = F/A \qquad F = P \times A \tag{14}$$
$$F = 1400 \times 60 = 84{,}000N = 84kN.$$

With the expected increase in strength of the heat treatment, this leaves a significant enough increase in overall tensile strength below the 100kN capacity of the Zwick Z100 tensile test machines.

50 Coupons were manufactured by the industrial sponsor's gear manufacturing subcontractors, and all were heat treated. In the interest of minimising the error in the experimental work and instrumentation, a minimum of 5 coupons were tested at each thickness. To understand the method, and to quantify the loads and displacements at which the coupons of each thickness fail, one coupon of each thickness was tested without an extensometer. This was at the request of the technical staff of the university to ensure there was no damage to the extensometer during the failure of the coupon.

Table 4-3: *Number of tensile coupons and ground thickness*

Thickness	Number of Coupons
6.0mm	7
5.5mm	6
5.0mm	6
4.5mm	6
4.0mm	6
3.5mm	6
3.0mm	6

To ensure repeatability, accuracy of measurements and to streamline the testing procedure, 10 coupons in mild and EN24T (817M40) steel were manufactured for initial testing. Results are not included in this Thesis as these coupons were primarily used for development of the experimental techniques.

4.3.2. *Tensile Fixture Design*

Due to the magnitude of tensile force required in this test, custom test fixtures were required. Having calculated the tensile load in Equation (14), the proposal to use a Zwick Z100 tensile test machine with 100kN capability and a 100kN load cell was therefore suitable. It was expected that the UTS would be increased by the case carburisation process, however the industrial sponsor advised that it would not increase from 84kN to beyond the capability of the tensile testing machine.

With a load case set, suitable fixtures could be designed. ‘H’ blocks machined from EN24T were identified as the most suitable solution. Figure 4-8 shows the completed CAD model.

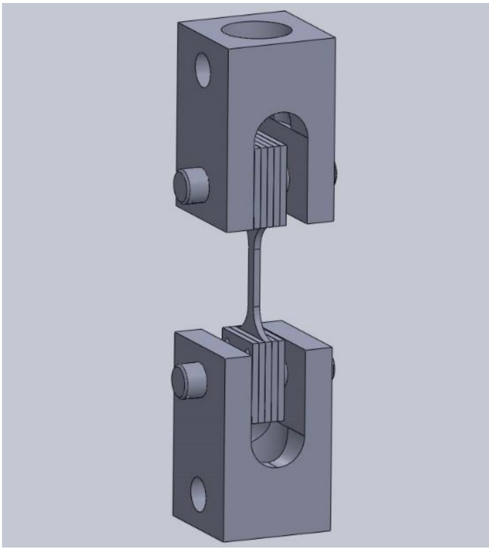

Figure 4-8*: Tensile coupon in fixtures*

To ensure that the fixture would withstand the loads required Equations (15), (16) and (17) were used.

Knowing that the shear stress is;

$$\tau = \mathrm{F/A} \tag{15}$$

$$\sigma y = \frac{My}{I} \tag{16}$$

Where σy is the bending stress, *M* is the maximum bending moment of the pin (WL/4), *y* is the distance to the neutral axis and *I* is the moment of inertia ($\frac{\pi}{4}r^4$).

Using the Tresca criterion for a shaft in bending;

$$^{1}/_{2}\ (\sigma 2 - \sigma 1) = {}^{1}/_{2}\ \sqrt{[(\sigma x - \sigma y)^2 + 4\tau^2]} \qquad (17)$$

To generate a 1400MPa stress in the parallel length of the tensile coupon, the stresses in the fixtures are as shown in Table 4-4.

Table 4-4: *Table of stresses in critical areas of the fixture pins.*

Location/Type of Stress	**Maximum Stress**
Maximum pin shear stress	36MPa
Maximum pin bending stress	395MPa
Combined stress (Tresca Criterion)	400MPa

The yield strength of EN24T from the material data sheet is stated as 650MPa therefore a 1.625 safety factor is included and deemed sufficient for this purpose. The 'H' blocks include a minimum CSA of $500\mathrm{mm}^2$, therefore the maximum stress at 84kN is 168MPa, giving a safety factor of 3.8.

Figure 4-9 below shows the fully manufactured fixtures with a tensile coupon in place with an extensometer fitted. In the background a DIC system is being used as a non-contact measurement system. Further information regarding DIC results can be found in Chapter 3.

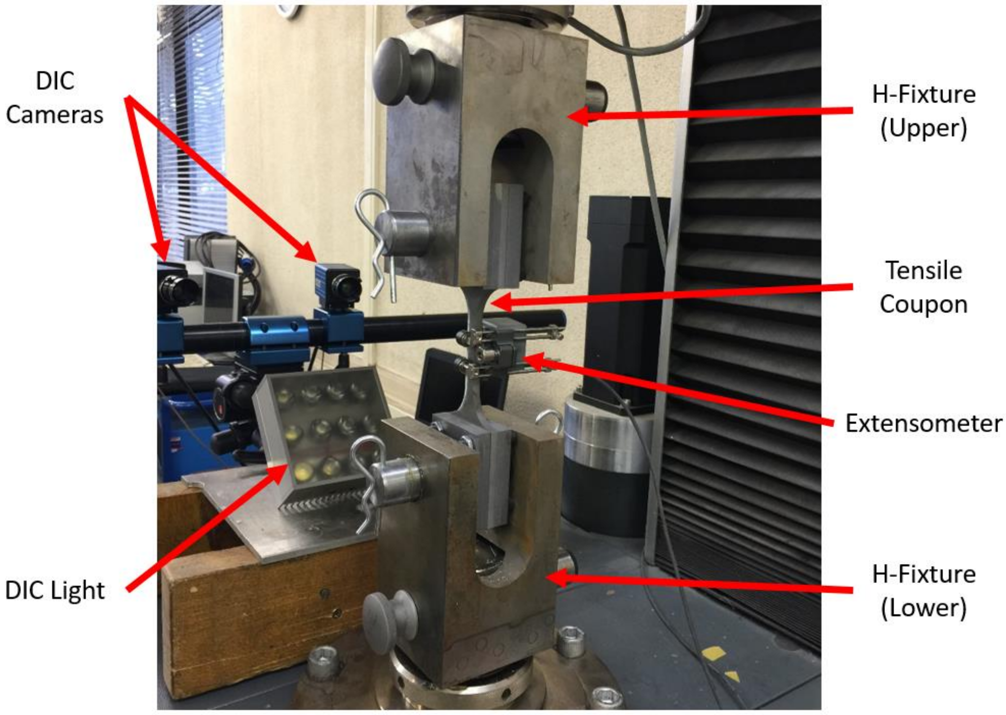

Figure 4-9: Complete fixtures testing EN24T coupon. DIC included in background.

4.4. *Theoretical Material Model - Ramberg Osgood*

The calculated strain in the material is derived from a Ramberg-Osgood relationship. Equation (18) was developed in 1943 by Ramberg and Osgood as part of the development of aluminium alloys for use on the Spitfire during World War II. The objective was to represent stress-strain curves using only three material parameters. Since then, the Ramberg Osgood relationship has been adapted for use in steels as shown in Figure 4-10 by Abudaia *et al.* (2004). The three parameters used are the Strain Hardening Exponent (Commonly denoted ‘n’), Monotonic Strength Coefficient (A) and the Uniaxial Stress. Since its first application it has been proven that the relationship can be further applied to any materials that strain-harden as they plastically deform.

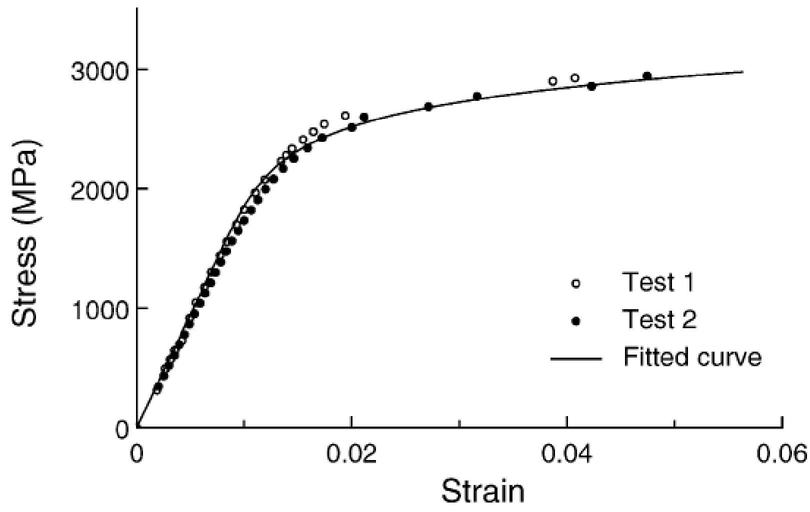

***Figure 4-10**: Stress-strain data for uniaxial compression of high-strength steel (Abudaia et al., 2004)*

$$\epsilon = \frac{\sigma}{E} + \left(\frac{\sigma}{A}\right)^{\frac{1}{n^m}} \qquad (18)$$

Naturally, as the applied range of material has expanded, variations of the relationship have been established. Equation (19) included by Barbato (1998) includes the additional parameter *'p'* within the formulation that refers to a given level of plastic strain (typically 0.2% in literature).

$$\epsilon = \epsilon_0 + \frac{\sigma}{E} + p\left(\frac{\sigma}{\sigma_p}\right)^n \qquad (19)$$

Radmussen (2006) introduced an expression for generating stress-strain curves over the full strain range of a material. The original Ramberg-Osgood relationship becomes inaccurate at proof stresses exceeding 0.2% due to the extrapolations of curve fits within the elastic and initial yield curves. To attain realistic and accurate stress-strain curves for stainless steel, the author derived two separate equations based on the proof stress and plastic strain. Equations (20) and (21) describe the stress-strain curves for proof stress below and above 0.2% respectively.

$$\epsilon = \frac{\sigma}{E_0} + 0.002 \left(\frac{\sigma}{\sigma_{0.2}}\right)^n \tag{20}$$

$$\epsilon = \frac{\sigma - \sigma_{0.2}}{E_{0.2}} + \epsilon_u \left(\frac{\sigma - \sigma_{0.2}}{\sigma_u - \sigma_{0.2}}\right)^m + \epsilon_{0.2} \tag{21}$$

Equation (22) includes the additional parameter *'m'* as an exponent where *'n',* the strain hardening exponent, is introduced for dependency on the proof stress above 0.2%. Equation (23) denotes the change, whilst Equations (24), (25) and (26) allow determination of the other parameters within Equation (23).

$$m = 1 + 3.5\,\frac{\sigma_{0.2}}{\sigma_u} \tag{22}$$

$$E_{0.2} = \frac{E_0}{1 + 0.002({}^{n}/_{e})} \tag{23}$$

$$e = \frac{\sigma_{0.2}}{E_0} \tag{24}$$

$$\epsilon_{0.2} = \frac{\sigma_{0.2}}{E_0} + 0.002 \tag{25}$$

$$\varepsilon_u = 1 - \frac{\sigma_{0.2}}{\sigma_u} \tag{26}$$

Figure 4-11 is a spreadsheet developed to take the parameters of a Ramberg-Osgood model, and generate numerical data required to input the elastic-plastic material model into the *ABAQUS* FE software. Each calculation has a section named '*ABAQUS* Input Data'. When the user has nominal stress-strain data from a physical test, it is required to be converted to true stress and logarithmic plastic strain. True stress is shown in Equation (27) and (28).

$$\sigma_T = \frac{F}{A_i} \tag{27}$$

Following substitutions

$$\sigma_T = \sigma\,(1 + \varepsilon) \tag{28}$$

Logarithmic plastic strain data is also required by *ABAQUS* and is shown in (29).

$$\epsilon_{ln}^{pl} = \ln(1 + \varepsilon_{nom}) - \frac{\sigma_{True}}{E} \tag{29}$$

These plastic material properties are then input to *ABAQUS* in the form seen in Figure 4-12. Using the material data generated in this chapter, it is possible to validate a material model. As described in the section above, the modified Ramberg Osgood model has sufficient parameters that control the curve around the yield that it can match a range of stress-strain behaviours. Due to the variable exponents that are generated from yield and UTS data, there are sufficient parameters to create a model with accurate yield characteristics.

Input values coloured				
S156 core at RT				
Modified Ramberg Osgood				
Ramberg Osgood param, n	26	<< Found in Mil handbook		
Initial Youngs Modulus, E_0	200000			
0.2% proof stress, $S_{0.2}$	1050			
Ultimate strength, S_{ult}	1500			
Elong at failure	0.11			
Total strain at failure	0.1175			
Non dim proof stress, e	0.00525			
Tangent Modulus at 0.2% proof stress, $E_{0.2}$	18340.61			
Transformed ultimate tensile strength, St_{ult}	450			
Transformed ultimate plastic strain, Et_{up}	0.1175			
m	3.45			
			Abaqus input data	
	Stress	Strain	True stress	Log plastic
	0	0		
	244	0.001218		
	787	0.003936	790.0	0.00000
	1009	0.005745	1014.4	0.00066
	1039	0.006718	1046.0	0.00146
0.20%	1050	0.00725	1057.6	0.00194
	1100	0.010036	1111.0	0.00443
	1150	0.013358	1165.4	0.00744
	1200	0.018083	1221.7	0.01181
Eqn changes for stress > 0.2% proof stress	1300	0.036346	1347.2	0.02896
	1466	0.119616	1641.5	0.10478
	1482	0.13313	1679.6	0.11659
	1500	0.149286	1723.9	0.13052

Input values coloured				
S156 full hard at RT				
Modified Ramberg Osgood				
Ramberg Osgood param, n	26	<< Found in Mil handbook		
Initial Youngs Modulus, E_0	200000			
0.2% proof stress, $S_{0.2}$	1807			
Ultimate strength, S_{ult}	2144			
Elong at failure	0.02			
Total strain at failure	0.03072			
Non dim proof stress, e	0.009035			
Tangent Modulus at 0.2% proof stress, $E_{0.2}$	29605.96			
Transformed ultimate tensile strength, St_{ult}	337			
Transformed ultimate plastic strain, Et_{up}	0.03072			
m	3.94986			
			Abaqus input data	
	Stress	Strain	True stress	Log plastic
	0	0		
	419	0.002096		
	1354	0.006772	1363.4	0.00000
	1736	0.009381	1752.0	0.00058
	1788	0.010463	1806.8	0.00137
0.20%	1807	0.011035	1826.9	0.00184
	1850	0.012496	1873.1	0.00305
	1900	0.014366	1927.3	0.00463
	1950	0.016905	1983.0	0.00685
Eqn changes for stress > 0.2% proof stress	2073	0.032002	2138.9	0.02081
	2096	0.037421	2174.0	0.02587
	2119	0.044134	2212.2	0.03213
	2144	0.053138	2257.9	0.04048

***Figure 4-11**: Material data calculated from Equations* (20) & (21) *for use in FE analysis.*

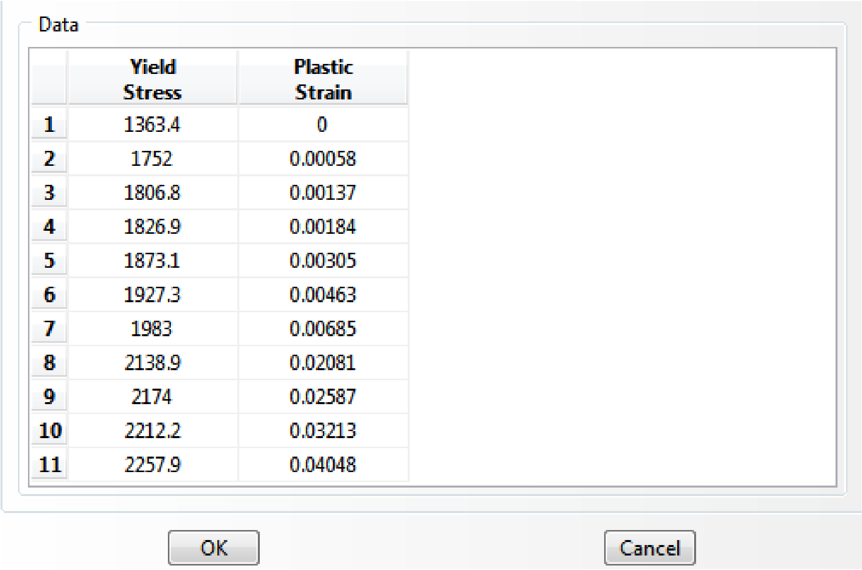

Data

	Yield Stress	Plastic Strain
1	1363.4	0
2	1752	0.00058
3	1806.8	0.00137
4	1826.9	0.00184
5	1873.1	0.00305
6	1927.3	0.00463
7	1983	0.00685
8	2138.9	0.02081
9	2174	0.02587
10	2212.2	0.03213
11	2257.9	0.04048

OK Cancel

***Figure 4-12**: Material data included in ABAQUS CAE.*

4.5. *Tensile Data (Room Temperature)*

All tensile testing was undertaken in conformance with the standards and experimental procedure outlined in Section 4.3. Figure 4-13 shows the raw data for the room temperature tensile test. All five curves are shown along with their average.

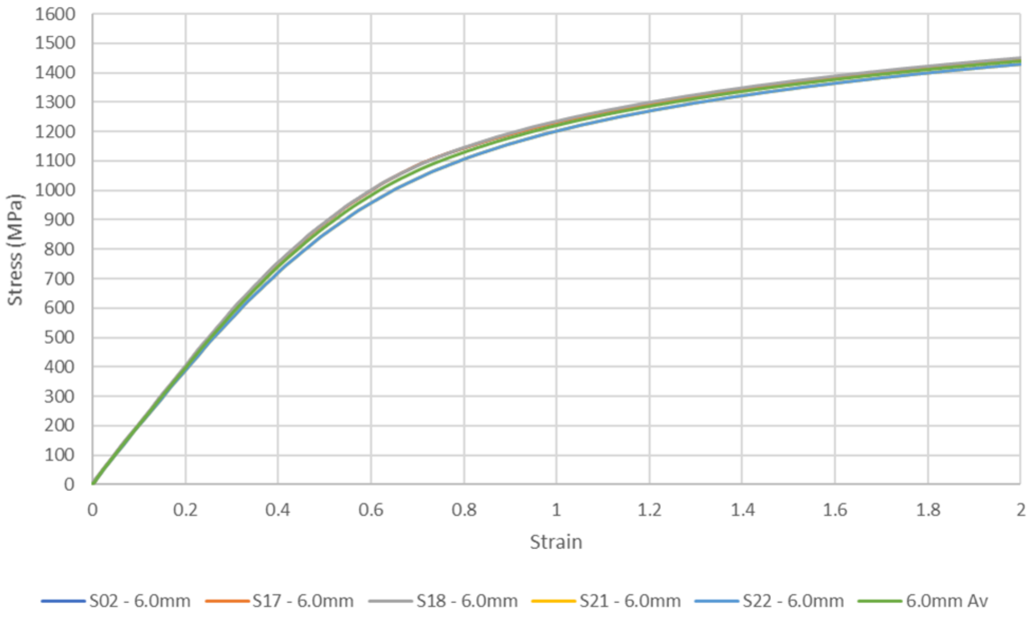

Figure 4-13: *Raw material for all 6.0mm tensile coupons (including average)*

Figure 4-14 shows the average raw data for all thicknesses of tensile coupons tested. There is a noticeable difference between the elastic and plastic areas of the stress-strain curves that becomes more apparent at higher strains.

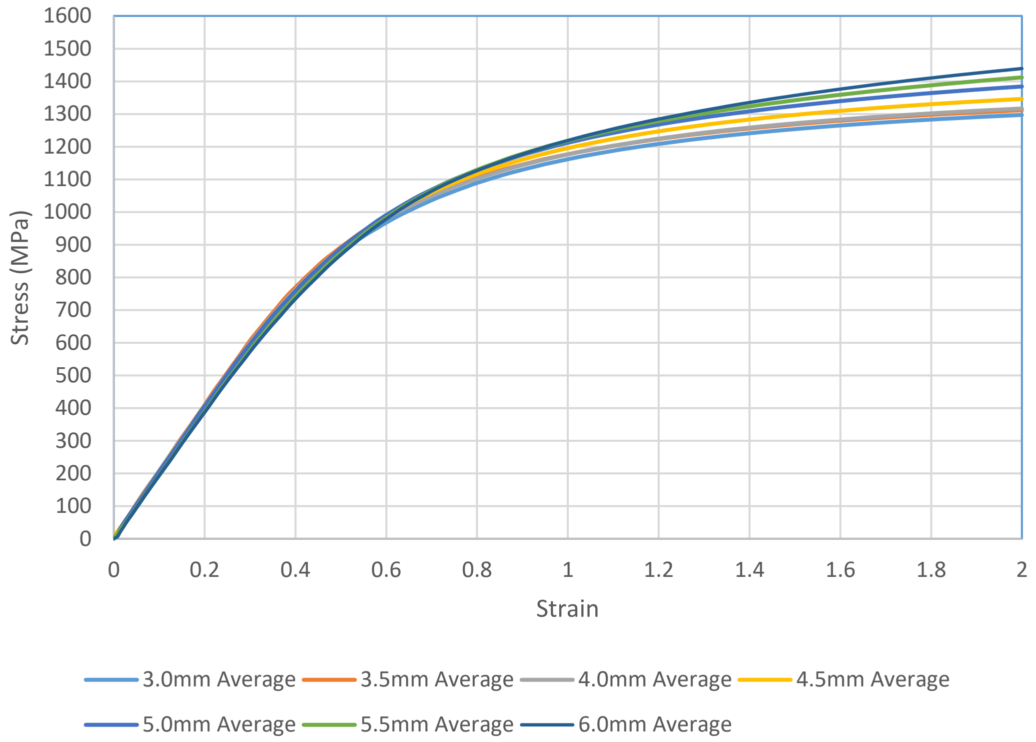

Figure 4-14: *Raw material data for averaged tensile coupons for each tested thickness*

Figure 4-15 shows a detailed view of the stress-strain curves from Figure 4-14 between strains of 1.8 and 2. This emphasises the additional capacity the case layer has to carry a higher load, therefore a higher stress.

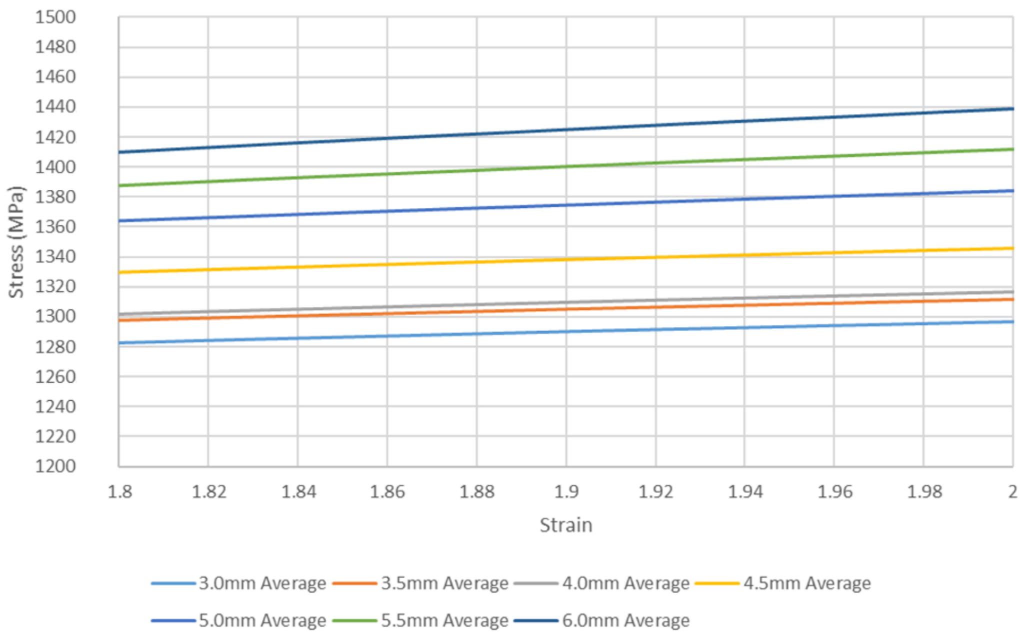

Figure 4-15: *Detailed Figure showing raw material data for each tensile test for strains between 1.8 and 2*

4.6. *Tensile Data (High Temperature)*

All tensile testing was undertaken in conformance with the standards and procedure outlined in section 4.3. All deviations from that procedure due to higher temperatures are explained below.

At the request of the industrial sponsor, a full test repeat at an elevated temperature was required. As per the sponsors' standard for material testing, all data must be taken in an environment as close to that of its intended use as possible. Within a transmission system, the temperatures of gears are typically at 130 °C although it is possible to be higher in exceptional circumstances. These tests were completed at 130 °C.

Due to the lack of a high temperature extensometer, high temperature oven and load machine capable of 100kN all within a single unit at Cardiff University, all high temperature testing was completed using the facilities of Westmoreland Mechanical Testing & Research (WMTR) in Banbury. All testing was completed on an Instron 5582 machine with an Instron 100kN load cell. A custom environmental chamber (Width – 540mm, Height – 650mm, Depth – 740) and fixtures were produced to house and fix the coupons in place. As per the room temperature testing, ASTM E21 was adhered to.

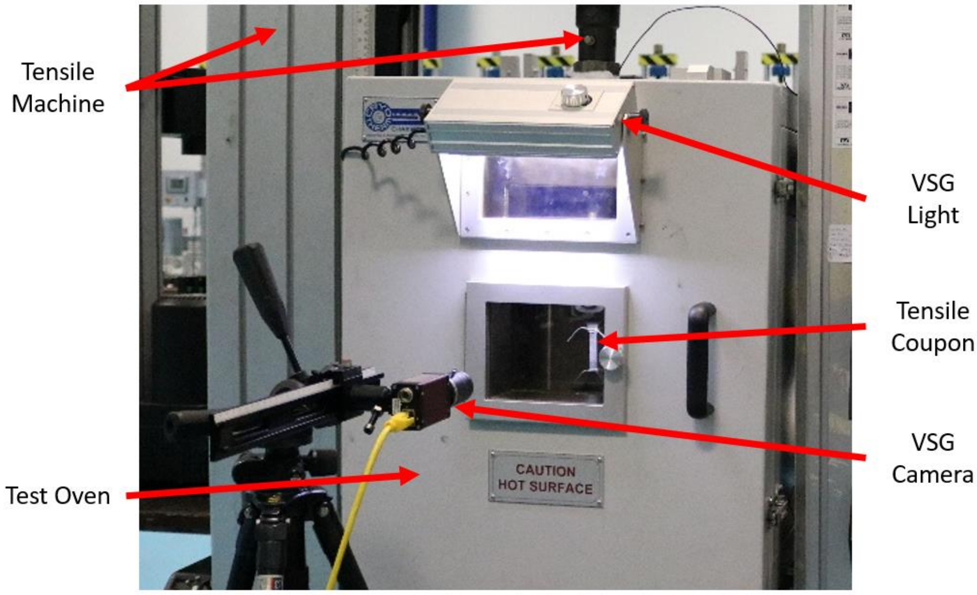

***Figure 4-16**: High temperature experimental setup*

Due to the nature of the high temperature test and the desire to not remove the extensometer at a pre-determined strain value, a VSG system (Imetrum system as described in Chapter 3, Version 5.3.5) was utilised through the quartz glass test window (chosen for its superior optical properties) in the environmental chamber door. Additionally, this ensures the test is entirely completed at the desired temperature. In previous testing completed at WMTR, an error of <0.5% was found between VSG and a mechanical extensometer in this condition (Personal Communication, 2017). As per ASTM E21, two thermocouples were attached to each test coupon such that temperature could be monitored in their heating up, stabilisation at 130°C, and 30 minute heat soak phases.

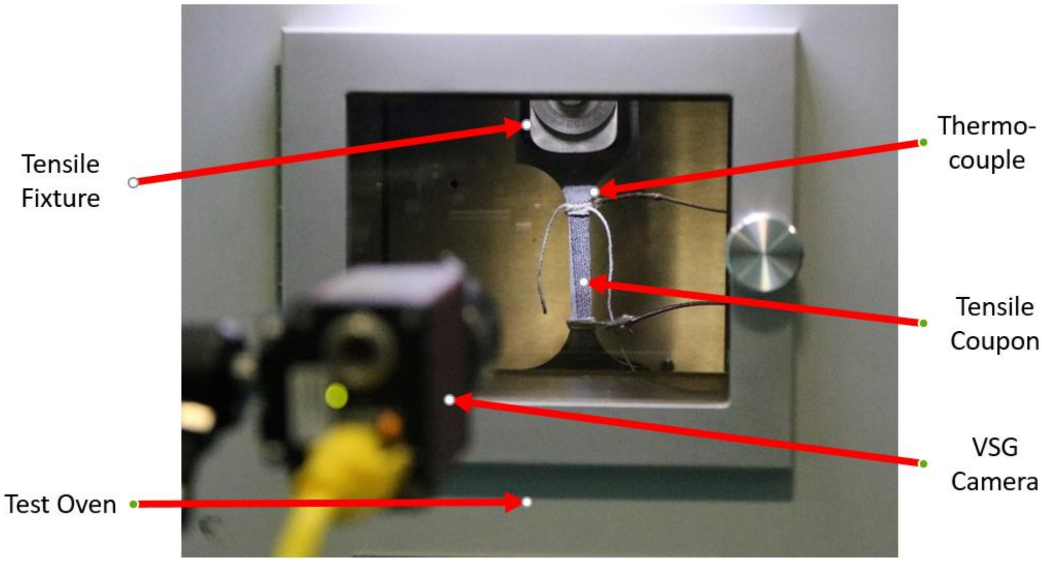

Figure 4-17*: Tensile coupon inside the environmental chamber. Note VSG camera in foreground.*

Figure 4-18 shows a failed tensile coupon following the test. The test setup can be more clearly seen here, including fixtures, thermocouple wires and the proximity of the VSG system to the test oven.

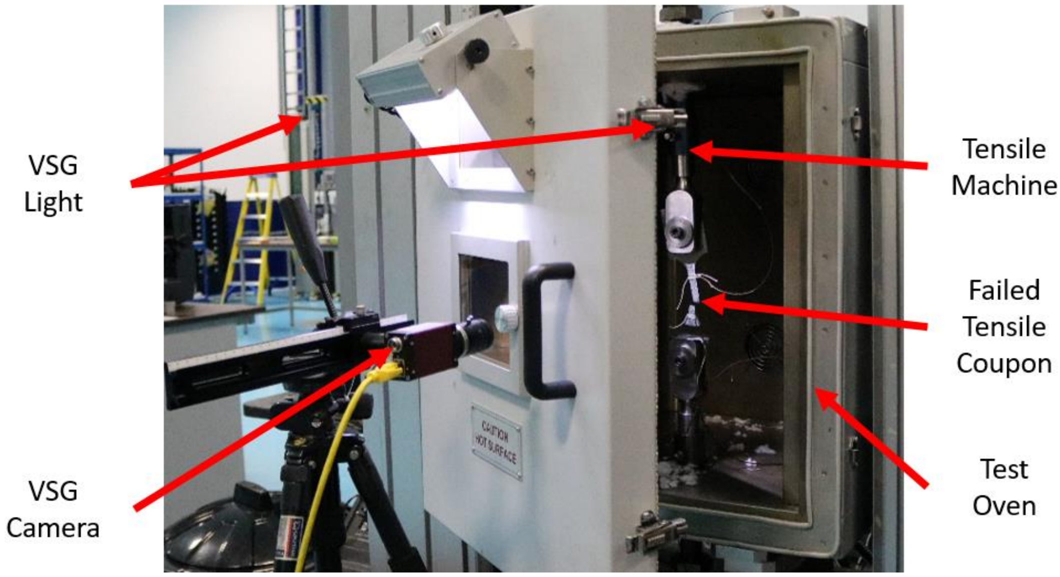

Figure 4-18*: Replacing the coupons in between each test. Note the unchanged camera position between each test.*

4.6.1. *High temperature Tensile Test Results*

Figure 4-19 displays the raw data from the VSG system used to monitor the high temperature tests. The Figure includes stress-strain for a single coupon at each variation of thickness, previously outlines in this chapter. Due to the nature of a VSG system, it is clear that significant post-processing of the data is required to create representative stress-strain curves akin to those of the room temperature tests shown in Figure 4-14.

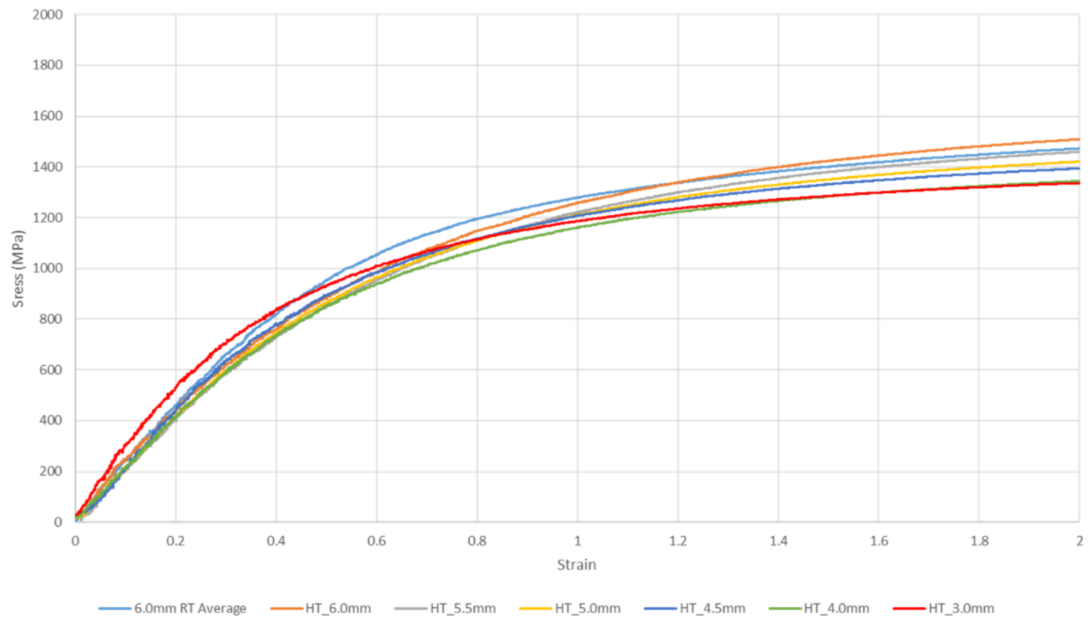

Figure 4-19: *Raw tensile test results (high temperature)*

4.6.2. *Tensile Test Results (Room & High Temperature comparison)*

Following post-processing of the raw data shown in Figure 4-19, Figure 4-20 shows the averaged data set of 6mm tensile coupons at high temperature (orange line) in comparison to that of the room temperature (grey). As the industrial sponsor has stated that strains up to 0.5% are of priority, there is little difference between the results from the extensometer and the VSG. For the remainder of this chapter and Thesis, the room temperature/extensometer data is used.

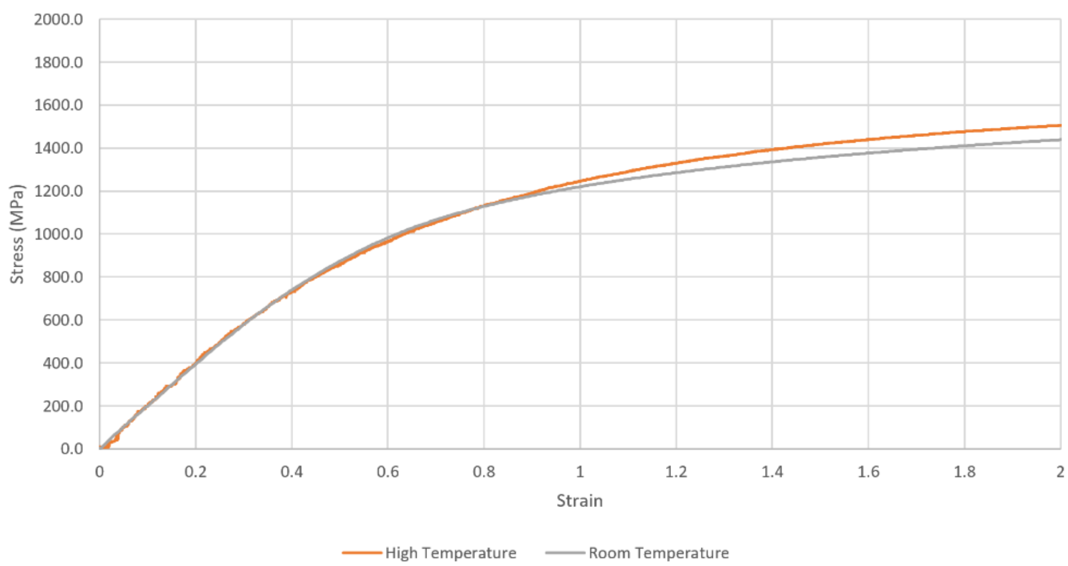

Figure 4-20: *Comparison of tensile data for 6.0mm tensile sample between 20°C and 130°C*

4.7. *Material Subtraction*

The stress-strain curves discussed thus far in this chapter outline the overall material properties of the tensile coupons with a specific case layer removed. This could be considered a composite between hardened and core material. With the view to providing representative material data to the industrial sponsor (and to improve gear analysis in general) a method of calculating the mean material properties within the case is required.

As there are several overall thicknesses of the tensile coupon tested to failure and stress-strain curves to describe the failure behaviour, a comparison between the layers is possible. The clearest means of explanation is an example.

Figure 4-21 demonstrates the comparison between the 3.0mm and 4.0mm tensile samples. As shown in Figure 4-15 earlier in this chapter, there is a difference between their stress-strain curves, therefore the case is adding to the strength/stiffness of the material as a composite of the 1.0mm overall thickness of hardened material and the 3.0mm thick core layer.

In the following example, these assumptions have been made.

1. No change in the CSA of the coupon. As there is no significant necking within the tensile coupon until substantially beyond the yield, this is a common and accepted assumption to make.
2. The strain is consistent between the two tests being compared. As the strain is being measured in real time using an extensometer, this is a fair assumption.

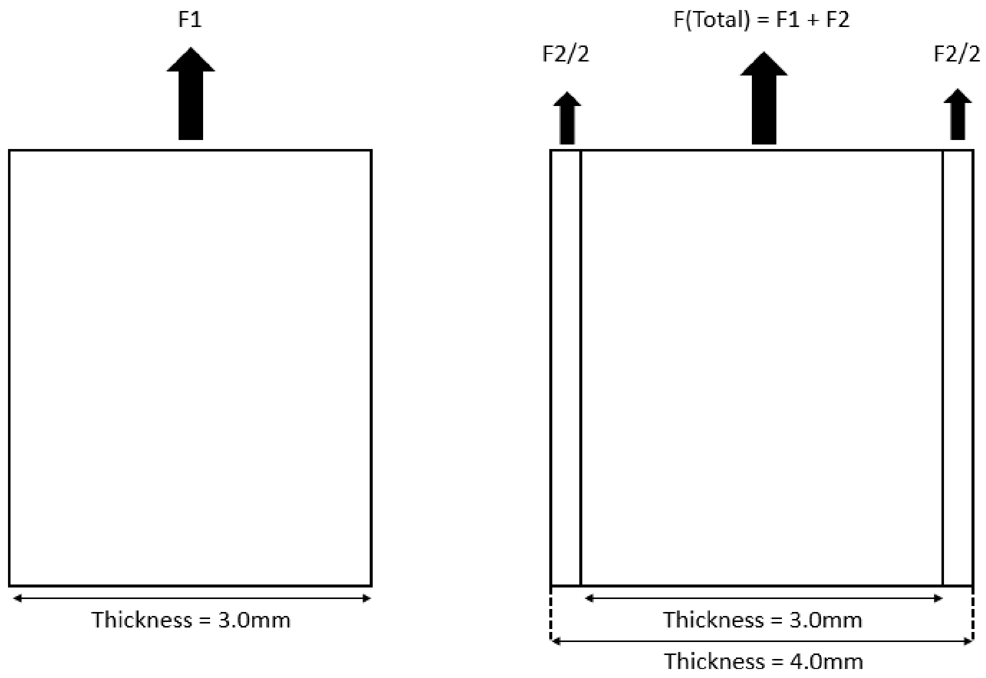

Figure 4-21: *Example of the subtraction method.*

If F_1 is the tensile force going through the 3.0mm wide coupon and F_2 is the tensile force being carried by the additional 1mm of the coupon, the total force (F_{Total}) is,

$$F_{Total} = F_1 + F_2 \tag{30}$$

Knowing that

$$\sigma = \frac{F}{A}$$
$$F = \sigma A \tag{31}$$

As the values for F_{Total} and F_1 are known, Equation (30) can be rearranged as

$$F_{Total} = \sigma_1 A_1 + \sigma_2 A_2 \tag{32}$$

Knowing $\sigma_1 A_1$ from the 3.0mm tensile test and that A_2 is the additional change in surface area between coupons, σ_2 becomes the only unknown variable. Thus Equation (32) can be rearranged as follows. Thus resulting in Equation (33).

$$\sigma_2 = \frac{F_{Total} - (\sigma_1\, A_1)}{A_2} \tag{33}$$

Using this equation, the stress averaged in the additional material can be found. Therefore a depth can be assumed for the material property. When a number of layers are analysed, they can provide a set of stress-strain curves that represent the variation in material properties over the entire case. This represented depth is shown in Table 4-5, noting that the material properties calculated using this method are effectively averaged over the layer thickness. These data represent the smallest increments available to be analysed.

Table 4-5: *Table of tensile layers (0.5mm increments) and their represented depths within the case*

Tensile Coupons to Compare	Represented Depth
3.0mm – 3.5mm	1.375mm
3.5mm – 4.0mm	1.125mm
4.0mm – 4.5mm	0.875mm
4.5mm – 5.0mm	0.625mm
5.0mm – 5.5mm	0.375mm
5.5mm – 6.0mm	0.125mm

Upon the completion of data analysis shown from Equations (30) to (33), each subtracted material layer for the smallest increment possible (0.5mm steps) is shown in Figure 4-22 to Figure 4-27. In these Figures, the thinner coupon is represented by the blue stress-strain curve, the thicker coupon by the orange curve and the subtracted stress-strain curve in grey.

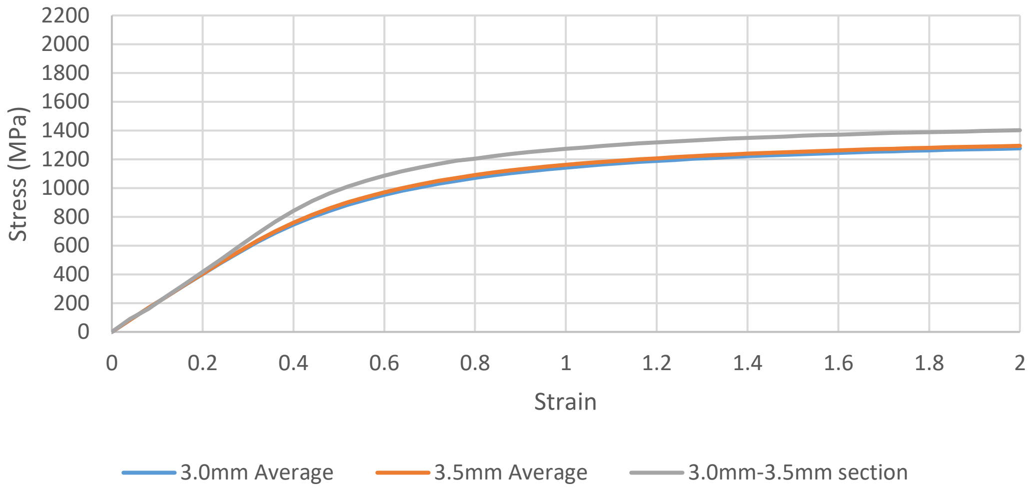

Figure 4-22: *Subtracted stress strain curve from 3.0mm and 3.5mm coupons*

Figure 4-22 and Figure 4-23 represent the subtractions at the largest depth from the surface of the coupon, and the closes to the core material properties. It is visible in both Figures that the grey line that represent the subtracted stress-strain curve are not as smooth as the orange and blue curves. As the averaged coupon data curves are quite similar to each other, any small errors or variation are emphasised in the subtraction calculations.

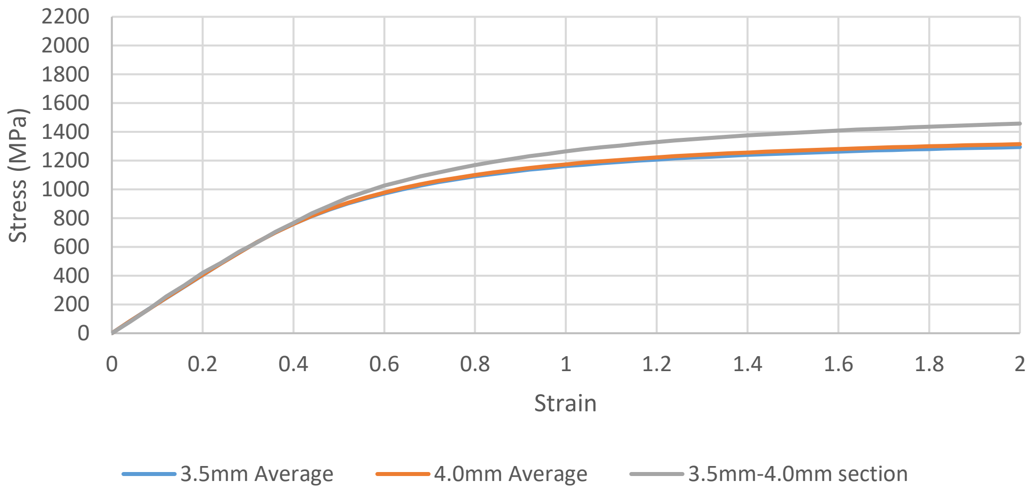

Figure 4-23: *Subtracted stress strain curve from 3.5mm and 4.0mm coupons*

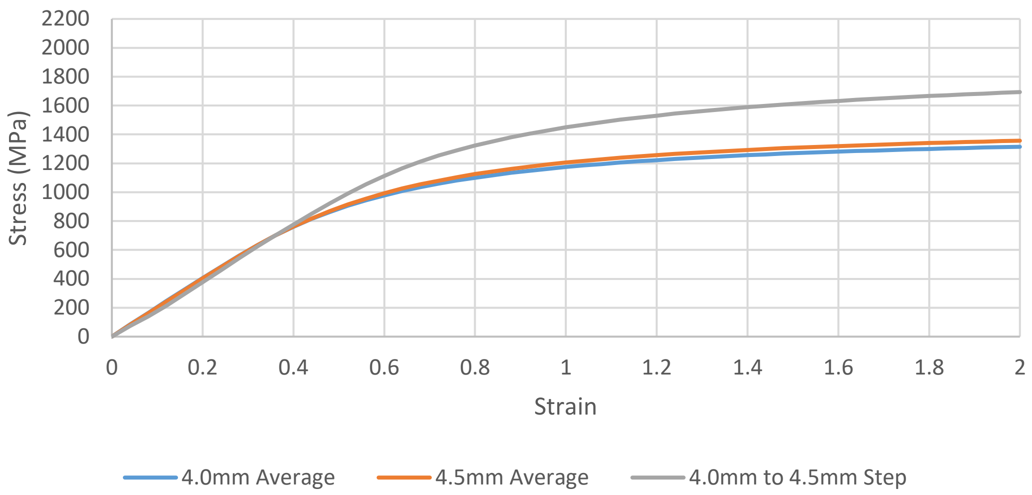

Figure 4-24: *Subtracted stress strain curve from 4.0mm and 4.5mm coupons*

Similar to the subtracted curves on the previous page, the grey line on Figure 4-25 has areas of apparent error around strains of 0.2-0.3 and 0.6. These errors are caused by small variations in the 'donor' curves and are emphasised by the subtraction calculation.

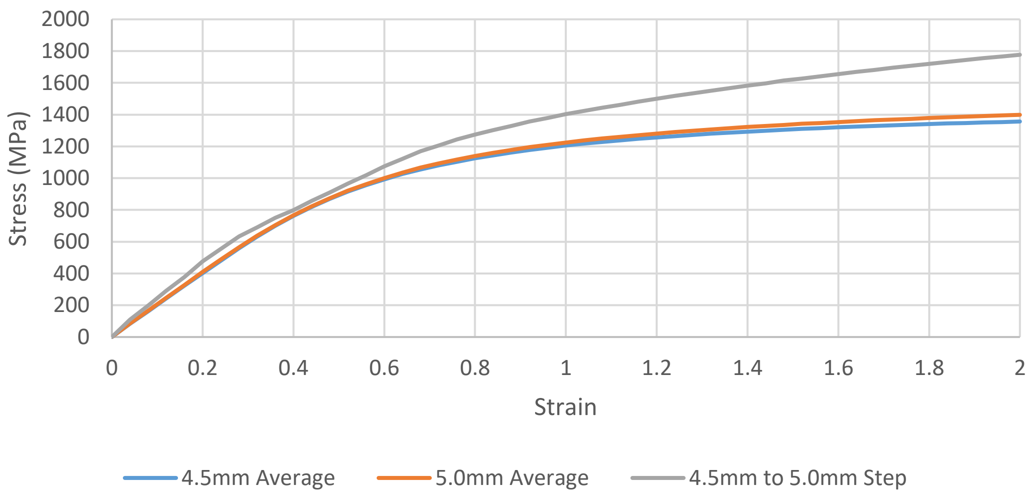

Figure 4-25: *Subtracted stress strain curve from 4.5mm and 5.0mm coupons*

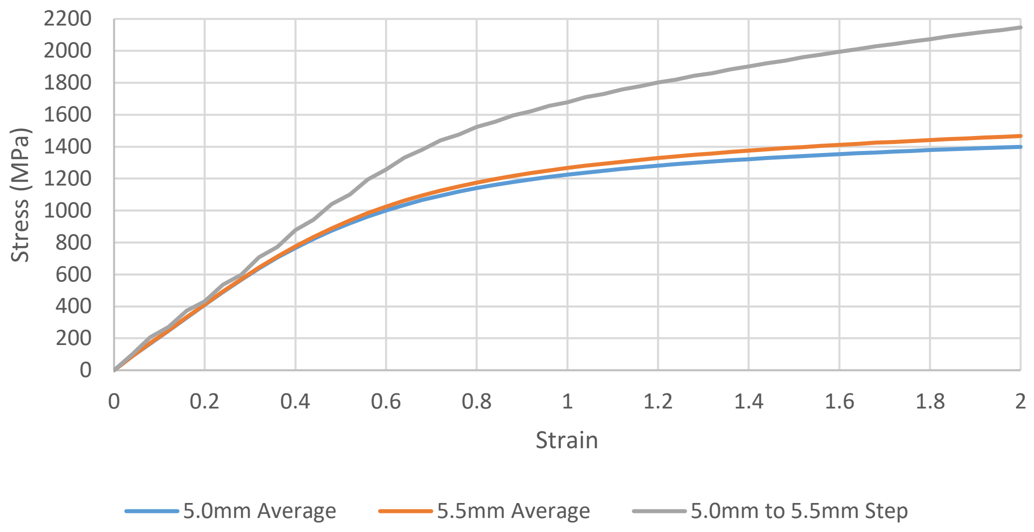

Figure 4-26: *Subtracted stress strain curve from 5.0mm and 5.5mm coupons*

Figure 4-26 and Figure 4-27 include the most obvious sensitivity between variations in the 'donor' curves.

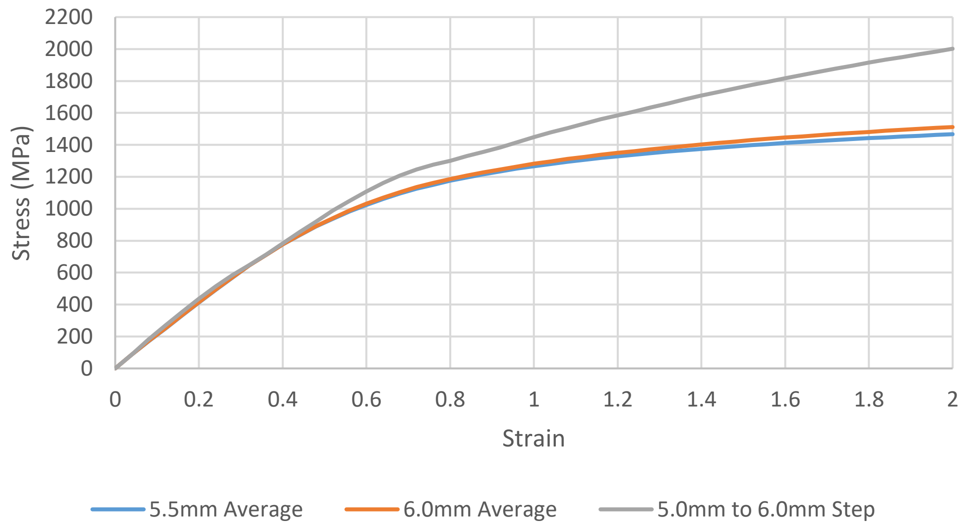

Figure 4-27: *Subtracted stress strain curve from 5.5mm and 6.0mm coupons*

Figure 4-28 shows all of the subtracted material data for each material layer. Note that the material stress strain curves for the harder layers appears as though the material is clipped to 2% strain. The material subtraction is sensitive to the gradient of the curve in the plastic zone, even as the stress-strain curves appear to become asymptotic. Additionally, the small measurement errors and the averaging of multiple data sets has caused the slopes to vary for the range of curves shown. Comparison between very similar data causes the results to become dominated by experimental error.

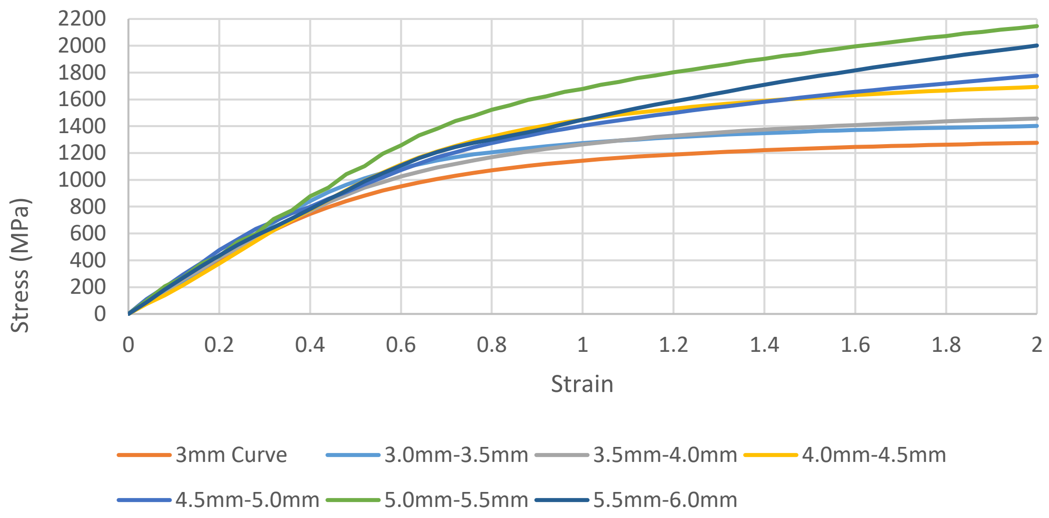

Figure 4-28: *Subtracted material data for all layers (0.5mm subtraction increments).*

To minimise some of the errors in the above measurement, the analysis was repeated however over larger steps of tensile coupon thickness. As opposed to completing the analysis over 0.5mm increments of heat treatment, a 1mm step was used as an alternative. The larger spacing between curves results in less sensitivity within the subtracted stress-strain curves to experimental error. Table 4-6 outlines the tensile layers that are used for the subtraction.

Table 4-6: *Table of tensile layers (1mm increments) and their represented depths within the case*

Tensile Coupons to Compare	Represented Depth
3.0mm – 4.0mm	1.25mm
4.0mm – 5.0mm	0.75mm
5.0mm – 6.0mm	0.25mm
3.5mm – 4.5mm	1.00mm
4.5mm – 5.5mm	0.50mm

Figure 4-29 through to Figure 4-33 show the subtracted curves for tensile coupon increments of 1.0mm thickness.

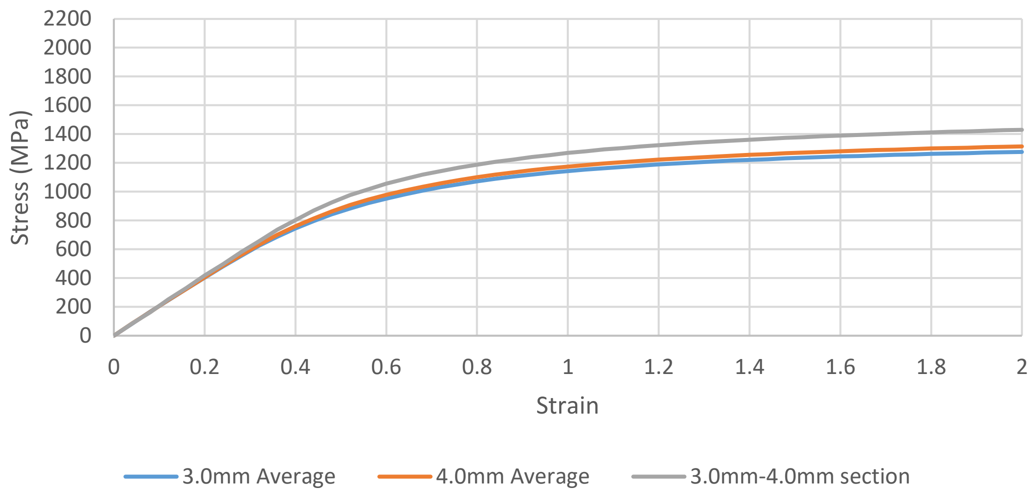

Figure 4-29: *Subtracted stress strain curve from 3.0mm and 4.0mm coupons*

From comparison to the previous analysis in Figure 4-28, the subtracted curves shown in Figure 4-29 and Figure 4-30 are considerably smoother due to the larger variation between the donor curves.

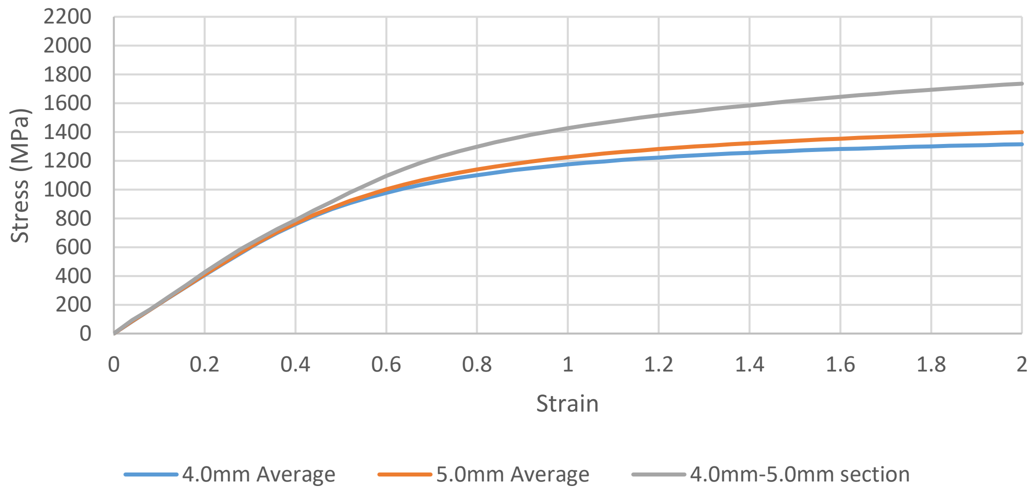

Figure 4-30: *Subtracted stress strain curve from 4.0mm and 5.0mm coupons*

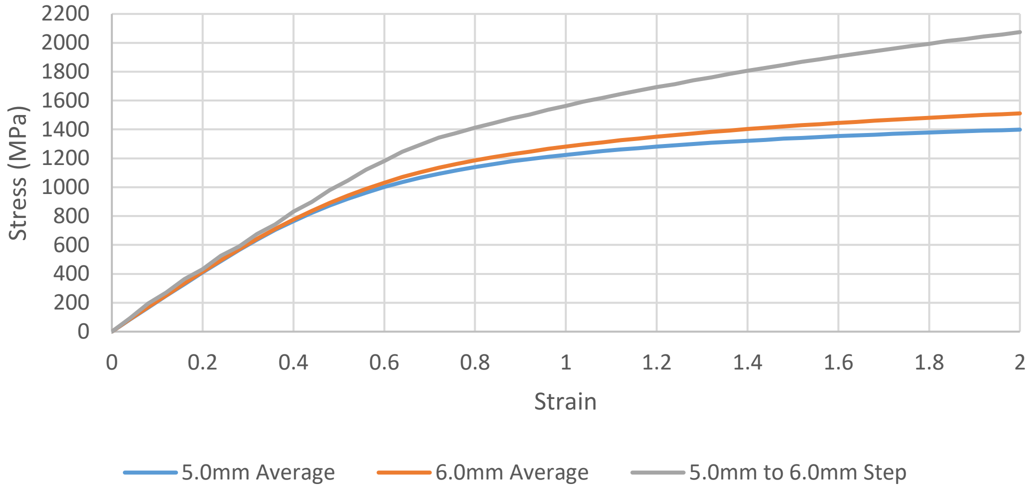

Figure 4-31: *Subtracted stress strain curve from 5.0mm and 6.0mm coupons*

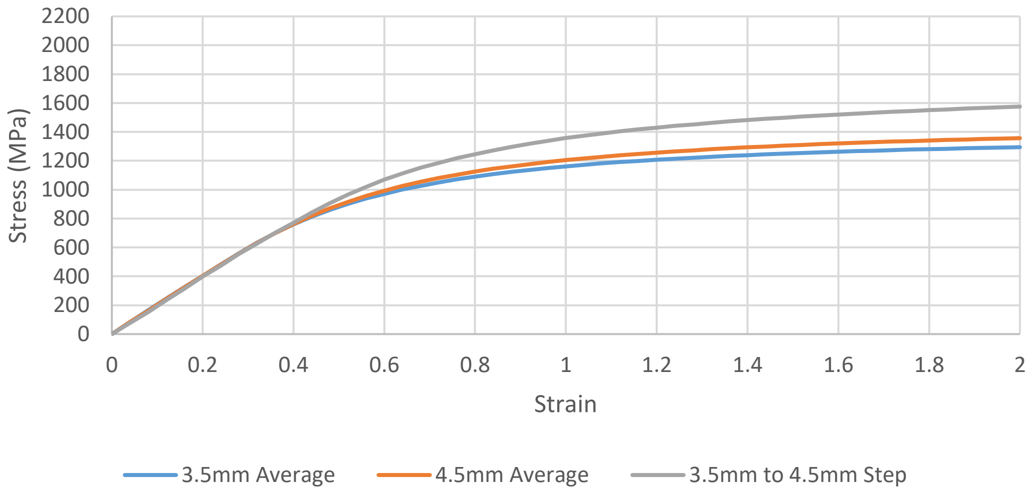

Figure 4-32: *Subtracted stress strain curve from 3.5mm and 4.5mm coupons*

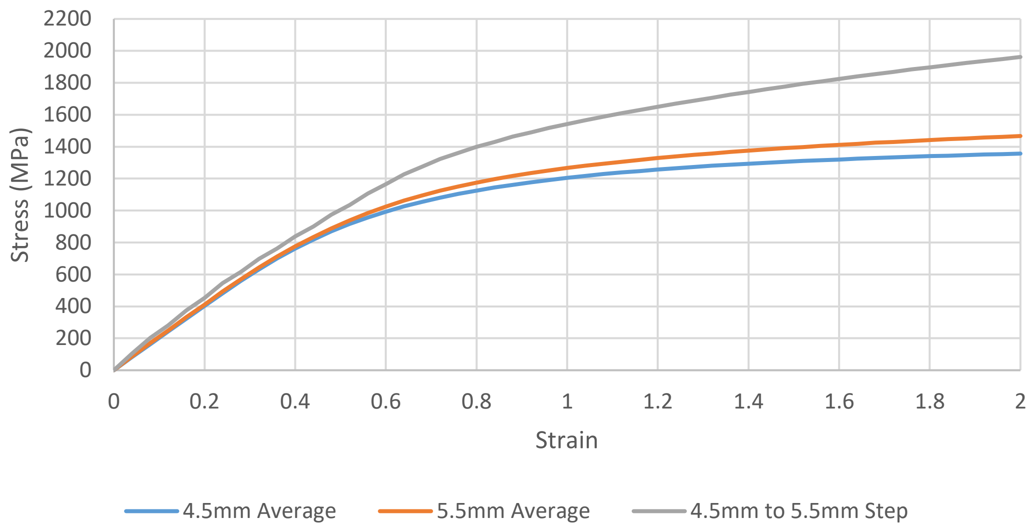

***Figure 4-33:** Subtracted stress strain curve from 4.5mm and 5.5mm coupons*

Figure 4-31, Figure ***4-32*** and Figure ***4-33*** all show that the subtracted curve is smoother than previous methods in this chapter.

Figure 4-34 shows a summary subtracted material data for 1mm increments.

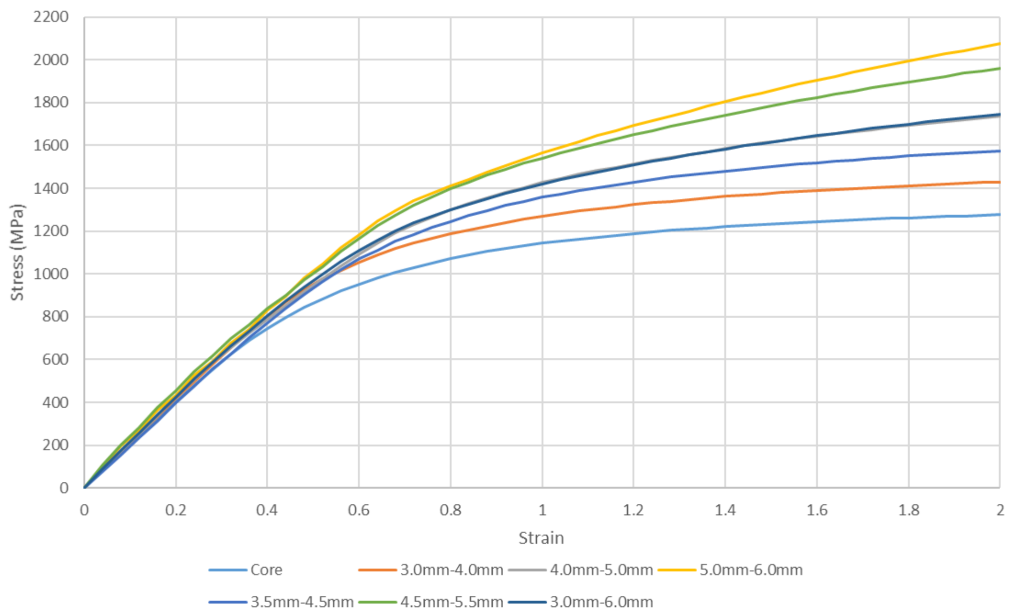

Figure 4-34: *Subtracted material data for all layers (1.0mm subtraction increments).*

As each of the stress-strain curves represent the material properties at a single depth, it is effectively averaged over the span of two data sets. By comparing the 4.0mm-5.0mm and 3.0mm-6.0mm data, the material stress strain curve generated represents effectively the same depth within the case. Figure 4-35 clarifies the location of the subtracted stress-strain curves, and demonstrates how the location is the same for each of the solutions described.

Both stress-strain curves are shown in Figure 4-36, and are in very good agreement with each other.

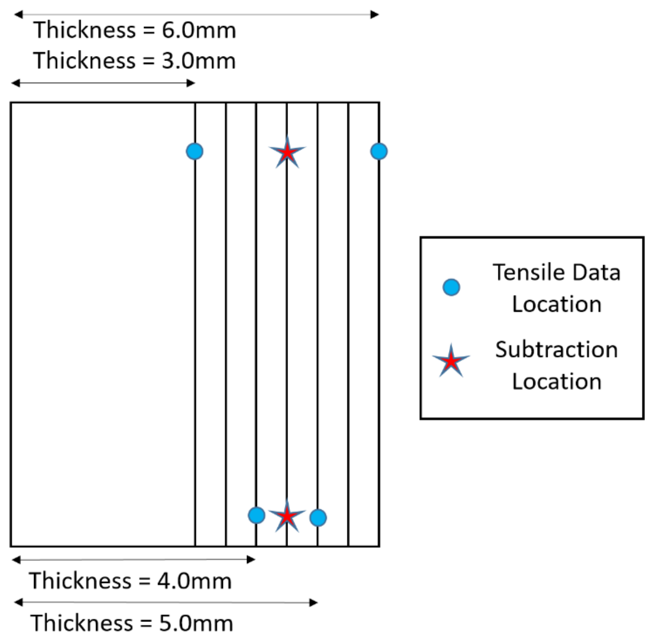

Figure 4-35: *Location of the subtracted material properties*

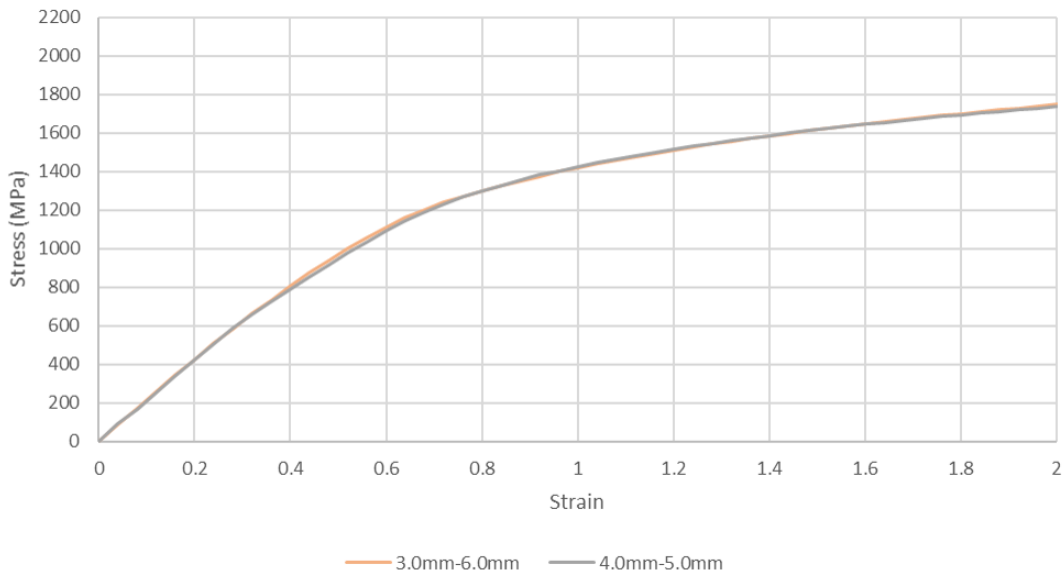

Figure 4-36: *Subtracted material data for a single depth from two separate subtractions*

Now that representative physical material data exists for positions within the heat treatment, the systematic variation of these properties with depth must be established, to allow the prediction of the stress-strain curves for any depth within the heat treatment. For such a relationship to be appropriate, a material model with multiple parameters to generate the complex geometries of a stress-strain curve and accurately model the post yield characteristics is required.

4.8. *Material Model Correlation (Ramberg Osgood)*

In order that a stress strain curve for any depth of material can be generated, some kind of model must be fitted to the stress-strain curves for each of the material layers. Using the subtracted data from the previous section of this chapter, the Ramberg Osgood approximation from Section 4.4 can be fitted to the stress-strain curves, and compared to determine how the model varies with depth. Using the *Solver* tool of *Microsoft Excel*, the variables of the Ramberg Osgood relationship can be fixed between user defined limits and optimised such that the error between theoretical and physical data can be minimised. *Solver* is an optimisation tool within *Microsoft Excel* used to specify specific limits to user defined variables in order to converge on desired values as an output. Figure 4-37 shows the Ramberg Osgood solution post optimisation from the *solver* tool against the experimental data for the core material property. It is clear that there is good correlation between the two.

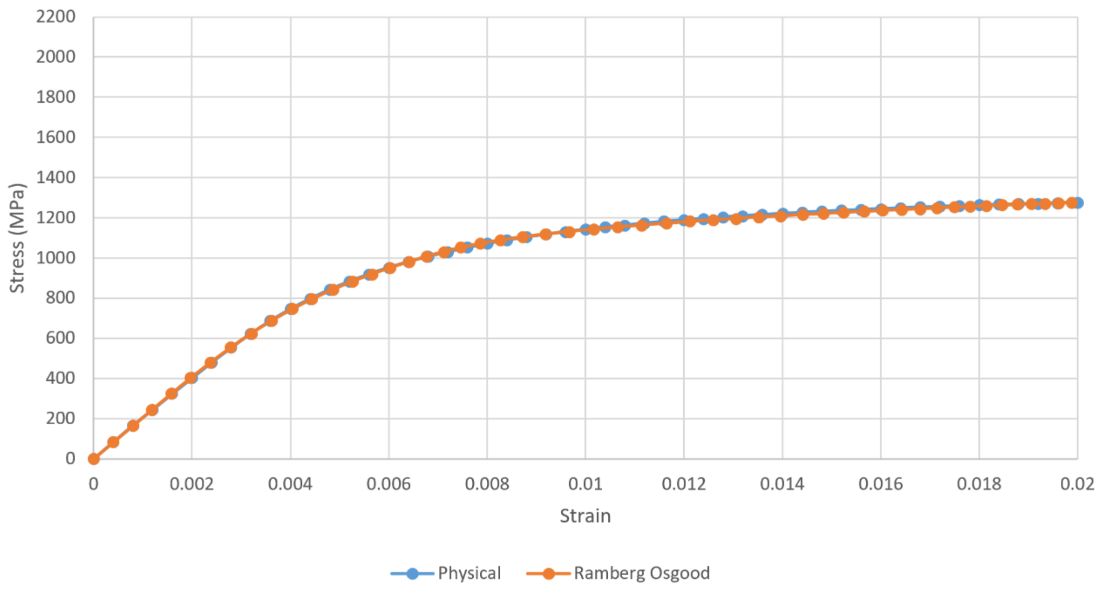

Figure 4-37: *Stress-strain curve for core material stress-strain curve and Ramberg Osgood relationship.*

Following the optimisation of the parameters in the theoretical material model for the core material, the remaining curves were analysed also. It was found that the solver solution was always compromised due to the curve of the plastic region and in replicating the linear section prior to yield as shown in Figure 4-38.

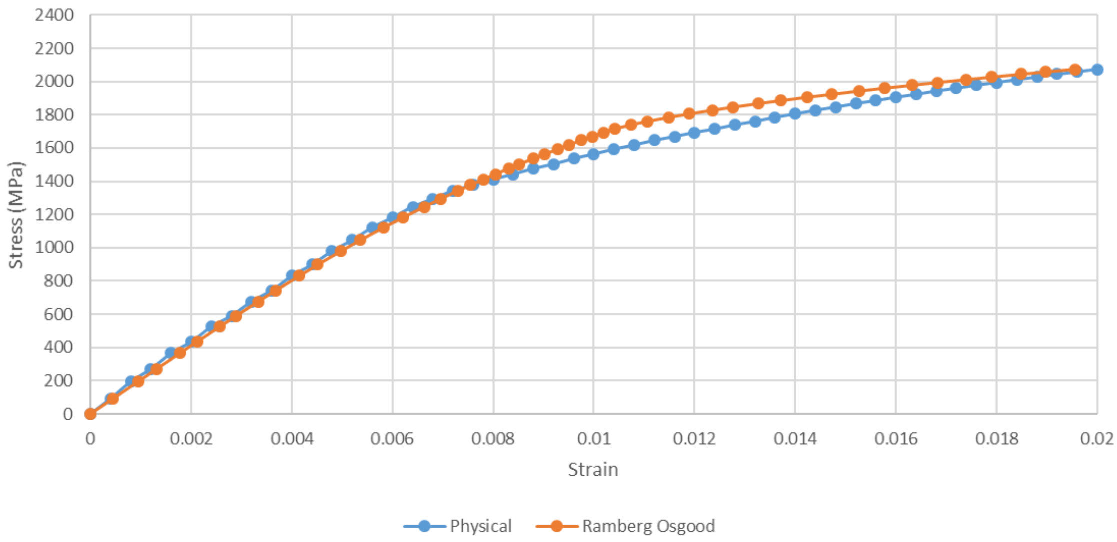

Figure 4-38: *Graph of Stress vs Strain for a simulated depth of 0.25mm into case*

The reader will notice that the strain calculated by the Ramberg Osgood equation does not match that of the physical data, i.e. at the same increments. This is because strain is the subject of the formula shown in Equation (21). As the strain is calculated from a specific stress value, the strain values between physical data points are not the same. As the material data for FE requires separation of the elastic and plastic sections (if the user desires to simulate plastic behaviour), and the strain must be in terms of plastic strain only, an alternative means of calculation is more desirable.

4.9. *Material Model Correlation (Johnson Cook)*

In order to generate a relationship for elastic and plastic material properties in a depth dependant fashion, the Johnson Cook Equation was used.

$$\sigma = A + B(\epsilon)^n \tag{34}$$

Where A, B and n are variables to be defined by the Microsoft Excel solver. Stress is calculated for a specific value of plastic strain through using parameter “A” which denotes the yield stress, “B” denotes the difference between the yield stress and the UTS and “n” is an exponent that controls the fit of the curve where 1 is a straight line between A and B. Further analysing the Johnson Cook material model described in Equation (34), at zero plastic strain, i.e. the yield point, the stress is equal to the yield stress. Thus, the equation does not combine the elastic and plastic behaviour in a single equation. As the elastic and plastic behaviour within FE is specified separately, this is an appropriate method of generating the data. The elastic properties were calculated from the experimental data and are included in Table 4-7 below.

Table 4-7: *Table of the elastic properties for a given depth into the case.*

Depth (mm)	Elastic Modulus (GPa)	Yield Stress (MPa)
0.25	200	1120
0.50	196	1020
0.75	193	963
1.00	190	910
1.25	187	860
1.50	185	775

The Poisson ratio is also required and assumed as being 0.3 as stated in the material data sheet. Therefore, a relationship for the Elastic Modulus/Yield Stress and depth can be made. This can be seen in Figure 4-39 and Figure 4-40.

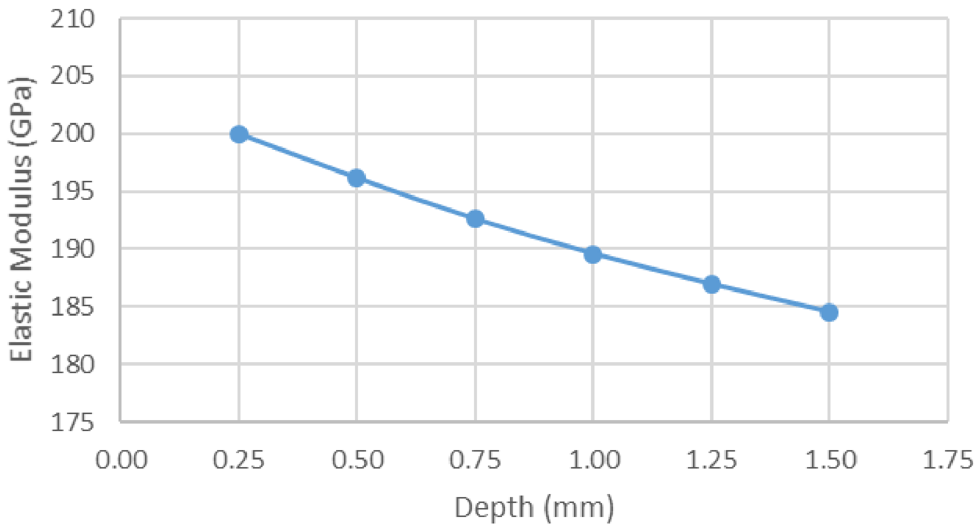

Figure 4-39: Graph of Elastic Modulus vs Depth

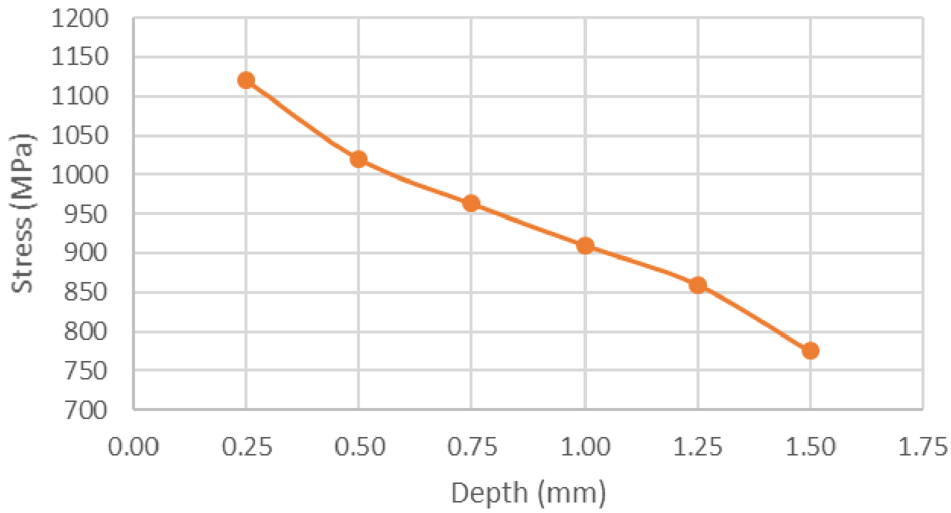

Figure 4-40: Graph of Yield Stress vs Depth

The plastic section of the stress strain curve can now be generated as the Johnson Cook parameter "A" is the yield stress. Figure 4-41 shows an example of a *Microsoft Excel* Spreadsheet used to calculate the "B" and "n" Johnson Cook parameters in matching to a set of experimental data. The blue section on the left hand side has stress and strain values from experimental data. The orange section includes the stress calculated using Equation (34) using the same values of plastic strain. In yellow, the values for the difference between experimental and calculated stress are compared using the *"ABS"* function, and then the total summed and squared using the *"SUMSQ"* function. On the right hand side of Figure 4-41, the Solver window is open. The aforementioned *"SUMSQ"* value is used as the objective for the solver and set to be minimised by changing the values of "B" and "n". The value for A is equal to the yield stress and is the value of stress at plastic strain = 0.

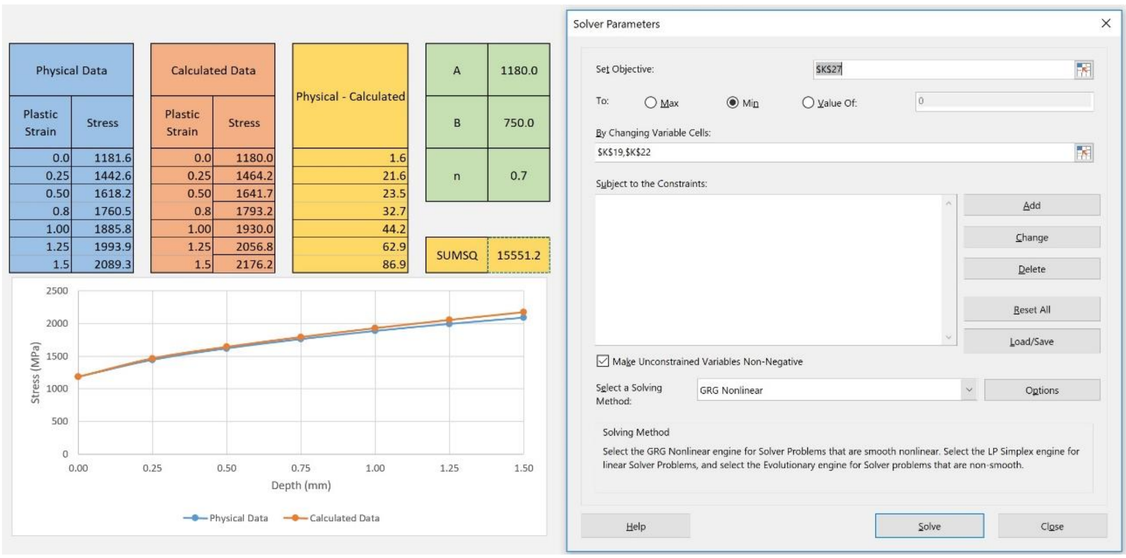

***Figure 4-41:** Johnson Cook calculation spreadsheet including Solver tool.*

When using a tool such as this, the plastic strain spacing must be altered to an appropriate value. If the spacing is too small, it is not possible for the solver to converge on a solution which is representative of the actual stress vs plastic strain behaviour of the material.

Figure 4-42 below shows a curve matched to that of the original data to prove the accuracy of the method.

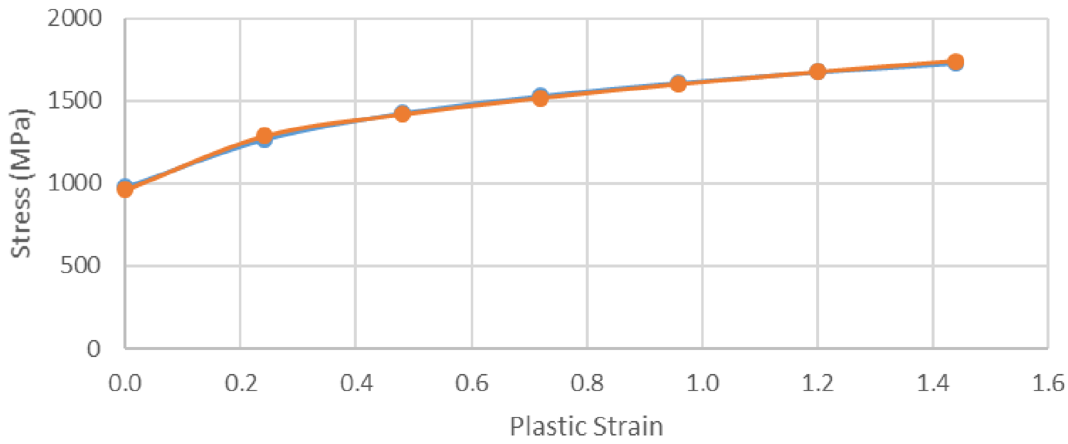

Figure 4-42: *Graph of Stress vs Plastic Strain for 0.75mm depth.*

The same process was repeated for each data set that represents a depth through the case.

Table 4-8 below includes the values for depth, elastic modulus and A, B and n parameters to create plastic stress-strain curves for a specific depth.

Table 4-8: *Table of Elastic Modulus and Johnson Cook parameters for a specific depth*

Depth (mm)	Elastic Modulus (GPa)	A (MPa)	B (MPa)	n
0.25	200	1120.0	780.2	0.60988
0.50	196	1020.0	740.0	0.54783
0.75	193	963.0	651.1	0.48840
1.00	190	910.0	576.0	0.44385
1.25	187	860.0	498.4	0.40151
1.50	185	775.0	442.4	0.38790

Figure 4-43 and Figure 4-44 below show the values of A and B, and n plotted against a specific depth, respectively. Each graph covers a depth range from 0 to 1.5mm, i.e. the surface through to the case penetration depth.

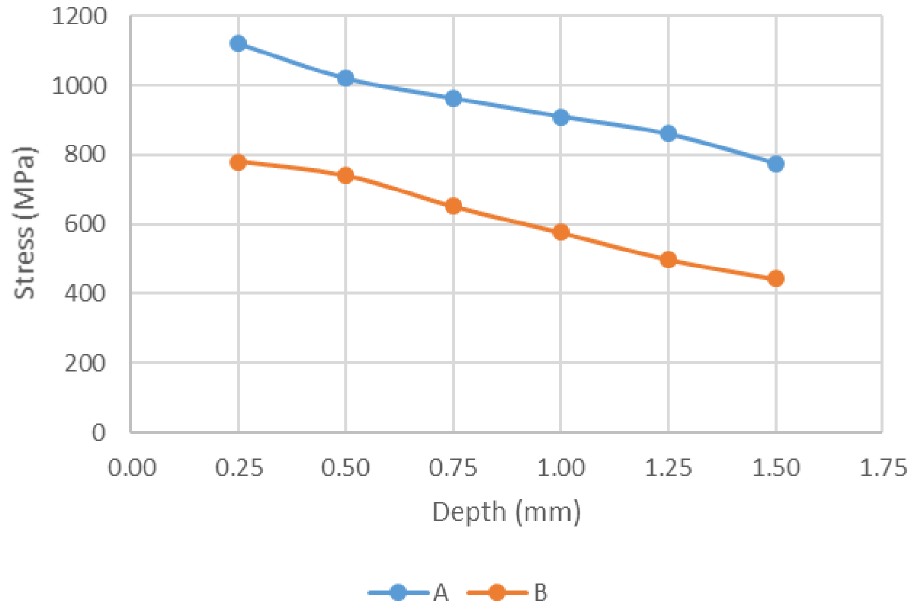

***Figure 4-43:** Graph of "A" and "B" parameter vs Depth*

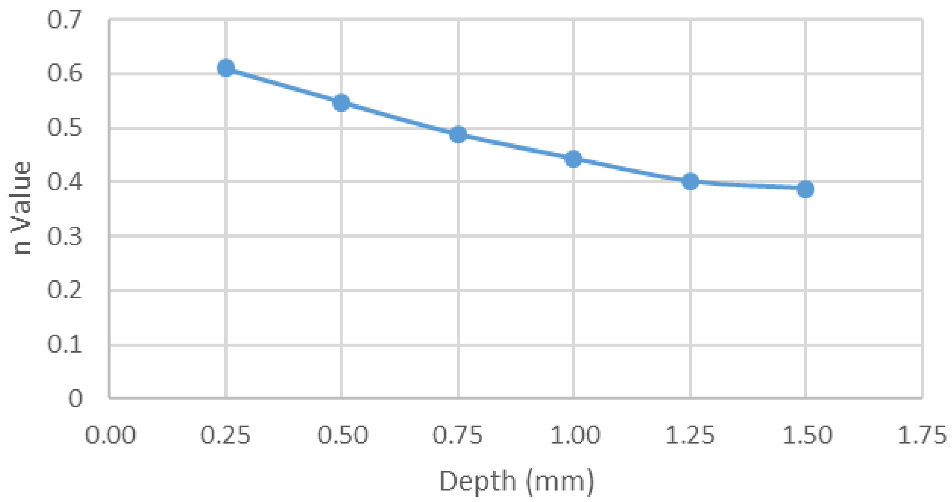

***Figure 4-44:** Graph of "n" vs Depth*

Using all data described thus far, the stress-plastic strain curves for each layer can be generated. This is shown in Figure 4-45.

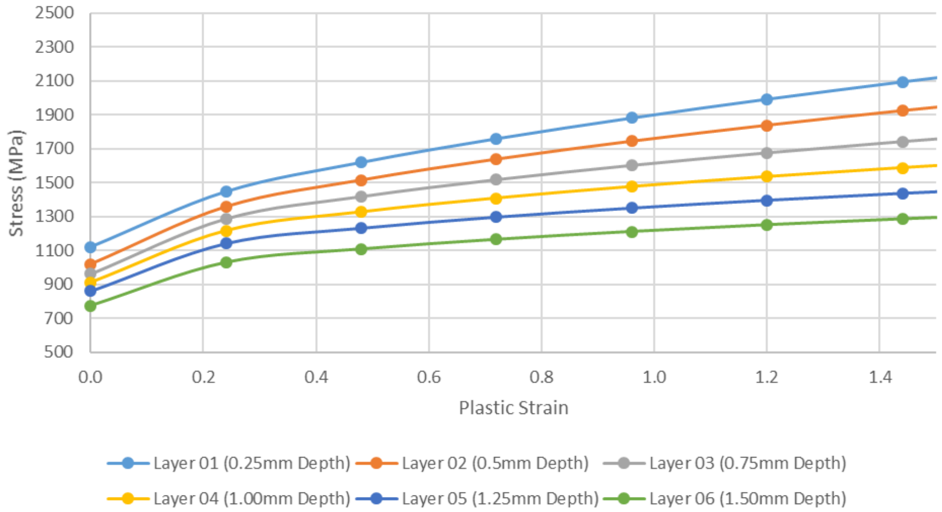

Figure 4-45: *Graph of the plastic properties*

Using the data contained in Table 4-7 and Table 4-8, Figure 4-46 Figure 4-47 and Figure 4-48 has plotted a polynomial equation the curves of A, B and n. Therefore each parameter now has a relationship for through the depth of a case layer.

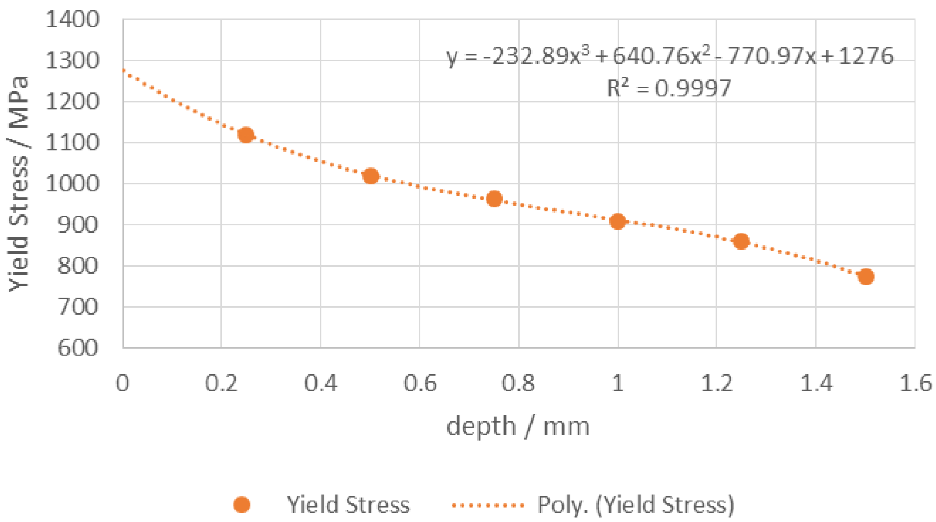

Figure 4-46: *Polynomial fit through the yield stress vs depth curve*

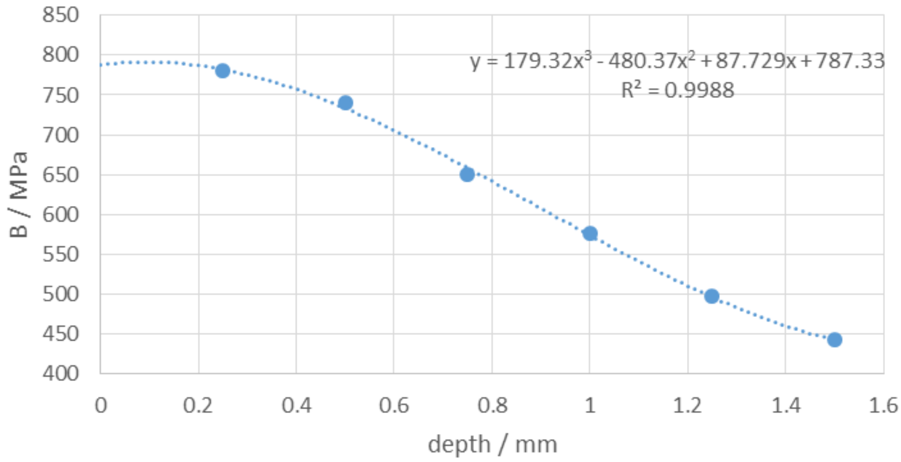

Figure 4-47: *Polynomial fit of B value vs depth*

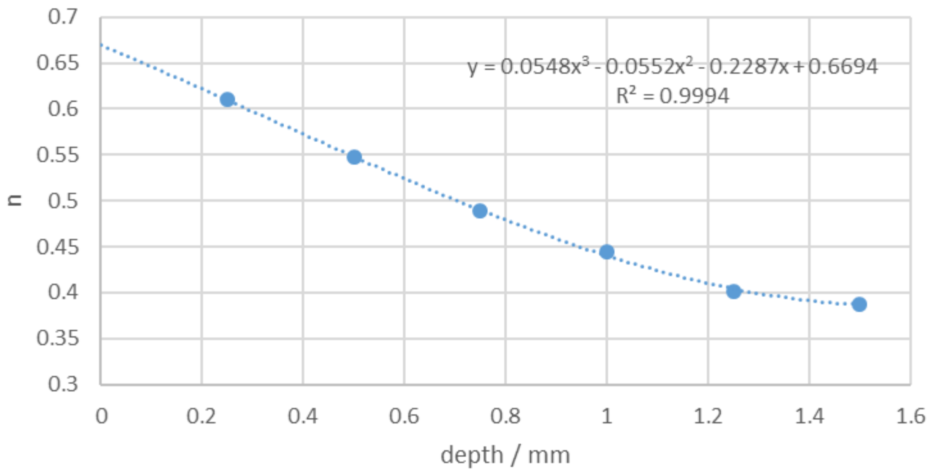

Figure 4-48: *Polynomial fit of n value vs depth*

The relationships for each of the A, B and n for a given depth from the surface (d) are described in Equations (35) (36) and (37).

$$A = -232.89d^3 + 640.76d^2 - 770.97d + 1276 \tag{35}$$

$$B = 179.32d^3 - 480.37d^2 + 87.729d + 787.33 \tag{36}$$

$$n = 0.0548d^3 - 0.0552d^2 - 0.2287d + 0.6694 \tag{37}$$

Therefore the material model may therefore be rewritten as in Equation (38). It must be noted that these equations are only valid for depths of up to 1.5mm.

$$\sigma = (-232.89d^3 + 640.76d^2 - 770.97d + 1276) + (179.32d^3 - 480.37d^2 + 87.729d + 787.33)(\epsilon)^{0.0548d^3 - 0.0552d^2 - 0.2287d + 0.6694} \tag{38}$$

Which gives the stress-plastic strain curve as a function of case depth (d).

4.10 Material Data Discussion

To improve on the quality of data produced for the use within FE analysis, further testing would be beneficial. By increasing the number of coupons tested, an increased confidence in the data can be achieved, and potentially would allow an understanding of the variability in properties to be gained. Providing further testing were possible, tests conducted at varying strain rates would be beneficial, again to increase confidence in the data to create material properties from the methods described in this chapter. In general, steel does not have great strain rate dependency, thus a higher strain rate would be of benefit by reducing the time taken to complete the testing of a batch of coupons. Depending on the coupon (between 3 and 6mm in thickness), the duration of each test ranged from 10-20 minutes. By increasing the strain rate, the time to complete testing could be reduced significantly. Were a batch of additional tests possible, an investigation into alternative heat treatments (not necessarily for gears) could be performed in parallel, for instance plasma nitriding, induction hardening or even an alternative specification of case carburisation could be investigated.

During tensile testing it was a requirement that the extensometer be removed prior to failure to prevent damage. Were it possible to leave the extensometer in place, further confidence in the data at high values of strain could be achieved. In addition to this, were an extensometer able to remain attached to the tensile coupon at an increased strain rate until failure whilst at the working temperature of a motorsport transmission, then the most representative data could be collected. In parallel to such a test, the inclusion of a VSG system to monitor strain over the parallel length would provide data for comparison in future investigations.

As an alternative to monitoring a tensile test with a VSG system, it has become common place for manufacturers of tensile test machines to collaborate with manufactures of non-contact measurement systems and incorporate the cameras into the crosshead. The added benefit to such a system is that the camera will move with the crosshead, thus the FOV remains in focus on the area of interest throughout the test. With a conventional system, materials failing at high strain rates can fail after the area of the interest has exited the FOV.

Within this chapter, all material data analysis was completed in *Microsoft Excel* using a standardised template for the input of raw data. Using *VLookup* functions, much of the analysis was automated. Were additional testing possible, a custom *MATLAB* script for the data analysis would be more beneficial as the time spent doing the analysis would be significantly reduced.

4.11 Material Data Conclusion

In summary, a method for determining the depth dependent mechanical properties of a material has been outlined. This includes a number of parameters plotted on graphs where one axis is depth, thus the end user can interpolate values for any depth through a case layer using a simple curve-fit to these specific results. These material parameters now require a way in which they can be applied to relevant elements within FE analysis, and this is the subject of the following chapter.

5. Functionally Graded Material (FGM)

5.1. Introduction

As described in Chapter 2, there are limited analyses reported in the literature of heat-treated components, which include varying material properties over the case-carburised layer. Traditionally, if FE models are required to include varying material properties, partitions are included in the model and separate material properties applied manually during the model's construction.

For complex shapes that undergo heat treatment, such as the involute geometry of gear teeth, or bearing components, it can be very time consuming to manually partition models in order to apply varying material properties to different layers. The most common and simple method is to apply a 'full hard' property to the surface of the material for the full thickness of the case and a core material for the remainder. As a solution, this is far from ideal since the model does not accurately represent the real variation in material properties produced by the heat treatment. Furthermore, making a significant step change in material properties is likely to lead to calculated results that are inaccurate due to the differences introduced in adjacent elements as opposed to the gradual and systematic change that will be the real variation in material properties for the hardened material.

The desired solution for both industrial and research analyses is therefore a method whereby the material properties are gradually varied from full hardness to the core material, as a function of depth from the heat-treated surface. This will model the material based on user-controllable parameters, as an FGM. Since within an FEA analysis material properties are allocated to each element, within the model the smallest possible change in material property is limited by the element size. Thus the model can never truly represent the continuous gradient in material properties from a heat treatment as it can only have a piecewise variation from element to element. If the elements are sufficiently small, the model can resolve the changes in properties in sufficiently fine steps so as to represent the material well; however, complexity in sectioning the FE model, application of material properties and computational efficiency become factors thereafter. The computational efficiency is especially compromised as the elements become smaller and therefore the number of elements increases (for a given volume).

5.2. Methods

This section discusses some methods of varying material properties within FE simulation.

5.2.1. Manually

As the name suggests, this method requires the user to section (partition) the FE models into the desired number of sections and apply varying material properties manually to each section. This becomes increasingly difficult and time consuming when complex geometry and multiple layers are required. Due to this, a more elegant, automated or semi-automated solution is often desirable especially when multiple models or iterations are required.

5.2.2. UMAT (User Defined Material Model)

In order to maintain compatibility with the FE solver used by the industrial sponsor, the FEA modelling in this Thesis has been conducted using *ABAQUS CAE*. Within this software, several user-definable sub routines are included which allow complex control of loading, motion and even material properties. A user-defined material subroutine (UMAT) is available and allows the user to vary the properties of a model throughout its analysis.

Writing a UMAT requires a substantial knowledge of *ABAQUS* and the FE solution process. In the interest of developing a method for the industrial sponsor where only the *ABAQUS* solver is used (See Chapter 1 for further detail of the Sponsors' analysis techniques), the UMAT was discounted as an option.

5.3. MATLAB Algorithm – Input File Manipulation

An Input File is a text based file created by an FE solver that contains all data required for constructing and running an FE model. Data for the geometry, loading conditions, boundary conditions and most importantly for this section, material properties, are included. To allow automation of the FGM process, a means of manipulating the FE input file was the most promising option to pursue. The input file format for *ABAQUS* is constructed in a comma separated value (CSV) format such that all the data for elements and node positions (Figure 5-1) are positioned in a form that can be easily accessed, extracted and manipulated.

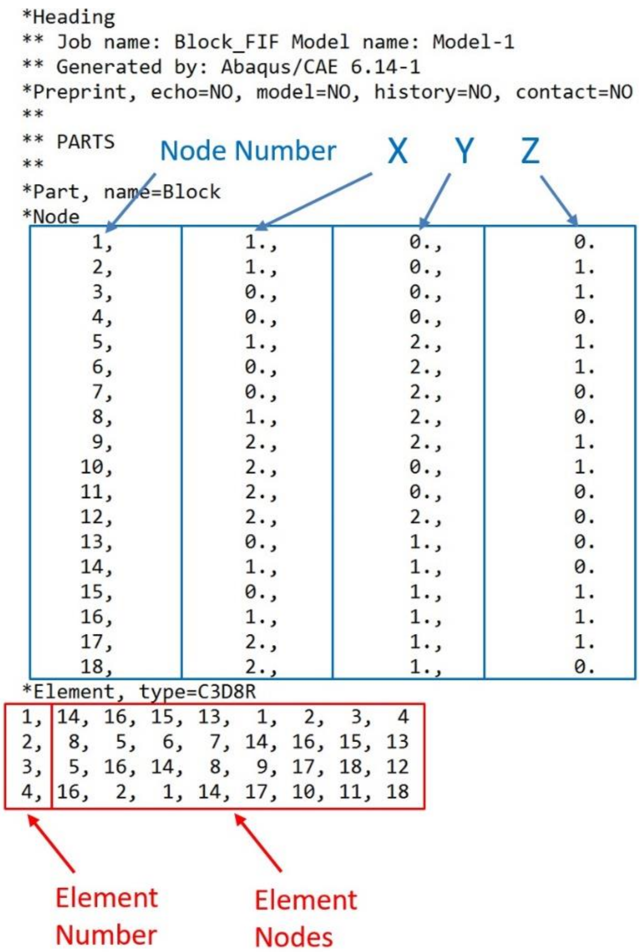

```
*Heading
** Job name: Block_FIF Model name: Model-1
** Generated by: Abaqus/CAE 6.14-1
*Preprint, echo=NO, model=NO, history=NO, contact=NO
**
** PARTS
**
*Part, name=Block
*Node
      1,           1.,           0.,           0.
      2,           1.,           0.,           1.
      3,           0.,           0.,           1.
      4,           0.,           0.,           0.
      5,           1.,           2.,           1.
      6,           0.,           2.,           1.
      7,           0.,           2.,           0.
      8,           1.,           2.,           0.
      9,           2.,           2.,           1.
     10,           2.,           0.,           1.
     11,           2.,           0.,           0.
     12,           2.,           2.,           0.
     13,           0.,           1.,           0.
     14,           1.,           1.,           0.
     15,           0.,           1.,           1.
     16,           1.,           1.,           1.
     17,           2.,           1.,           1.
     18,           2.,           1.,           0.
*Element, type=C3D8R
1, 14, 16, 15, 13,  1,  2,  3,  4
2,  8,  5,  6,  7, 14, 16, 15, 13
3,  5, 16, 14,  8,  9, 17, 18, 12
4, 16,  2,  1, 14, 17, 10, 11, 18
```


Figure 5-1: *Example of an ABAQUS input file*

The approach adopted was to create the necessary FEA model using the graphical tools that are part of the *ABAQUS* software. In the normal course of running an analysis, the Graphical User Interface (GUI) produces a text file for the *ABAQUS* numerical solver. This file was the target for manipulation. To extract and manipulate the data within the input file, a *MATLAB* script was developed as part of this research. The steps required to manipulate the FE input file within this *MATLAB* program are described in the next section of this Chapter. Each step is explained thoroughly, in turn. The *MATLAB* script can be found in the Appendix of this Thesis. To aid in explaining the process of manipulating the input file, examples of a 27 element (3x3x3) cube and simplified tensile coupons are used. Using these simple models was advantageous as it allowed hand calculation of the outcomes of each scenario to validate the method, and aid in the debugging and verification of the code. Figure 5-2 shows the 3x3x3 cube within the *ABAQUS* GUI.

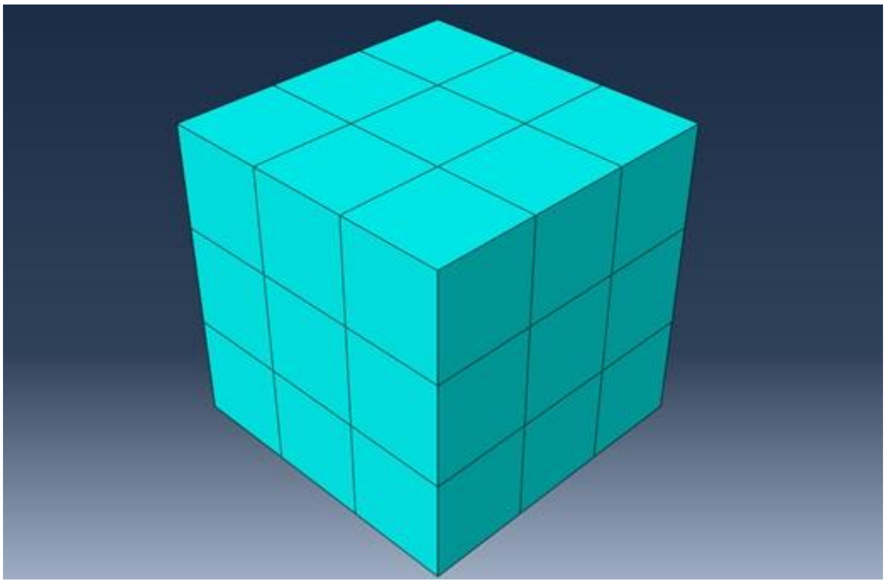

Figure 5-2: *Model of the input file discussed in this section*

5.3.1. Requirements of the user within the ABAQUS GUI.

The following steps are required in the *ABAQUS* GUI to create an input code that can be modified.

a. Mesh quality. In the next section it will become apparent that the model mesh needs to be of a sufficient mesh quality. Careful attention must be paid to the skewness of elements especially near surfaces that will be subject to case hardening.
b. As this step focuses on the application of the most appropriate material properties, it is not necessary to apply layered material allocations in the *ABAQUS*/CAE interface. As previously mentioned, it can be very time consuming when partitioning complex geometries into entities for individual mesh assignment. Within the *ABAQUS* GUI, the mechanical properties are assigned in the 'Material' option. To allow the relevant information to be easily found in the model text file, the material was named 'FGMMATERIAL'. The application of a material to a component is done with a 'Section'. This links the mechanical properties of the material to the desired geometry. This section is named 'FGMSECTION', for easily identification within the input file. The custom naming of these parameters was not essential to the outcome or success of theA. As a user becomes more familiar with the construction of an input file, these keywords become less important, however it is good practise within FE simulation to ensure that continuity in keywords is applied.

c. In order to identify which surfaces are exposed to the heat treatment and therefore have a case layer below them, all of the heat-treated surfaces must be identified within the GUI. In *ABAQUS*, a 'Surface' can be defined and a boundary condition applied. To generate a set node list in the input file, a number of boundary conditions can be used. To generate the surface node list in this application, a temperature offset boundary condition was applied. Care should be taken that any boundary conditions applied to generate a node list do not affect the analysis should they remain in the input file following its manipulation. In the GUI, the offset to the temperature offset was set to zero. To ensure that the analysis was not affected, the boundary condition was deleted in the input file.

   For ease of locating the boundary condition in the input file, and continuing good practise for naming conventions, the surface was named 'FGMSURFACE'.

Figure 5-3 gives an overview of how the *MATLAB* algorithm uses and modifies the *ABAQUS* input file. The key donates the inputs to *MATLAB*, actions that the code takes and its outputs. Each section is explained in detail subsequently.

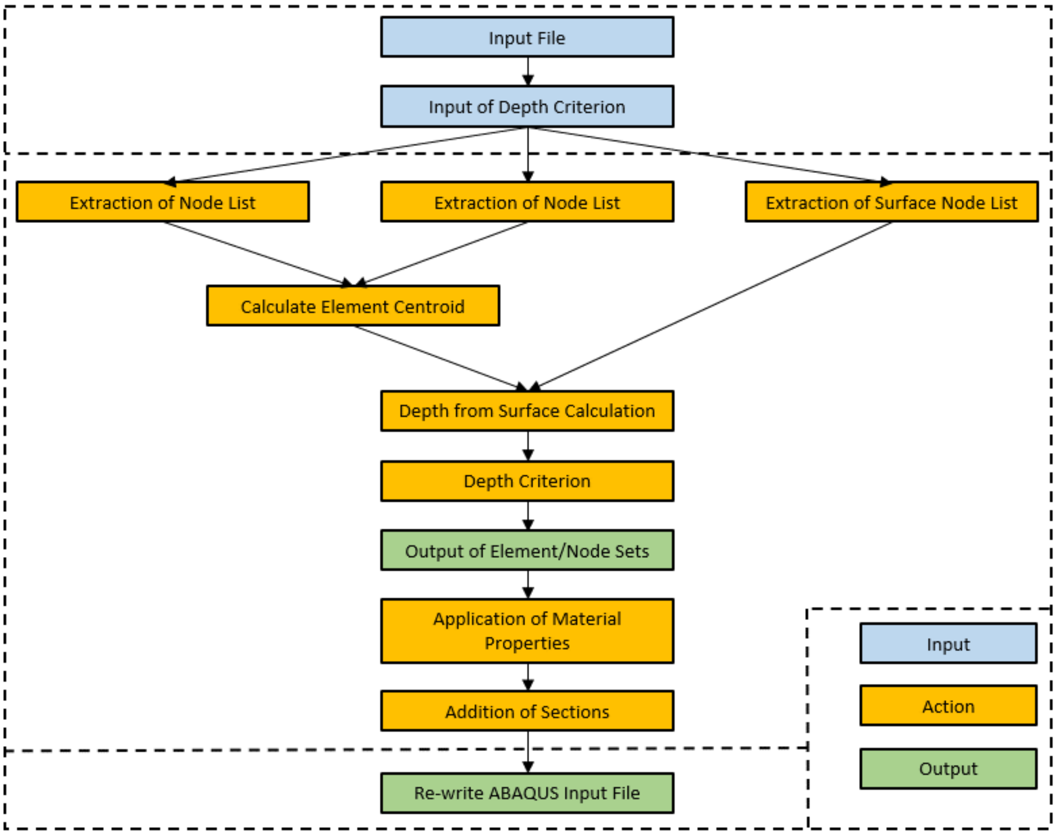

Figure 5-3: *Flow diagram demonstrating how MATLAB script manipulates the ABAQUS input file*

5.3.2. Input to MATLAB & Additional Data

The original *ABAQUS* input file created in the GUI is imported into *MATLAB* which includes within it the list of nodes, elements and the surface nodes that represent the penetration surface for the heat treatment.

At the beginning of the code, the user is required to manually input the line number for the start and end of the node, element and surface node lists. This ensures the code manipulates the correct data. A means of autonomously finding them is possible, however at this proof of concept phase, this solution is adequate.

5.3.3. Extraction of Node List

From the input file, the node list is the first item of data to be extracted. An example of the node list can be seen in Figure 5-1. This is extracted using a *cell2mat* function which creates a matrix containing the data where the commas are removed. The node list is kept in its original column format including node number and its x, y and z coordinates, respectively.

5.3.4. Extraction of Element List

In a similar way to the node list, the element list has a consistent format within the input file. It is visible at the bottom of Figure 5-1 and follows the form of the element number followed by the ID number of the 8 nodes that make up its construction. The order of the node numbering is specific however is not required to achieve the goals of this Thesis. The nodes are ordered such that the closest to the origin is defined first and ordered clockwise in the x, y and z axis. The element list is also extracted using a *cell2mat* function, creating a matrix containing the data.

5.3.5. Extraction of Surface Node List

The surface nodes list has a different format to the node list shown in Figure 5-1. As the surface node list is included in the boundary condition section of the input file, it is written as a list using the maximum 16 comma separated values. An example for the surface node and element list is shown in Figure 5-4.

```
*Nset, nset=FGMSURFACE, instance=Rubik -1
 1,  2,  3,  4,  5,  6,  7,  8,  9, 10, 11, 12, 13, 14, 15, 16
17, 18, 19, 20, 21, 24, 25, 28, 29, 30, 31, 32, 33, 34, 35, 36
37, 40, 41, 44, 45, 46, 47, 48, 49, 50 ,51, 52, 53, 54, 55, 56
57, 58, 59, 60, 61, 62, 63, 64
```

```
*Elset, elset=FGMSURFACE, instance=Rubik -1
 1,  2,  3,  4,  5,  6,  7,  8,  9, 10, 11, 12, 13, 15, 16, 17
18, 19, 20, 21, 22, 23, 24, 25, 26, 27
```

Figure 5-4: *Format of the surface node list*

As per the node and element list, the surface nodes are extracted using the *cell2mat* function. For ease of coding later on in this section, it was desirable to match the format of the surface node list to match the node list. Using a *"for loop"*, the matrix format for the surface nodes was matched to the node list.

5.3.6. Element Centroid

As previously explained, the resolution of the depth-dependent change in material properties is dependent on the element size. To identify the relevant material property values for each element, it is necessary to know the position of the centroid of the element. After that, its distance beneath the surface can be calculated and the material properties applied based on this.

The node list consists of four columns as described previously. The element list consists of 9 separate values, the element ID and then the node ID of the nodes that construct the element. As previously mentioned, the elements used in this project are quadrilateral (C3D8) due to the requirements outlined by the industrial sponsor and their common use throughout literature concerning FEA of gears. If another element type such as tetrahedral or another hexahedral element (others are available with nodes positioned along midpoints of a typical 8 node element) were to be used, further refinement to this step would be necessary.

To calculate the element centroid position, the *MATLAB* algorithm takes each element in turn, finds its constituent nodes, and identifies their Cartesian coordinates from the node list matrix. These nodes are stacked for the element and their coordinates are averaged to calculate the centroid coordinates for the element. An example of a single element centroid can be seen in Figure 5-5.

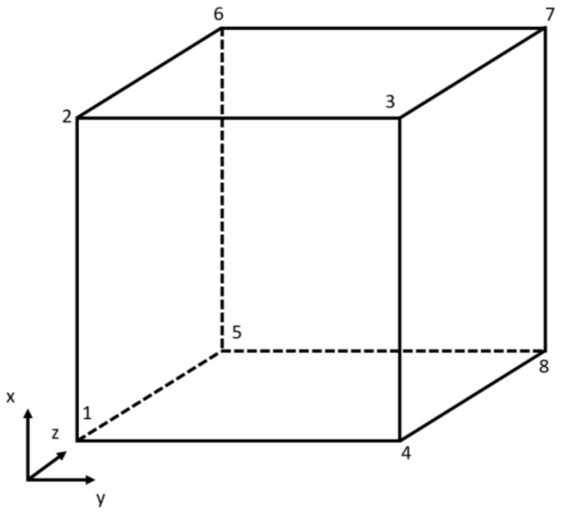

NODE	X	Y	Z
1	0	0	0
2	1	0	0
3	1	1	0
4	0	1	0
5	0	0	1
6	1	0	1
7	1	1	1
8	0	1	1
Sum	4	4	4
Average	0.5	0.5	0.5

Figure 5-5: *Calculation of a centroid for a single element.*

This solution can be considered a simple one, however is practical and efficient yet has scope for improvement in future.

A concern with this method of centroid location is that elements are not always perfectly cube-shaped. When deformed it is defined as skewed. When there is substantial skewness the centroid location may not be considered accurate. However, as the material properties are allocated to the whole element, the accuracy of the approach is governed by the fineness of element resolution of the case layer. Inaccuracy in centroid location will then be a secondary effect. There should therefore be sufficient geometry refinement at the model creation and meshing stages within the GUI to ensure a sufficient quality of mesh, avoiding heavily skewed elements.

As an alternative, it is possible to modify the code such that the node closest/furthest away from the surface is selected for the depth selection. Using this approach, it is possible to raise or lower the effective accuracy/safety factor of the analysis. Additional techniques for finding the element centroid position are discussed in the further work section of this Thesis.

Within the code, two *"for loops*" are used. The first to obtain the first element, and the second to retrieve the coordinates of its nodes. The node coordinates are averaged to find the centroid position then stored in another matrix of *"Element Centroid Coordinates"* which is three columns consisting of X, Y and Z coordinates. As the element numbering will go from 1 up to the maximum number of elements in the model, the row number is equal to the element number.

5.3.7. Depth from Surface Calculation 1

Now that the centroids for each element have been calculated, they can be compared to the known positions of nodes on the surface. In section 5.3.5 any surfaces that are exposed to a case are specified in *ABAQUS*/CAE as a surface. This surface is represented in the Input File as a node set (nset=FGMSURFACE) and an element set as shown in Figure 5.1. Some boundary conditions used to identify the surface nodes may generate a list of surface elements also. The surface element list is of no importance to this section. As each of these nodes has been converted into its own matrix with node number and X, Y and Z coordinates, the position of each element centroid can be compared to every surface node in turn. This calculation is completed using a number of "*for loops"* with the "*pdist"* function of *MATLAB* initially calculating the distance between element centroids and each surface node in turn. The minimum distance for each element centroid gives the depth from the surface and is saved along with the element number. These data are held in a vector. Each row contains the minimum distance and is assigned to the row number which corresponds to the element number. Due to the large amount of computational time required to perform the "*pdist"* function, an alternative was required. When calling a function included within *MATLAB*, there is a time taken to implement it when compared to including code behind it in the user's script. Due to the number of nodes and elements expected within a detailed gear model, calling a function such as "*pdist"* would not be a viable solution. Instead a custom section to the script was added where the depth is calculated though basic trigonometry. In a study on a small model, the latter solution was considerably quicker.

5.3.8. Depth from Surface Calculation 2

To further investigate the concept of the previous surface depth calculation an alternative approach was also applied. A concern regarding the previous version is that the centroid position may not be completely representative of the position of the element if it is sufficiently skewed.

The alternative method which compares the minimum and maximum distance of the element's nodes from the surface nodes was proposed. Due to the calculation time to compare all element centroids to each surface node, this solution would require every node from every element be compared to every surface node. Due to the increased number of calculations, it was not considered an appropriate alternative.

5.3.9. Depth Criterion 1 (Unused)

The following criterion was used for initial testing, investigation and validation of the *MATLAB* script.

1) Depth greater than 0.0mm and less than 0.5mm
2) Depth greater than 0.5mm and less than 1.0mm
3) Depth greater than 1.0mm and less than 1.5mm
4) Depth greater than 1.5mm

Using this criterion three material properties would be assigned to the case layer with a single property being applied to any element with a depth greater than 1.5mm to represent the core material.

This information is held in a matrix consisting of four columns. Each column represents a material depth/property and each element number is placed in the column corresponding to its calculated depth from the surface. It should be noted that this selection of three layers is arbitrary and could be increased without any changes to the technique being described.

5.3.10. Depth Criterion 2 (Final)

As an alternative to the previous depth criterion, a more automated means of specifying a depth criteria is desired. Including a user defined input for the case depth and the desired number of materials case layer, it allows for the user to create multiple models for an iterative analysis. The total number of materials included in the analysis is then increased by one to include the addition of the core. Figure 5-6 shows the code specifying the number of materials.

```
HAZDepth=1.5;
HAZMaterials=4;
HAZLayerIncrements=HAZDepth/HAZMaterials;
TotalMaterials=HAZMaterials+1;
```

Figure 5-6: *Code to for user to define the number of materials within the case layer*

Using the depth parameters outlined earlier in this chapter, each element is considered in turn and assigned to a layer from this depth criterion. As an output to this step of the code, a .txt file is created that has the node and element numbers for each of the desired layers included. The node and element numbers are included in the correct format of 16 comma separated variables per row, therefore able to be directly added back to a rewritten input file.

5.3.11. Application of Material Properties

As per the format of the *ABAQUS* input files, the material properties are assigned as shown in Figure 5-7. For an analysis consisting of only elastic material properties, only the data in the blue box of Figure 5-7 is included. For an analysis where elastic-plastic properties are required, the data in the red box is also required. The first line in the red box denotes a stress of 600MPa at zero plastic strain. This value of stress is the yield stress. The remaining lines follow the same format of stress and plastic strain. The final line is the UTS and the corresponding plastic strain at failure. Unless element failure is included within the model, the gradient of the last two points is extrapolated to infinity. The stress-strain curve for plastic behaviour is shown on the right of Figure 5-7. The example shown here is a simple plastic behaviour with effectively two tangent-moduli, but more stress and plastic strain data points can be used to accurately model the real stress-strain curve.

```
** MATERIALS
**
*Material, name=Steel
*Density
7850.,
*Elastic
20000.,0.3
*Plastic
600.,    0.
1100.,0.02
1400.,0.06
```

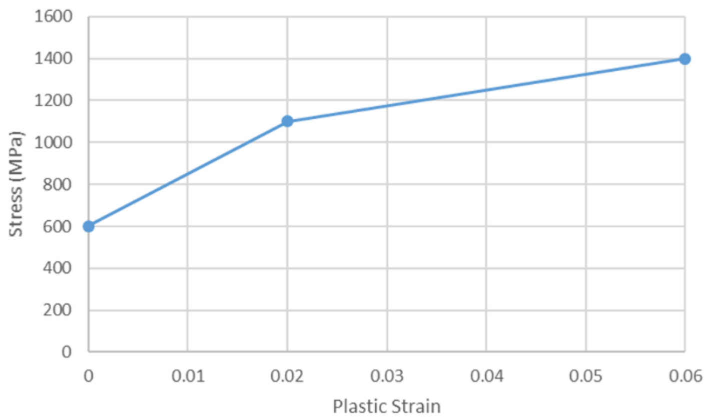

Figure 5-7: *Material properties (elastic and plastic) in the ABAQUS input file.*

At this stage, the finalised material properties from chapter 4 are required. In their finalised form they have elastic properties in the form of an elastic modulus and a Poisson ratio and a curve that describes the stress-strain (plastic strain) behaviour. It is important to ensure sufficient data points are included for the plastic properties. When only a few points are included, the solver will linearly interpolate between the points, therefore a larger plastic strain will be associated to a specific value of stress, potentially creating results which are unrealistic. When using an insufficient number of data points in this section, the importance of the data from chapter 4 will be diminished. Additionally, this may cause some issues in the FE solver failing to converge.

A spreadsheet (Figure 5-8) using the A, B and n values calculated from Chapter 4 was constructed to generate material data for the FE section of this research. The Johnson Cook equation is used to generate a stress for a given plastic strain. To ensure sufficient detail in the generated stress-strain curve, strain increments of 0.005 are made. Using the *Concatenate* function within *Microsoft Excel*, the stress and plastic strain were generated in the correct format to be imported into the input file. The *Concatenate* function joins two or more text strings into a single string. A screen shot of the spreadsheet is shown in Figure 5-8 below. The Figure shows a section of the spreadsheet where the columns in green represent the calculated stress at the given value of strain for Layer 1 (for up to 0.1mm into the case). The orange column in-between them uses the *Concatenate* function to merge the necessary data. Layer 2 represents the next layer into the case (for up to 0.2mm into the case), where the stress and stain are in blue columns with the orange column again combining the data. This data can then be copied and pasted directly from the cells to the input file.

Layer 01 - 0.1mm			Layer 02 - 0.2mm		
Stress	Combined Data (Concatenate)	Plastic Strain	Stress	Combined Data (Concatenate)	Plastic Strain
1240.000	1240, 0	0.000	1190.000	1190, 0	0.000
1262.983	1262.98263870727, 0.0005	0.005	1215.936	1215.93592558638, 0.0005	0.005
1276.567	1276.56705516919, 0.001	0.010	1230.585	1230.58514749804, 0.001	0.010
1287.981	1287.9812027814, 0.0015	0.015	1242.738	1242.73780887882, 0.0015	0.015
1298.181	1298.18085298114, 0.002	0.020	1253.509	1253.50859513197, 0.002	0.020
1307.563	1307.56313495618, 0.0025	0.025	1263.356	1263.35612371222, 0.0025	0.025
1316.342	1316.3415946941, 0.003	0.030	1272.525	1272.52536601952, 0.003	0.030
1324.648	1324.64778079125, 0.0035	0.035	1281.166	1281.1664587121, 0.0035	0.035
1332.570	1332.56998240495, 0.004	0.040	1289.380	1289.37974614557, 0.004	0.040
1340.171	1340.17108347186, 0.0045	0.045	1297.236	1297.23644606692, 0.0045	0.045

Figure 5-8: *Spreadsheet to generate material data to input into a re-written input file*

5.3.12. Manipulating Data for the Rewrite of the ABAQUS Input File

As previously mentioned, as the objective of this Thesis is to prove a concept for an algorithm to create an FGM, there is further work required to streamline the process to integrate effectively with gear analysis in industry. To create an algorithm to manipulate an input file, rewrite new sections and assemble it all in the correct format would require a great deal of precious experience, expertise and considerable time for debugging. FE software developers dedicate substantial resource to such activities, therefore is deemed to be outside of the remit of this research, which is concerned with the development of the underlying principles and analysis methods. From previous experience in working with these documents, using copy and paste functions to manually assembly the file is a far more time effective means of achieving the end goal for this research.

5.3.13. Writing the ABAQUS Input File

Previous Figures in this chapter have demonstrated the format for various sections of an *ABAQUS* input file. Figure 5-1 shows the node and element lists that make up the vast majority of the input file (on a gear model at least), however this section is only imported (not modified) to the Authors' script and manipulated to achieve the objectives of this chapter.

When writing the input file to include the FGM, the donor input file is the starting point. The input file is a '.inp' format as default and will not open in some text editors. By changing the file extension in the files name to .txt, it can be opened in all text editors.

The next section of the input file is *'Sets'.* An example of this can be seen in Figure 5-4 where node sets (nset) and element sets (elset) are created, and contain the desired nodes and elements to be included for that section. They can be given a specific naming convention to later be called. An instance is also specified in the first line of the section. An instance refers to a component. Therefore, there is scope to apply this approach to assemblies, rather than the single components used in this Thesis. For sets to be assembled, the .txt file created by the *MATLAB* algorithm will need to be manipulated such that the node and element sets for each material later are linked and given a naming convention that can later be referenced.

Figure 5-7 shows the format for a simple elastic-plastic material included in the input file. For multiple materials, the spreadsheet shown in Figure 5-8 was used and multiple materials included into the input file. Again, an appropriate naming convention should be applied.

To assign a material to specific layers within the FE model, element sets are linked with the materials in the next part of the input file, named with the keyword *'Sections'*. Figure 5-9 shows an example of how the sections are assigned. *Section_01* on the first line of each section entry is then linked to *Set01* (the first element set) and *MatLayer01* (the material properties for the first layer).

```
** Section: Section01
*Solid Section, elset=Set01, material=MatLayer01

** Section: Section02
*Solid Section, elset=Set02, material=MatLayer02

** Section: Section03
*Solid Section, elset=Set03, material=MatLayer03
```

Figure 5-9: *Example of how 'sections' assign a property to element sets*

Following the inclusion of the generated sets and sections, and new material properties, care should be taken to ensure that the formatting is correct. It is good practise to ensure that no blank lines are included in the code as it can lead to importing errors when opening in the ABAUQS GUI.

Following the completion of the modified input file, it should be converted back to a '.inp' file format. As previously mentioned, some text editors can directly open and modify a '.inp' file, in which case, this step is not necessary.

5.3.14. Running the ABAQUS Input File

Two options are available for the running of an *ABAQUS* input file.

The first option is to run within *ABAQUS* CMD. To achieve this, the input file must be located in the temporary directory specified by *ABAQUS*.

The second option and the one recommended by the Author is to import the input file into the GUI. In importing, it gives the user the opportunity to perform checks on the file to ensure no errors have occurred. Due to the addition of multiple sets, sections and materials, a visual check is possible within the *'materials'* viewer. The user is given the option to display the model by material definition, thus providing a visual check that the FGM code has had the desired effect. This will be described in more detail further in the next section of this chapter.

5.3. Proving the FGM code

To prove the code, input files of varying complexity were constructed using the *ABAQUS* GUI, manipulated with the *MATLAB* Algorithm and then opened within the *ABAQUS* GUI for inspection. For each step in the analysis, each image from the *ABAQUS* GUI includes a colour plot view in the materials section of the GUI, where the various materials that make up the component are viewed with elements coloured differently according to their assigned material.

5.3.2. Example 1 (six elements modelling a bar)

A simplified tensile coupon/bar (Figure 5-10) consisting of six elements in a row was constructed in *ABAQUS* GUI. The model consisted of 0.5mm solid elements. A temperature offset boundary condition was applied to identify the nodes on the end face of the bar, and to create the surface that the FGM would propagate from. No loading boundary conditions were included in the model.

The input file was then run through the *MATLAB* algorithm and manually manipulated as previously described in this chapter, where sets, sections and additional materials were incorporated into the input file. The case depth specified in the algorithm was 1.5mm and specified that three materials would be incorporated into the case layer.

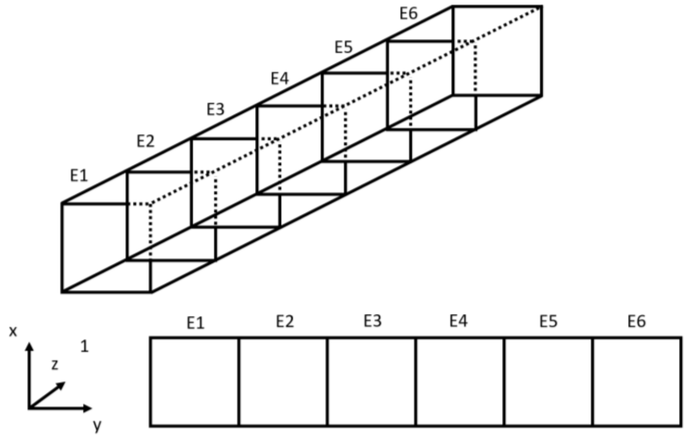

Figure 5-10*: Graphical interpretation of six elements in a tensile arrangement.*

Figure 5-11 shows the result of running the *MATLAB* algorithm, modifying the input file and re-importing into the *ABAQUS* GUI. The Figure shows the model in a colour plot of the materials assigned to each element. Therefore, it is clear and obvious that four different material properties have been applied; three in the case layer and one to represent the bulk of the remainder of the model/core.

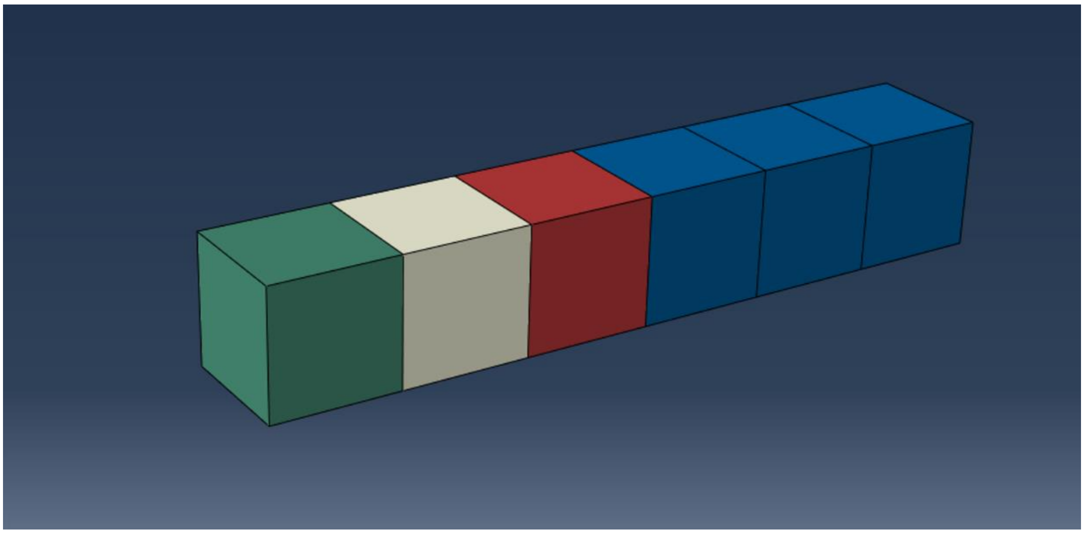

Figure 5-11: *Tensile result of the six element tensile sample with independent material properties applied*

In summary, the algorithm has successfully manipulated an input file for a simplified tensile coupon to aid in applying an FGM to an FE model. Therefore, the goals set for this section of development have been successfully achieved.

5.3.3. Secondary Investigation (Tensile Coupon)

As described in Chapter 4, the material properties for the Case Carburised S156 steel were found via tensile coupons that have been manufactured such that they have only a case beneath one pair of surfaces on opposite sides of the sample. As per the FE modelling summary of Chapter 2, the tensile coupon has been simplified to a 1/8th model with symmetrical boundary conditions applied to minimise the size, number of nodes/elements and complexity of the model, and also to reduce computational power and run time during an iterative analysis. To simplify the model, the pin detail has been removed. The simplified model of the coupon is shown in Figure 5-12. The *MATLAB* algorithm was then applied to this coupon model with a specified 1.5mm case and 5 materials specified within it.

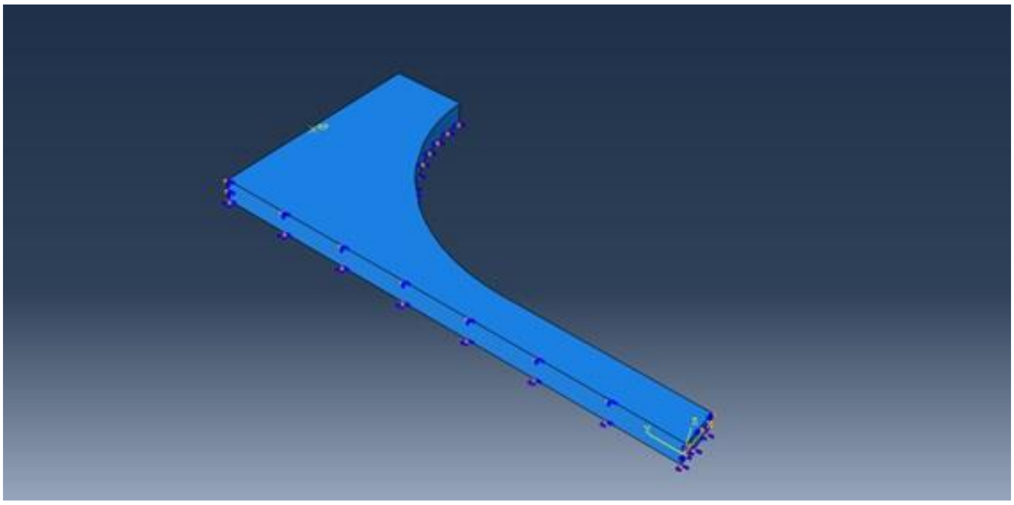

***Figure 5-12**: 8th model of a tensile coupon*

The tensile coupon included in this section was specified with a mesh seed of 0.2mm such that there are multiple elements through its thickness to allow sufficient layers to be allocated a material property to prove the method. The top face of Figure 5-12 was specified as a temperature offset in the boundary conditions to generate the node list on its surface. This face is the one that the case penetrates from. The boundary conditions for the simulation of the coupon are *Symmetric* and applied to an X, Y and Z face.

Following the initial modelling in the *ABAQUS* GUI, generating the input code, running it in the *MATLAB* algorithm and rebuilding the modified input file, the model can be re-imported into *ABAQUS* and success of the process evaluated. As shown in Figure 5-13, viewing the model in the materials tab, the colour plot shows that the application of the FGM code has been successful. The colour plot makes it clear and obvious where the case layer properties have been applied over a depth of 1.5mm and the core material applied thereafter.

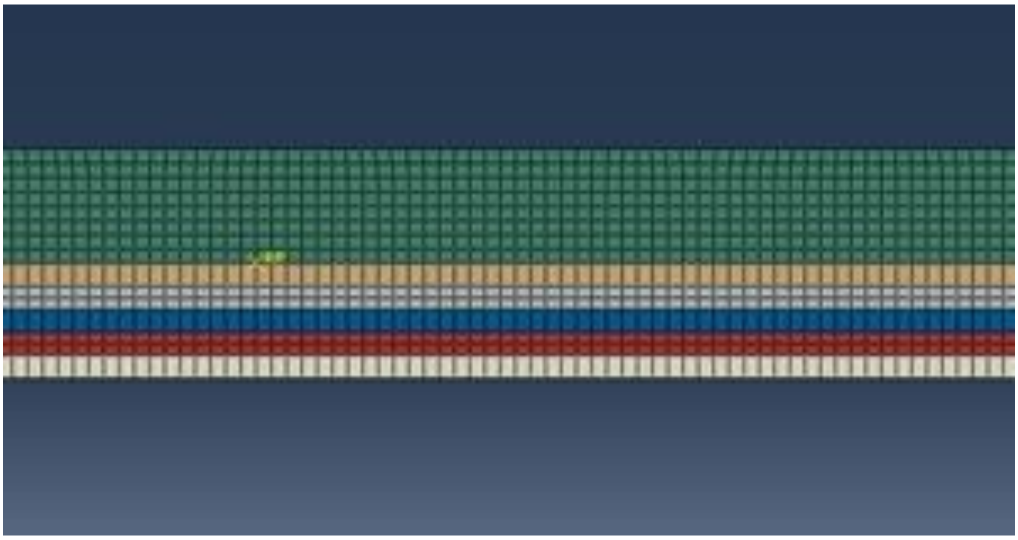

***Figure 5-13**: Section of the case within the tensile coupon*

In summary, the algorithm has successfully manipulated an input file for a tensile coupon (as tested in Chapter 4) to aid in applying an FGM to an FE model. Therefore, the goals set for this development model were successfully achieved.

5.3.4. Final Investigation (Involute Geometry)

The previous examples (Figure 5-11 and Figure 5-13) have been quasi two-dimensional models. The last stage of proving the FGM code is to apply it to a three-dimensional geometry. To be in line with the research of this Thesis, the code is applied to a gear, specifically a model of a single tooth.

A model was built in the *ABAQUS* GUI with no loading boundary conditions, only the temperature boundary conditions required to generate the surface node list. Figure 5-14 shows the gear in question. In the Figure, radial faces over the root, flank and addendum are chosen from which to have the case layer propagate from. The mesh size used on the model is 0.1mm (globally), therefore comparable to that required if 15 layers were to be simulated through the case layer. The *MATLAB* algorithm specified a case depth of 1.5mm and three material layers.

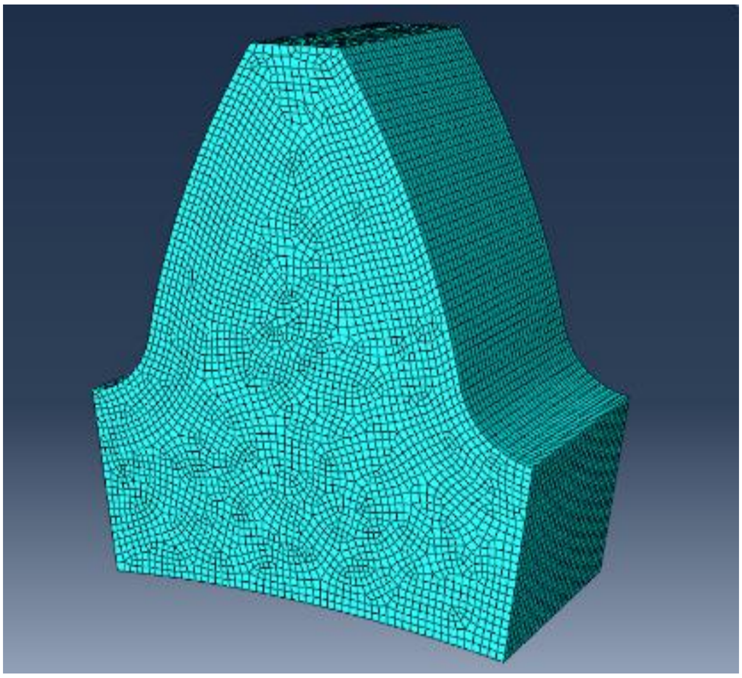

Figure 5-14: *FEA model of a single tooth with surfaces specified for heat treatment material application*

Following the application of the *MATLAB* algorithm to the input file, manipulation and re-writing, the input file was re-imported into the *ABAQUS* GUI to inspect the success of the addition of a case layer. Figure 5-15 demonstrates that the application of an FGM to a gear geometry has been a success.

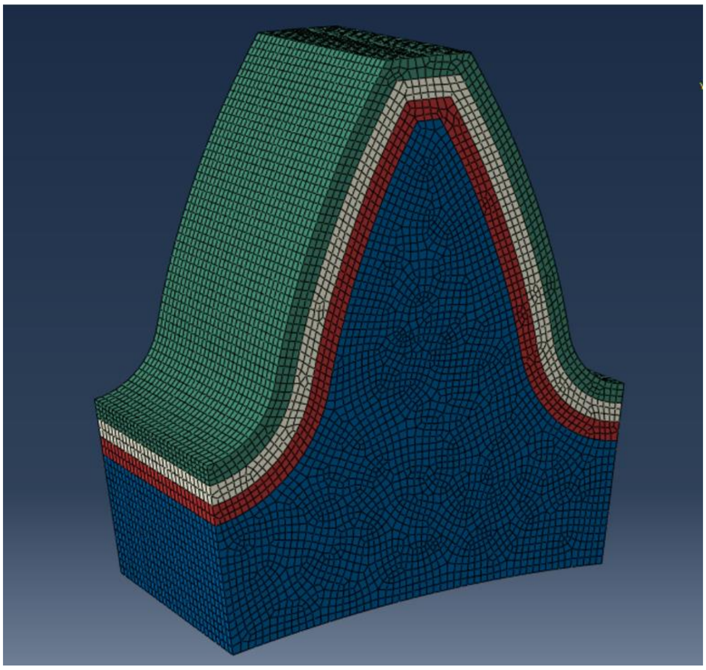

Figure 5-15: *FGM applied to the involute geometry of a gear*

In summary, the algorithm has successfully manipulated an input file for a gear geometry to aid in applying an FGM to an FE model. Therefore, the goals set for this development model have been successfully achieved.

5.4. FGM Discussion

This chapter outlined that the user creating the initial model in the *ABAQUS* GUI was required to produce a mesh of sufficient quality for the analysis. During an early iteration of the gear model where the mesh was not sufficiently refined, the FGM code was applied to investigate the effect of a poorly-refined mesh. **Error! Reference source not found.** s ubsequently shows the effect of the FGM code on an unrefined mesh. It is clear that the material properties are not applied in uniform bands parallel to the surface and instead are scattered, based on centroidal distance from each element to the surface. The scattered application of material properties will not affect the running of the model, however the unrefined nature of the mesh can have some influence over the accuracy of the results.

In addition to the depth criterion, a means of calculating the position relative to a concave or convex surface would be of benefit. As presented in Chapter 2, during the manufacture of gears, the heat treatment takes place prior to the final grinding process. This is to ensure there is no tooth distortion due to the high temperatures and oil quenching during the heat treatment process. As there is typically more distortion closer to the addendum of the tooth, there would subsequently be more case removed by grinding. Using a hardness plot over the full involute comparable to that of Figure 4-4, could identify how the penetration of the case varies over the full geometry. Within the FGM code, comparing the element centroid to a series of surface nodes may identify whether the element is closest to the tip, flank or root of the tooth and therefore a more appropriate material property be applied.

Computational efficiency is a factor in FE modelling. The FGM section of this research is no different. In the example of the gear model, the model consists of 384,000 nodes, 344,000 Elements and 14,000 surface nodes from which the heat treatment is specified to penetrate. Therefore the number of calculations involved in calculating each element's centroid, comparing it to each surface node, allocating a depth criterion and writing the node and element sets is substantial. With an early iteration of the FGM code, the expected time to finish the calculations was measured in years. Through analysing the percentage of time taken for each aspect of the code, the Euclidean function that calculates distance between two sets of Cartesian coordinates took over 90% of the run time. This was due to the overheads associated with the high level function. By doing the trigonometry calculation directly, the calculation time was reduced considerably. When using a PC consisting of 16 CPUs with 2.9GHz processors and 128 GB of RAM, the code for the aforementioned number of nodes and elements took 25 minutes to run. Further to this, there is still the requirement of modifying the input file manually prior to importing the model to run. As with the FE modelling, cloud computing or the allocation of more computing power could reduce the run time for the code, and the calculations would lend themselves to parallelization. To mirror the approach of FE analysis once again, the codes could be left to run overnight on a less powerful PC. Due to the time required in partitioning a gear model for a heat treatment, running this code overnight, in the background or on cloud space is likely to be the most efficient use of an Engineer's time.

As Chapter 4 produced a relationship between elastic modulus, and the Johnson Cook material model parameters (A, B and n), there is scope to include a relationship for these values directly within the code. Were this included, a bespoke material property could be generated for each element and its specific depth from the surface, as opposed to the banding approach used in this Thesis. Despite the benefit of improving how the model represents the case layer, there is the risk of added complexity in the processing. Considering the number of calculations required in the FGM code in its current state at the time of writing, there could be a limitation for the sake of computational efficiency in the FGM code and the *ABAQUS* solver itself. However, the concept of having the code generate material properties based on the depth of each element is worth pursuing as opposed to the banding approach used in this Thesis, although it could be argued that increasing the number of bands towards the number of elements within the case depth leads to the two approaches converging anyway. The user could specify a number of layers that they desire, then the code determines the average depth of all the elements in that criterion. Thus a more representative case layer could be generated and included in the analyses.

This chapter also highlighted the different approaches considered in allocating the depth of an element. The method of comparing the element centroid to the surface nodes was chosen, however alternatives were discussed but not implemented. Were the depth assigned based on the shallowest node and not the centroid of the element, then it is ensured that the hardest layer of the case is always represented irrelevant of the mesh density. This would require all node coordinates be compared to each defined surface node therefore increasing the number of calculations required within the FGM code. In the case of the gear model used later in chapter 7, this would cause only a 10% increase in calculation time. For a model where the case would be simulated from all external surfaces, this calculation time would be substantially increased.

In the development of the FGM code, it was found that if the mesh size on the surface was sufficiently large and the number of layers in the case sufficiently small, then no elements were assigned the hardest material property. To ensure this does not happen within a model, there is scope for an alternative approach to element depth calculation where the minimum and maximum node depths for each element could be averaged and that depth assigned to the element. To ensure that the layer of elements on the surface are assigned the hardest material property, an additional command in the code should be included that ignores the averaging of minimum and maximum node depths if any node within an element is found to have depth of zero from the surface.

5.5. FGM Summary

As demonstrated, a FGM was created using a custom *MATLAB* algorithm that manipulates the FE Input File. It has successfully applied material properties based on a user-defined depth criterion. A process for the re-writing of the input file has been described and a means of assessing the success of the process discussed. Using this algorithm and process, a case layer can be incorporated to a model based on a few user defined parameters for the case depth and desirable number of materials.

The FGM code has been trialled on three-dimensional components through its development including a simplified tensile coupon, another tensile coupon as tested in Chapter 4 of this Thesis and a gear/involute geometry.

6. *Validation*

6.1. *Introduction*

To assess the performance of the modelling approach a physical test is required. The model should replicate the physical testing environment as accurately as possible and care should be taken to understand the limitations of instrumentation, measurements and modelling outputs. This short chapter reports on a physical test subsequently used in Chapter 7 to validate the material model and FE approach developed in Chapters 4 and 5.

6.2. *Experimental Setup*

To generate experimental data for comparison with a finite element gear model, a quasi-static test was most appropriate. A dynamic test would be complex to simulate and would also present challenges in capturing empirical data such as strain. Therefore, fixtures were designed and manufactured that would restrain a gear in place for compression over the span of four teeth. The concept for the test method is comparable to a test conducted by the industrial sponsor in which gears are compressed over the span of four teeth. This industrial test was initially used to compare different gear steels to establish stiffness and 0.2% proof stress values. With a gear test of this nature, it is possible to make rapid comparisons between multiple components with minimal error. If a tooth bending test was conducted with the gear restrained by mounting on a shaft, shaft bending and misalignment can result in misalignment at the point of load and therefore leads to errors in the simulated torque, and also misalignment in any non-contact measurement techniques used in this validation process. Compressing across a span of four teeth leads to relatively few potential sources of error. The fixtures (shown in Figure 6-1) are effectively two anvils that include a mounting bracket to position the gear in the correct position. The fixtures were mounted to a 50kN Interface load cell on a LOS hydraulic test machine, controlled by an MTS Flex GT Controller software. The RDP 5mm LVDT was logged using a Vishay 7000s logger system.

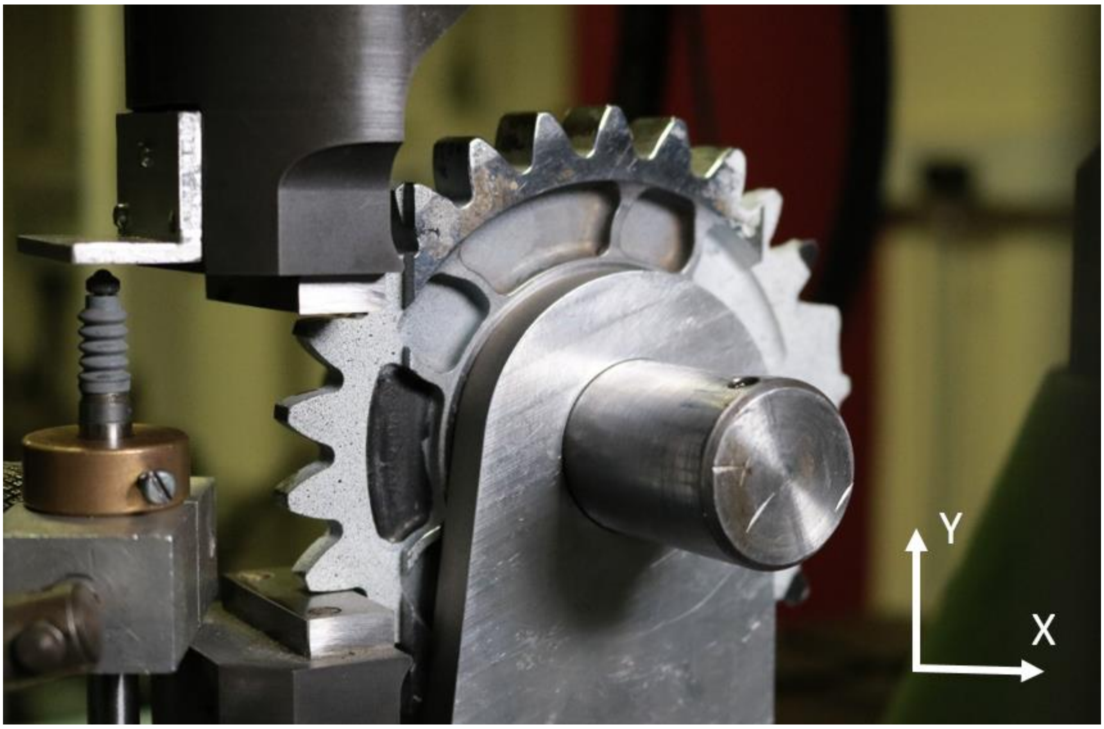

Figure 6-1: *Test setup for the compression of a gear tooth to failure.*

The anvils were manufactured from EN24T steel, and following manufacture were heat treated by plasma nitriding. Due to the discrepancy between material properties (namely hardness and yield strength) of the EN24T and the S156 gear steel, a section of the tensile coupons tested in Chapter 4 was used as a contact interface between the gear and anvil. This ensures that the fixtures do not yield prior to the gear and creates a comparable contact interface. Not only does this reduce the cost of material and heat treatment for the fixtures, it also reduced lead time for manufacture.

To monitor the tooth during loading, the test gear was modified with half of its face width removed via the wire EDM process. Figure 6-2 shows the modification of the gear along with a schematic clearly showing the narrowed face width of the gear. The modification was performed to opposing sides of the gear so that two tests could be completed on each gear if required. This section was removed to negate the end effects of the case, and reduce the forces in the test such that they could be performed using the facilities available at Cardiff University and simplify any FE analysis required. Additionally, with the end sections of the gear removed, the case layer can be monitored face on by the VSG system.

Figure 6-2: *Validation test gear, note the wire cut sections and speckle pattern applied.*

The gear under test is a ratio gear from the 2014 gearbox provided by the industrial sponsor. As it was not a current design under mass production, the number of test gears available was limited, thus a series of tests within the elastic range of the gear were first conducted to ensure all instrumentation and machinery was set up appropriately, prior to loading the gear to beyond yield.

A compressive preload of 200N was applied to remove slack in the setup and load machine. The test was conducted under displacement control at 0.4mm/minute until failure of the gear tooth. The loading rate was chosen to ensure that the test did not exceed the maximum memory of the VSG system whilst monitoring the component at the highest resolution and framerate possible. To ensure the maximum amount of data is collected, LVDT's and a VSG system was used to monitor the test. The position of the LVDT can be seen in the left hand side of Figure 6-1. The LVDT was used to measure the vertical displacement over the four tooth span of the gear under test. The VSG system was set up to monitor the root fillet of the lowest tooth visible in Figure 6-1. The lowest tooth was monitored due to it being the side that will experience the minimum translation due to the crosshead travel. This allows better control over the area of the gear that is kept in the FOV. Figure 6-3 shows the entire experimental set up with the LVDT and VSG camera shown clearly.

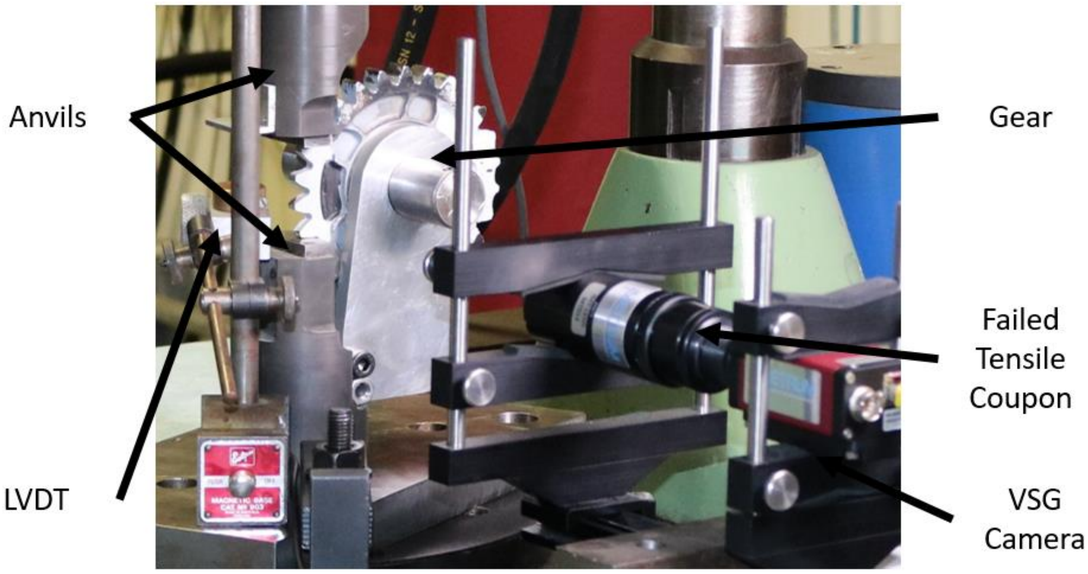

Figure 6-3: *Experimental setup with VSG visible.*

6.3. *Test Results*

Initial testing of a gear ratio concluded with the failure of the upper most tooth under load shown in Figure 6-4. As previously stated, the VSG system was set up so it was monitoring the lowest tooth being spanned by the fixtures, thus the failure was not captured. As such, there was a requirement to repeat the test with the aim of capturing the tooth failure with the VSG system. As previously mentioned, each gear had two locations where the case was removed, thus the test could be repeated immediately. As only a single VSG system was available and it was focused on the lowermost tooth shown in Figure 6-4 (marked with red box). This side of the gear tooth was monitored due to its loading in tension, therefore the expected failure criterion for a metallic component. Compression failure is not associated with bending failures for gear teeth. A repeat of the test yielded a failure in the monitored tooth.

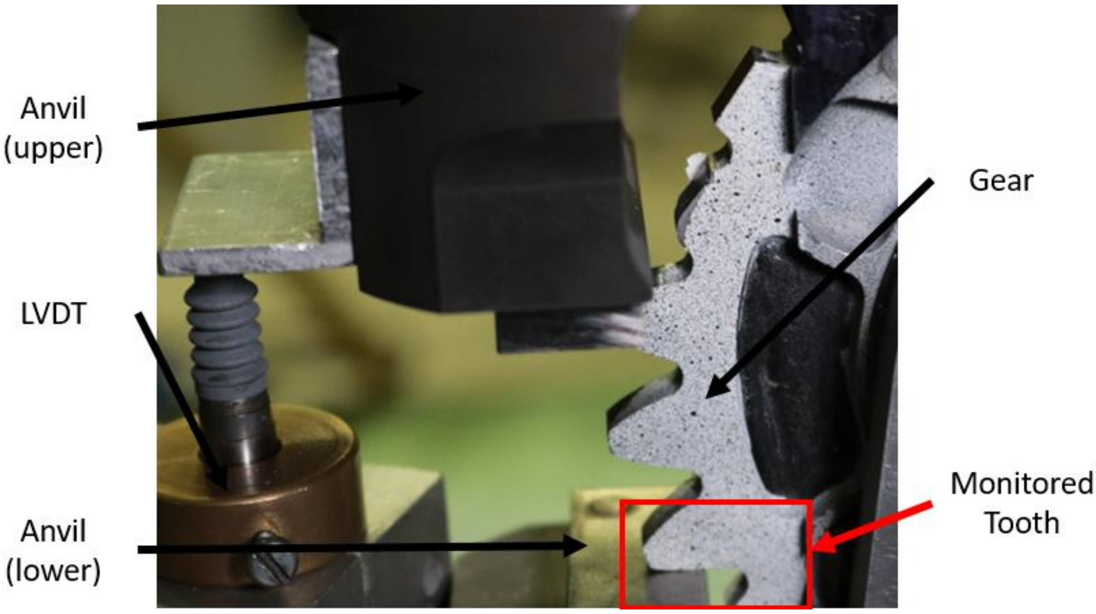

Figure 6-4: Failure of gear tooth under compression.

Following the repeated test, the failed gear tooth was monitored by the VSG system. Figure 6-5 shows the load cell force and the displacement from the LVDT. It is clear at around 35kN load that a yield point was reached as there is a noticeable change in gradient (line through the linear section of the graph to emphasise). At 0.7mm of displacement and 45kN load, the gear tooth slipped on the anvil. This was likely caused by the slight rotation of the tooth combined with any compliance in the load machine actuator causing some misalignment in the loading.

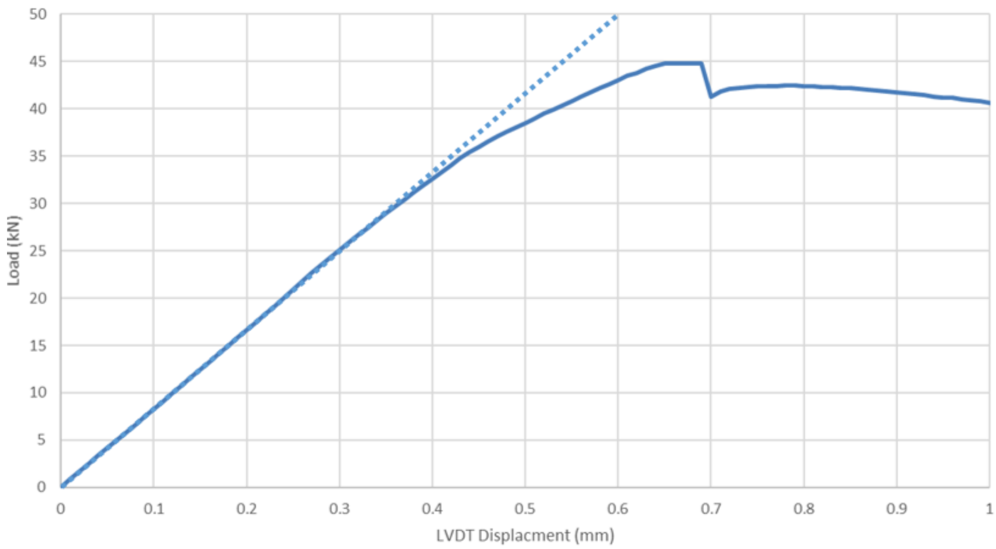

Figure 6-5: Graph of Force v Displacement from validation test

Figure 6-6 shows a colour plot of the Y displacement as measured from the VSG system. This will be used to compare against the same load conditions within FE analysis.

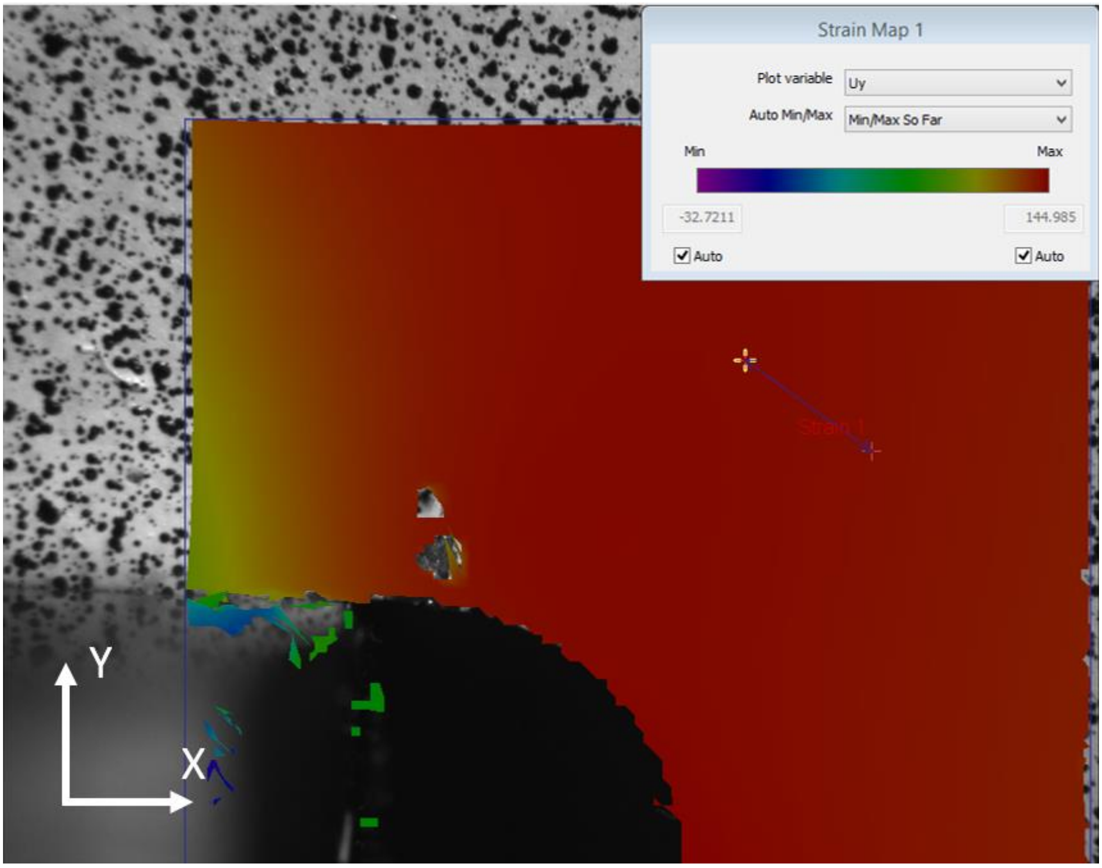

Figure 6-6: *Colour plot from the VSG showing displacement in the Y axis*

As test data was collected from the VSG, LDVT and load cell, it can be used as a comparison to FE models using the material properties generated from Chapter 4 applied to mimic the case layer using the method outlined in Chapter 5.

6.4. ***Validation Discussion***

During the validation test, alternative VSG cameras and lenses would have been of benefit to maximise the field of view for the monitored gear. The cameras and lenses were selected as they were the most appropriate of the ones owned by the University. Increasing the number of pixels, reducing the speckle size and increasing the field of view would provide further detail through the case layer. This however is something that would only be possible when the technology in this area of non-contact measurement improves further. With the VSG setup used in this Thesis, there is very little displacement/deformation within the case during loading and this cannot be seen even when changing the boundaries of the colour plots (Figure 6-6). This is due to the monitored component being of a high stiffness with the small FOV being monitored. Despite the mapping of strain on a gear tooth McRory (2010), this was looking at a section of a single gear, but over several teeth. The gear was manufactured from a steel with lower yield strength and no case hardening. Therefore there was more displacement and therefore strain captured in the FOV.

As an alternative validation approach, using a VSG system over the span of four teeth in the gear test may be a viable alternative. As there would be larger displacements over a span of teeth, more accurate measurements can be made. As an alternative approach, it may provide data that is a better comparison to that of FE. Figure 6-2 shows how the face width of the gear was taken from 12mm down to 6mm to negate the end effects of the case and reduce the loads required to yield the tooth. To increase the deformation of the gear tooth, this face width could be further reduced. As a secondary benefit, further reducing the face width of the tested gear would result in a lower force from the load machine, which in turn will result in less compliance in the test fixture, giving more accurate displacements from the LVDT and crosshead. With less compliance, the tooth slip shown in Figure 6-5 would be either reduced or negated completely. TWO CROSSHEAD ADJUSTORS.

As an additional means of validation, strain gauges could be placed on the gear teeth. As described in the literature review, with the size of gears analysed in this Thesis, positional accuracy of the strain gauge is difficult to achieve thus may prove difficult to compare to FE. In addition to this, were strain gauges to be positioned on the surface of the gear then it would provide less area for a systems such as VSG to monitor the surface. As an alternative position, strain gauges could be positioned on the root fillet themselves, therefore on a face that is not being monitored by the VSG system.

6.5. ***Validation Conclusion***

This chapter has produced a means of testing a gear in a quasi-static nature. Custom test fixtures were designed and produced such that they are able to load the gear whilst ensuring a non-contact measurement system has full view of a tooth root that is being loaded in tension. The instrumentation included in the test have provided data that can be directly compared to values from FE analysis. The VSG system provides a strain map as well as displacement colour plots in either the x or y axis, thus matching an output possible within *ABAQUS*. An LVDT was included that provides the displacement over the four teeth being loaded. Once again, this is a displacement that is possible to extract from FE.

7. Finite Element Analysis

This chapter combines the findings of the literature review, the experimentally measured material properties for the case layers, and the FGM model developed in previous chapters, to create a validated FE model for the tensile coupon and gear geometry.

7.1. Tensile Coupon (3mm – Single Material)

To provide the foundations of a validated FE analysis, the core material model must first be correlated. Therefore, an FE model of the 3mm tensile coupon was created with a uniform material property applied, using the experimentally measured core properties. With optimisation to the boundary conditions and mesh density the FE model can be validated by the tensile test data from Chapter 4.

In light of the simplification of FE models outlined in the Chapter 2, the same concept was applied to the tensile sample. Using symmetry boundary conditions, the model was simplified to one-eighth of the original dogbone geometry. Therefore, nominally one-eighth of the elements exist compared to a full model, substantially speeding up iterations and minimising computational power. The model is shown in Figure 7-1.

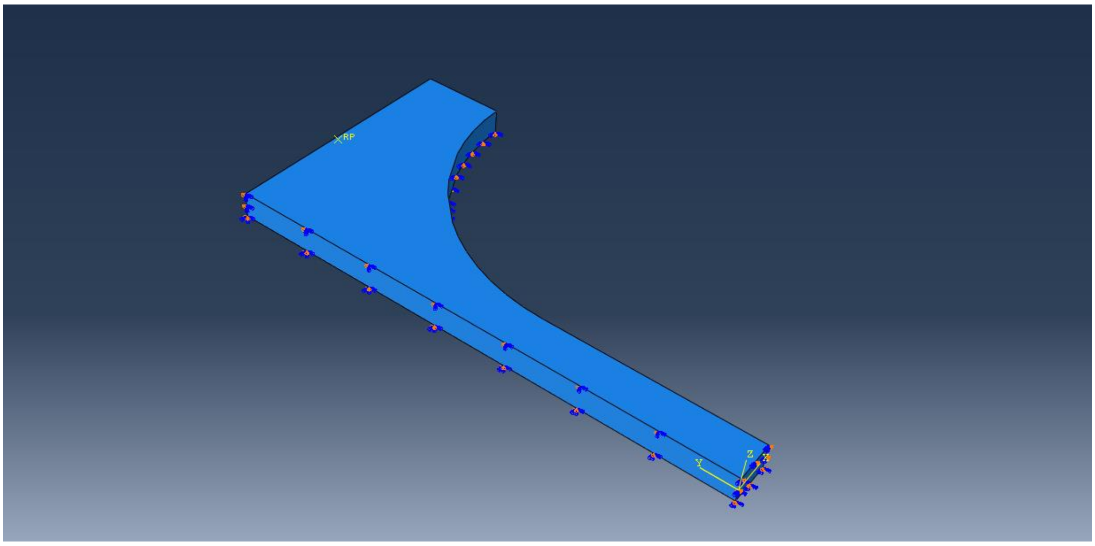

Figure 7-1: *1/8th model of the 3mm tensile coupon*

The boundary conditions include a displacement applied to the end of the coupon as if mounted in a tensile machine. The applied displacement (2mm) was taken from the experimental data in Chapter 4. The step size of the analysis was set at 0.05, therefore increments of 0.1mm of displacement are applied until the simulation cannot converge and the step size becomes smaller. The model has a global mesh seed of 0.2mm. Figure 7-2 shows the stress versus strain for the 3mm tensile coupon over its parallel length. The physical data is an averaged data set of 5 tensile coupons.

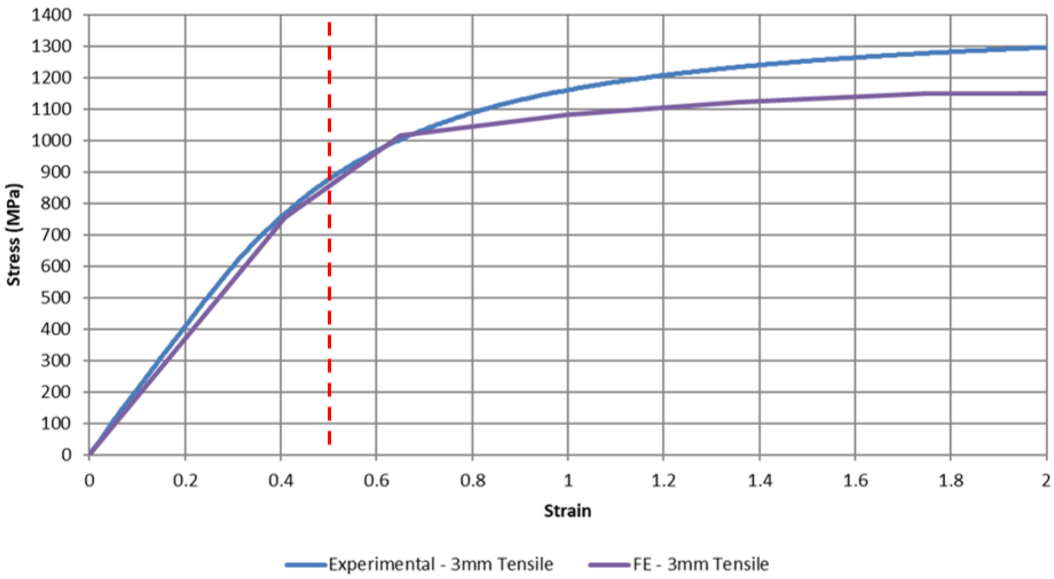

Figure 7-2: *Stress v Strain for 3mm tensile coupon of core material properties – FE and Experimental data. The transparent region represents the range of strains of least importance to the industrial sponsor.*

Figure 7-2 shows the experimental data and FE simulation are comparable in the elastic region and initial phase of yielding. There is some difference in the elastic stiffness, however. Plastic behaviour is largely comparable up to 0.65% strain. This comparison is acceptable as the industrial sponsor requires comparable behaviour up to 0.5% strain (left side of red dotted line) only (Personal Communication, 2017). To better represent the model at strains of above 1%, the B value used to generate the plastic stress-strain curve could be re-investigated. The B value is a value that represents the stress increase from the yield to the UTS. Increasing this value by the order of 150MPa would generate more comparable behaviour between the FE and experimental results, however may compromise the immediate behaviour post yield. Figure 7-3 shows the stress-strain curve generated by the Johnson Cook equation with current and suggested values of B.

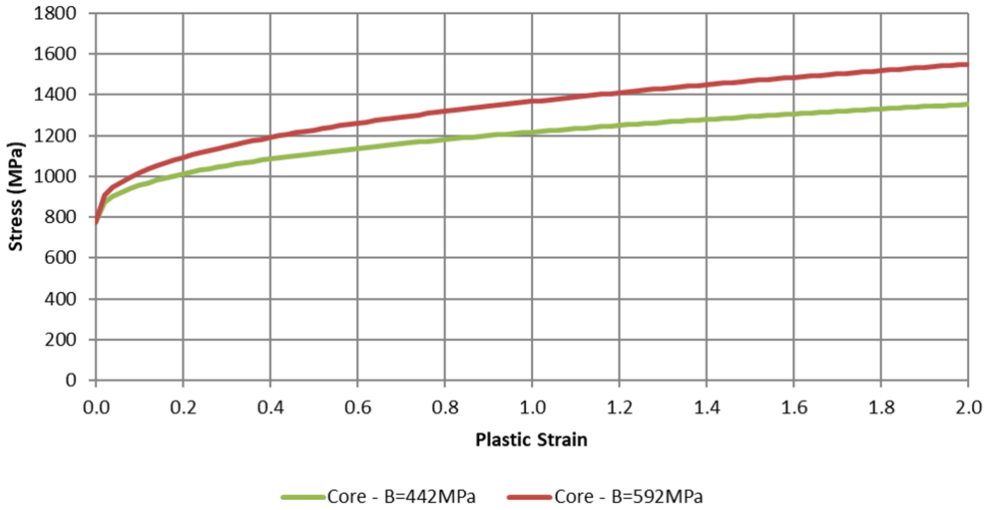

Figure 7-3: *Comparison of stress versus strain for different Johnson Cook "B" values*

7.2. Tensile Coupon (6mm – Variable Material)

Similar to the 3mm tensile coupon model, the 6mm sample follows the same philosophy of a one-eighth model. The difference here, along with the thickness, is the inclusion of a case layer, which requires the use of data from Chapter 4 and the application process from Chapter 5. Figure 7-4 shows the meshed model with a 0.1mm mesh with material properties applied.

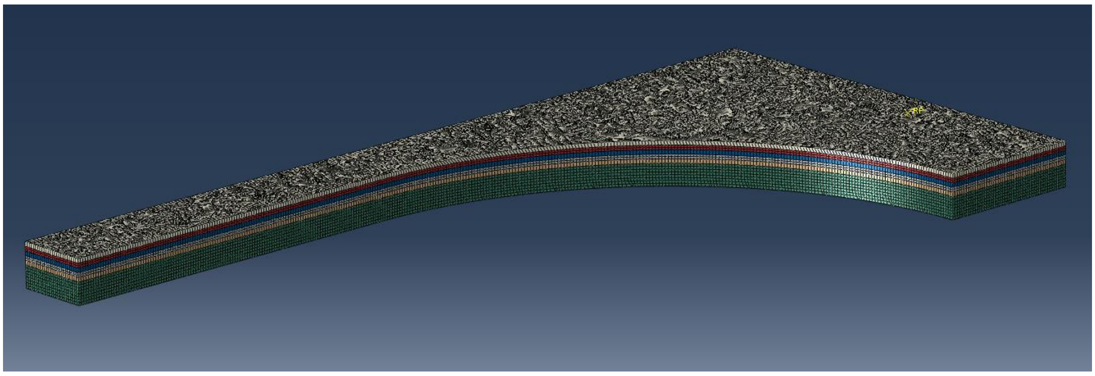

Figure 7-4: *6mm tensile coupon model completely meshed with material properties applied.*

The various materials assigned to the case by the FGM code are clearly shown in Figure 7-5.

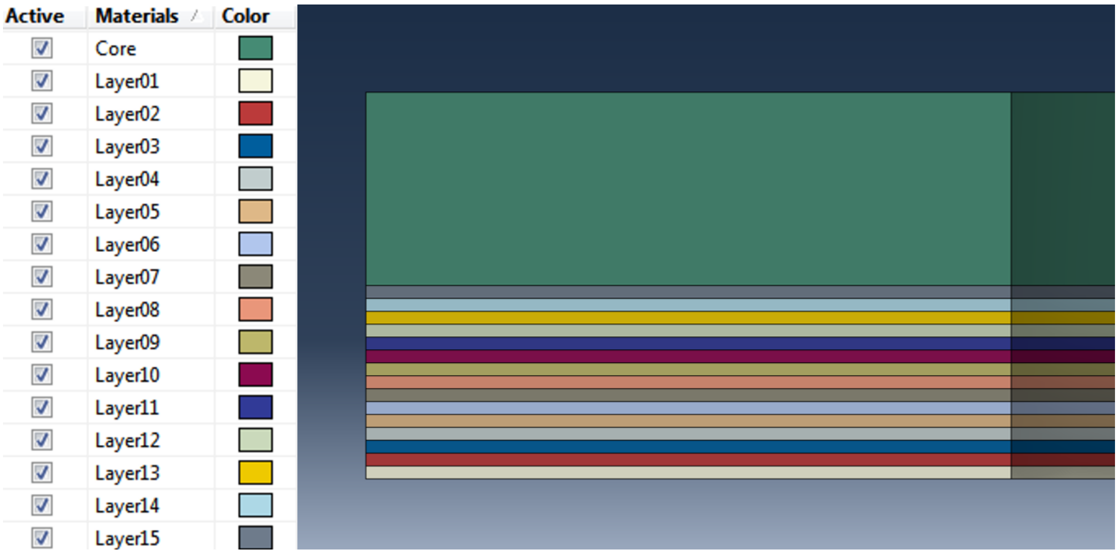

Figure 7-5: *6mm tensile coupon model with materials applied within the case depth.*

Boundary conditions and step size are identical to that of the 3mm section.

Figure 7-6 shows the Stress v Strain comparison between the experimental and FE model. The physical data is the averaged data set of 5 tensile coupons.

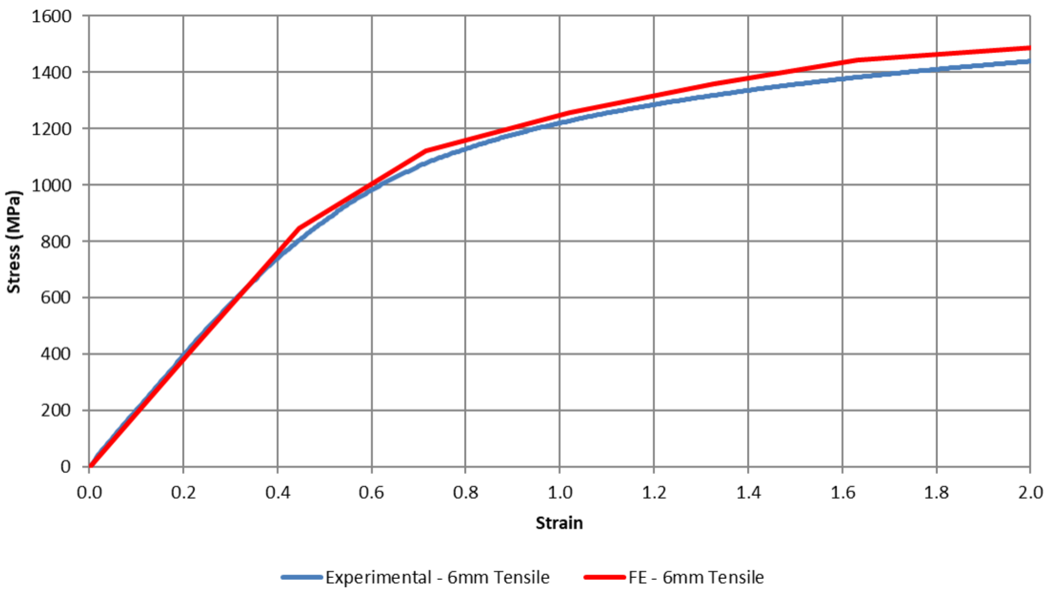

Figure 7-6: *Stress v Strain for 3mm tensile coupon of core material properties – FE and Experimental data*

Figure 7-7 shows a Von Mises stress contour plot of the 6mm tensile coupon with the case layer included. The case layer is at the bottom of the figure, where the mesh density is higher. The stress contour clearly shows how the load capacity of the case layer is higher than that of the core. There is considerably more stress (500MPa) being carried by the case layer in this instance.

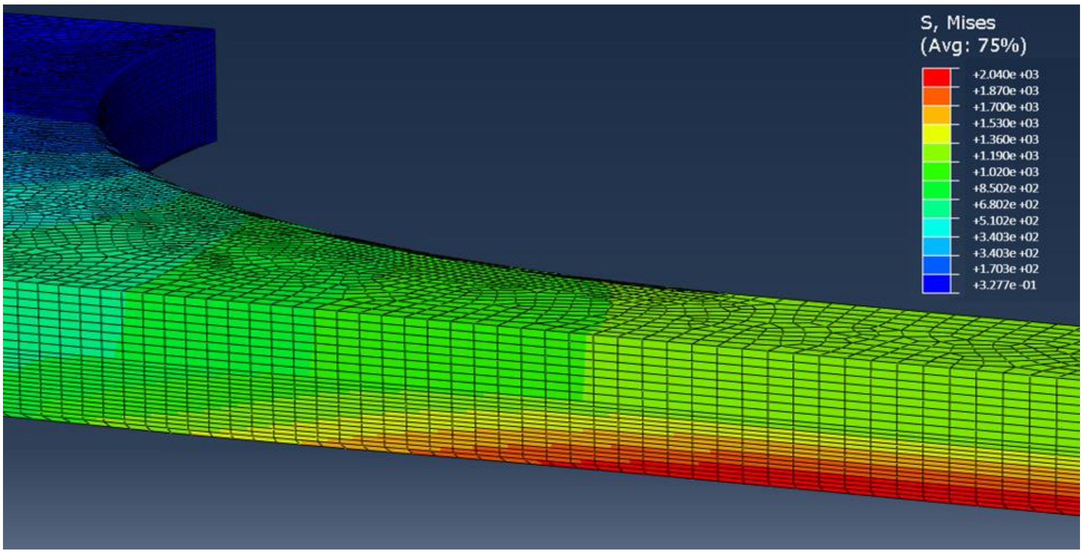

Figure 7-7: *Von Mises stress contour for 6mm tensile coupon with case layer*

The experimental and FE results are comparable through all regions of the stress-strain curve. Behaviour at the yield is satisfactory, however as the strain increases above 1% the FE and experimental data diverge by a consistent 3%. As with the 3mm tensile model, the B value from the Johnson Cook equation can be reinvestigated. A lower value over the layers would generate more comparable results at the UTS, however could compromise the comparison of behaviour immediately post yield.

As a comparison between FE and experimental data, the 6mm tensile coupon with full case layer modelled has produced satisfactory correlation. To increase confidence in the modelling of the case layer, additional simulations of a partial case could be of benefit. As there is sufficient experimental data from Chapter 4, this should be considered as an area for further work.

7.3. Gear Model

To create a representative computational model, the necessary complexities of the real gear must be incorporated into the model. As discussed in Chapter 2, FE models of gears have little to no specific standards for their modelling. The following points were included in the FE gear model. Figure 7-8 shows the gear model used for the remainder of this chapter.

1. Symmetry based boundary conditions were applied to create one-quarter of the model. The gear was sectioned axially and radially.
2. The number of gear teeth were reduced to four. Two adjacent teeth either side of the loaded tooth are included to produce representative geometry and therefore behaviour during the simulation.
3. Simplification of geometry around the unloaded side of the model that reduces the complexity of the geometry and volume, thereby reducing the number of elements.
4. Reduced mesh density in the unloaded area of the model. The mesh size increased from 0.1mm (around the loaded gear teeth) to 2mm on the left hand side of Figure 7-9.
5. Material was removed from either side of the tooth to replicate the gear test from Chapter 6. Thus creates a two-dimensional case penetration.
6. Anvils are represented by discreet rigid shell elements. All nodes are coupled to a single master node, which is assigned the displacement boundary conditions representing the movement of the crosshead.

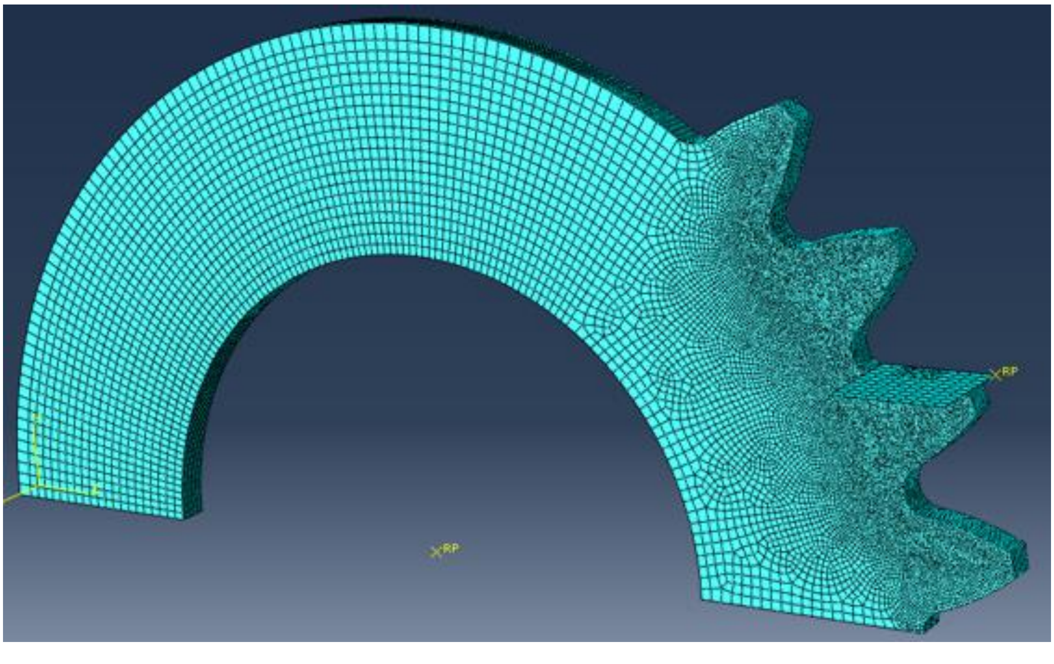

Figure 7-8: *Fully meshed validation model*

Figure 7-9 below shows a detailed view of the element density changes from the flank of the loaded teeth through to the core.

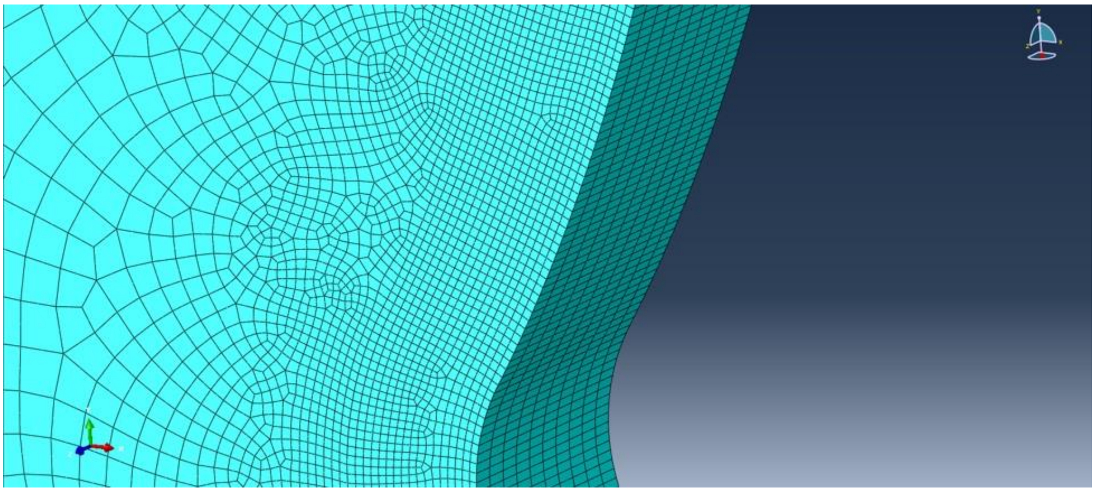

Figure 7-9: *Detailed mesh on the gear flank on the full validation model*

Figure 7-10 shows the material properties applied to the gear by the FGM code. Using the FGM code outlined in Chapter 5, a mesh of 0.1mm was applied to the loaded teeth (shown clearly in Figure 7-9, and 15 material properties were applied within the 1.5mm case layer. Note the change in material property (via colour plot) on the left hand side of the Figure where the flank of the adjacent tooth has a larger mesh size.

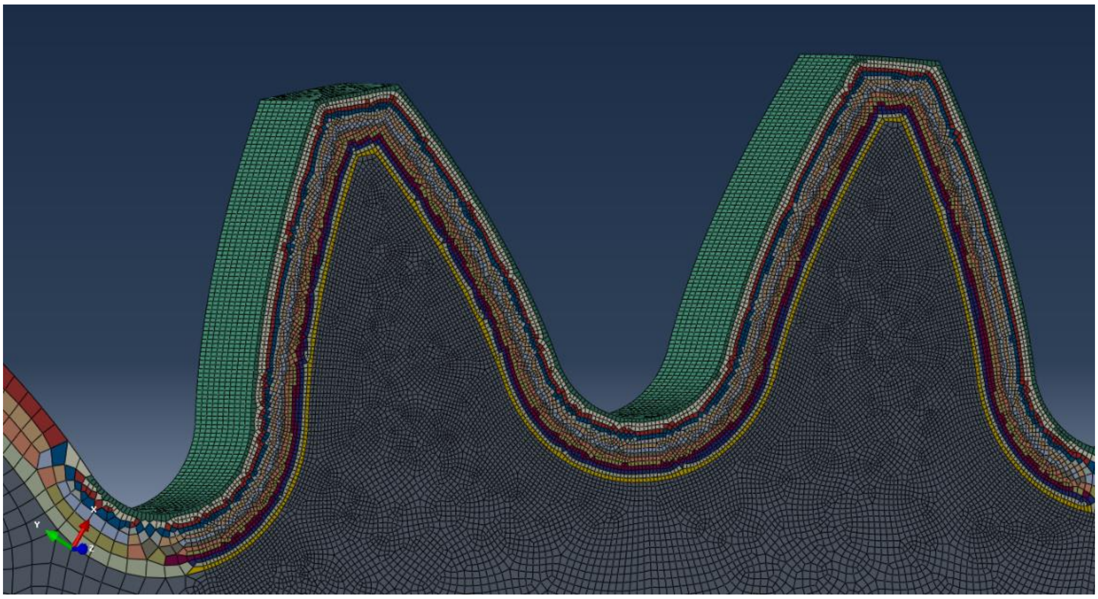

Figure 7-10: *15 layers of materials properties within the case layer*

7.4. FE Results

Figure 7-11 shows the load versus displacement results for both the experimental and FE simulations of the gear validation test. The experimental load and displacement is taken from the load cell and the LVDT, respectively. The FE load is calculated as the reaction force (in the vertical Y axis) of the master node of the anvil (discreet rigid shells). The displacement was calculated as being the time step of the model multiplied by the specified displacement rate. In this instance, the displacement applied is 1mm, therefore the same as the step. Three FE results are shown for comparison - a case layer consisting of 15 materials (the same as the tensile coupon in Figure 7-7, a single (hardest/strongest) material property over the case layer and another model with core material properties applied to the case.

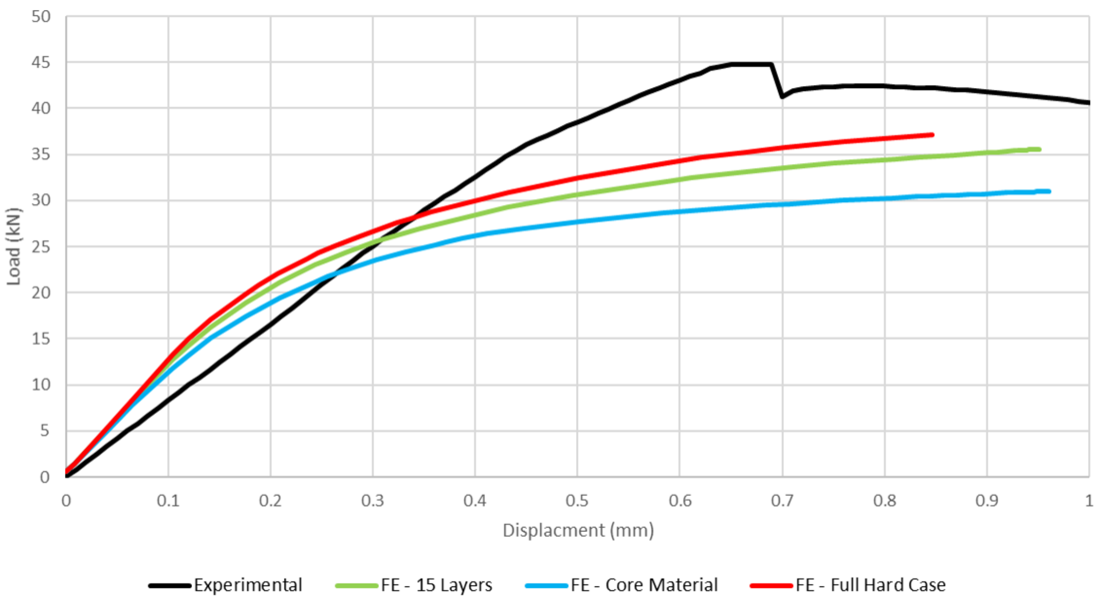

***Figure 7-11:** Load v displacement for experimental and FE simulations*

To account for the symmetrical boundary conditions, a factor was applied to the load and displacement data to make it directly comparable to the experimental data. There is some discrepancy between the FE and the experimental results. It is apparent that the experimental setup is less stiff than that represented in FE. This is expected as there will inevitably be compliance within the load machine, fixtures and LVDT mounting, which are modelled as rigid bodies in the FE model. Additionally, the gear is modelled as a single axial thickness, which equates to the test sample used in Chapter 6 in the region of the loaded teeth, but away from this region the gear thickness varies. Figure 6-1 shows how the body of the gear has been pocketed to minimise the mass of the component. This missing material also contributes to the mismatch in elastic stiffness between experimental and FE.

The FE results themselves are as expected. In the elastic region, all models display comparable behaviour. The 'full hard' case layer is clearly stronger post-yield than the layer controlled by the FGM or the core material applied to the case, however the 'full hard' model is not representative of a case hardened layer. The contribution of the case makes a substantial increase to the strength of the gear when compared to the model featuring only the core material. In terms of load capacity, there is 16% increase between the model using only the core material and the model with a representative case layer.

Figure 7-12 shows a Von Mises Stress contour plot of the gear validation model. Note the stress in the adjacent teeth is minimal; therefore there is scope to further refine the model. This could involve removing the left hand tooth seen in the Figure, and further increasing the mesh size to reduce the number of elements and thus reduce the time taken to run the FGM code and Finite Element simulation. Increased computational efficiency would also result. Note, the shell mesh that represents the anvil has been hidden.

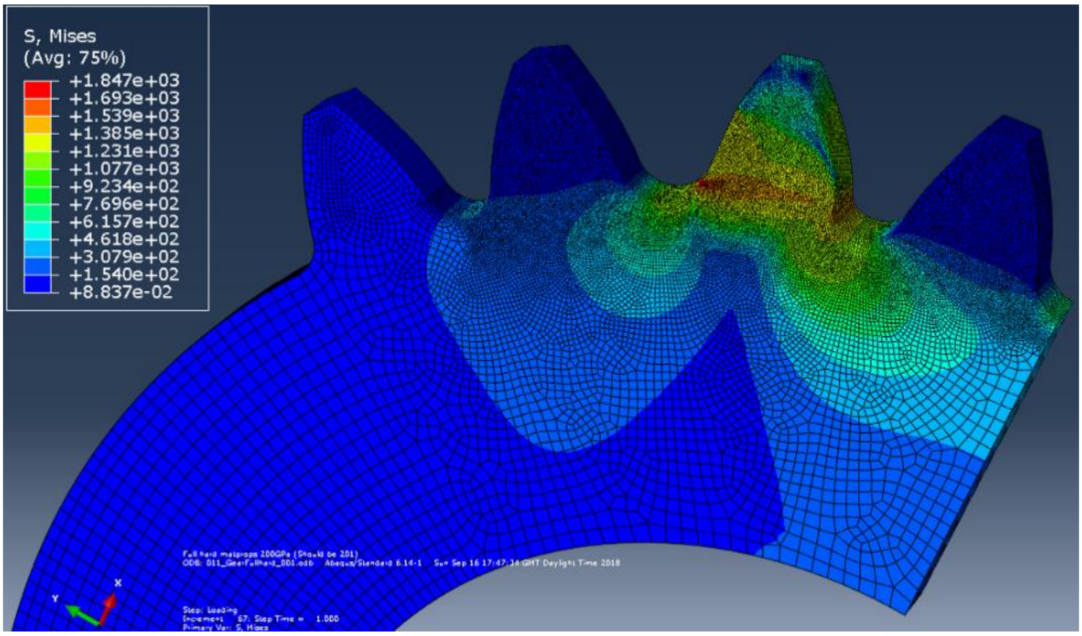

Figure 7-12: Full validation model loaded in FE

In the validation test from Chapter 6, the VSG system was used to monitor the tooth and displayed a colour plot of the displacement in the Y axis. Figure 7-13 shows four colour plots for the Y displacement at different loadings. The order of increasing load within the Figure is top left (lowest load), top right, lower left, lower right (highest load).

It is clear that as the load increases that the band of yellow becoming increasingly apparent and moving closer to the root. This band indicates less displacement on the flank of the gear tooth, as expected due to its restraint against the anvil. The red area of the colour plot indicates the most displacement over the colour plot shows that the gear tooth is plastically deforming at this point.

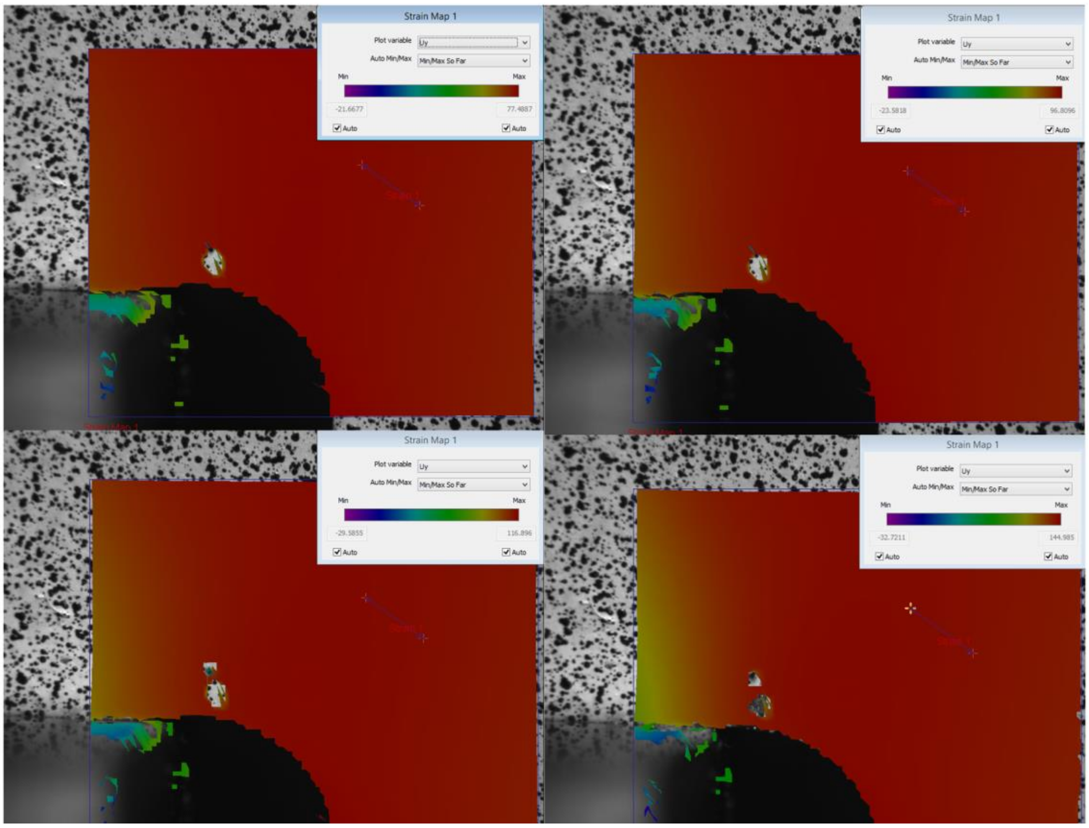

Figure 7-13: *Y (Vertical) displacement colour plot from the VSG system during loading*

Figure 7-14 shows a Y displacement colour plot generated from *ABAQUS* for the same FOV as monitored by the VSG system. It is clear that the behaviour of both are comparable from visual inspection as fringes of the colour plot at comparable angles. The displacement at the edge of the anvil from the VSG system is 0.12mm as calculated from the bottom right plot of Figure 7-13. For the same location on the FE plot of Figure 7-14, a displacement of 0.102mm is found. These values of displacement are given at 0.35 mm of crosshead/anvil displacement when the force v displacement curves of the experimental and FE cross over as shown in Figure 7-11. Therefore the values are of the same order, and comparable to each other.

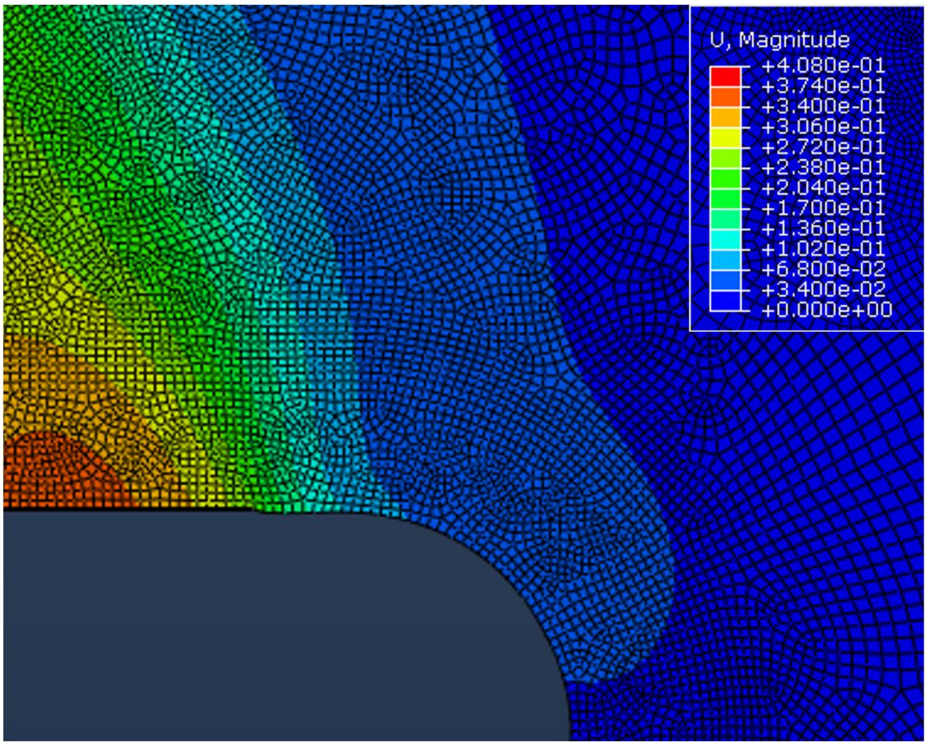

Figure 7-14: *Y (vertical) displacement colour plot from FE.*

Figure 7-15 shows the gear after failure. The crack propagating through the tooth is obvious. The colour plot was still applied in the VSG GUI as can be seen by the green section on the left hand side of the crack. Due to the sudden movement of the tooth during failure, the colour plot can no longer track the displacement over the speckle pattern.

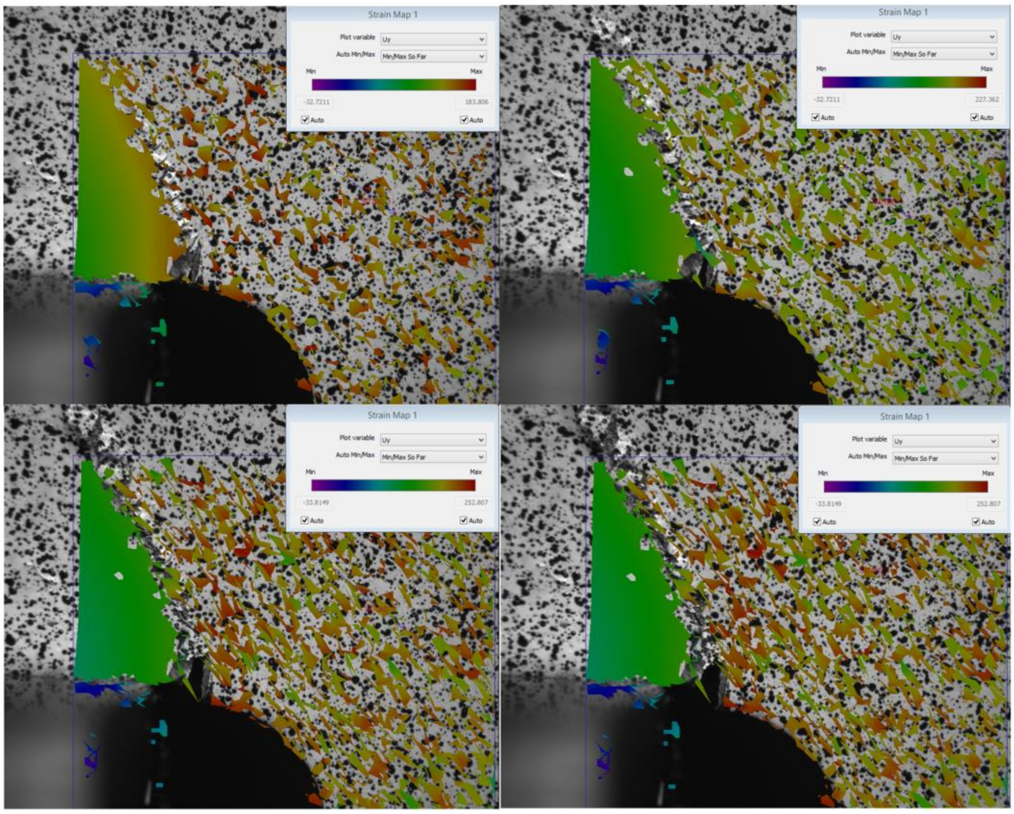

Figure 7-15: *Y (Vertical) displacement colour plot from the VSG system during failure*

7.5. FE Discussion

Chapter 2 outlined the importance of computational efficiency when running complex FE models. With the development in computing power, including cloud based computing, speeds are ever increasing and therefore run times for the models are decreasing. As in any sector in engineering, limits are constantly being pushed by the Engineers/Researchers. If a small gain in performance is possible from running an increased number of model iterations, it is usually worth the additional time and effort, especially if there is a gain to be made in performance, material or manufacturing costs. When small models (two-dimensional models or simple three-dimensional models for instance) are iterated, results are attainable in a matter of minutes. In the time it takes for an Engineer to plot the results, understand them, record them and make an informed decision on the next step, another iteration could have run. The FE models of 3mm tensile, 6mm tensile and gear models run as part of Chapter 7 of this Thesis took approximately 15 minutes, 30 minutes and 4 hours respectively to solve.

With these solution times in mind, an Engineer could simulate dozens of iterations of a tensile coupon through a working day and make iterative decisions (performance or correlation) based on their results. Inversely, with the models which take longer to run, the Engineer would queue iterations of the gear model overnight and analyse the results in a single block. With this insight, the computational efficiency does not seem of substantial importance. However, efficiency will always be considered in the model build by simplifying areas of complexity or changing the density of the mesh to reduce run times. This efficiency is not a conscious decision to be efficient, it is usually due to the impatience of the user.

In the simplification of the gear FE models included in this chapter, the number of teeth was reduced to two adjacent to the loaded tooth. This has proved to be a reasonable assumption as shown in Figure 7-12. The Figure shows the Von Mises stress distribution through the gear. The minimum stress shown on the colour plot is 8.8MPa and apparent through the main body of the gear. When comparing this stress to that of the peak stress (1847MPa) and the yield stress of the material (775MPa) it is apparent that there is negligible stress within the left hand side of the model, including the left hand tooth. Therefore there is scope to further simplify the model by removing the tooth on the left of Figure 7-12. Additionally, the mesh could be made coarser in this area to further reduce the time required to run the simulation. Having a coarser mesh in this area would also reduce the time required for the FGM algorithm to be applied. As the second lowest stress distribution in the colour plot is 154MPa, the removal of another tooth may affect the stress in this area. If it is desirable to remove the tooth completely it is recommended to take the approach of Çelik (1998) shown in Figure 2-8, where the radius of the gear body is that of the base radius of the involute rather than the diameter at the apex of the root fillet, as used in the cimulations of this chapter.

Chapter 2 discussed the mesh size used for gear simulation within literature. As previously stated, the mesh size must be appropriate for the model, thus sufficiently small to achieve the detail required of the model. Within literature, mesh sizes were discussed and found that a mesh size of 0.2mm was suitable for the flank of a gear tooth to produce representative behaviour for bending stresses (Personal Communication, 2017) and 0.5mm for the root fillet (Lisle, 2017). Within the FE models presented in this Thesis the mesh around the surface of the teeth is 0.1mm such that sufficient detail can be produced and in order to demonstrate the application of an FGM. Within industry, this is a mesh size that is not typical of this analysis however with increasing detail and complexity being included in simulations, may take place in future.

7.6. FE Conclusion

In summary, FE simulations of tensile coupons were validated by experimental data from Chapter 4. The 3mm tensile coupon FE models demonstrated a deviation in the elastic region, and good correlation in post yield behaviour, however they deviated further as the material approached its UTS. The 6mm tensile coupon (with representative case layer) had good correlation to the experimental data and matched over the elastic and plastic range.

Knowing that the material data of tensile coupons has been correlated, the case has been successfully applied to a gear model. Simulations using 'full hard' and 'core' properties applied to the case provided insight into the increased load capacity of a case hardened gear. The gear was compared to the validation data and some disparity found. This has been attributed to the compliance of the fixtures and measurement error. As the UTS of the 3mm tensile coupon comparison is lower than in the experimental test, the model would perform closer to the experimental data for the gear test, should the UTS/B value of the Johnson cook equation be revisited. When compared to the VSG system, the gear demonstrated comparable behaviour when approaching failure

8. Discussion, Conclusion & Future Work

8.1. Material Data Discussion

During the experimental work conducted in Chapter 4 of this Thesis, a method was developed of measuring the variation of elastic-plastic material properties over a case depth for an S156 gear steel and the specified heat treatment for the industrial sponsor. Were the industrial sponsor to change the specification of its gear steel in future or investigate an alternative heat treatment, repeat testing would be required. However, the sponsor has converged on this composition of material through the testing of S156 against alternative gear steels such as NC310YW and FND-YW, therefore the content of this Thesis relevant for the near future.

When a suitable replacement for S156 or an alternative specification of case hardening is found, the method outlined in Chapter 4 of this Thesis can be implemented to understand the properties of the new material and heat treatment. Additionally, this method could be applied to alternative heat treatments such as induction hardening, plasma nitriding or tempering. Therefore this method has further scope within material science and is not limited to the application stated in the initial brief of this research.

It is important to note that when implementing the data Chapter 4 of this Thesis, that any variation within each material or heat treatment batch be understood and quantified. This can be done either as a hardness check through the case, or with the inclusion of tensile coupons in a batch of gearbox components. From these batch checks,

8.2. Functionally Graded Material Discussion

This aspect of work has successfully allowed the user to apply depth dependant material properties to complex FE models without the time consuming operation of partitioning models within the FE GUI. The method in which the FGM is applied within this Thesis is design as such that it fits in with the process currently conducted by the simulation engineers within the industrial sponsor. As the sponsors engineers produce an *ABAQUS* input file from an Altair software, it is possible at this point to use the FGM algorithm prior to its running. As emphasised in Chapter 5, the engineer creating the FE model is required to produce a model of sufficient quality for the FGM code to be effective. Figure 8-16 shows an example of bad mesh quality along the flank of a gear tooth. The input file for the gear was generated, run through the FGM algorithm, input file re-written and imported back into the *ABAQUS* GUI. Were the mesh of a higher quality, elements would run in parallel rows relative to the flank of the gear tooth. It is clear that the elements in the center of the case layer (coloured elements) are highly variable in size, skewness, aspect ratio and the properties applied to them. Were the elements of a sufficient quality, then the colour plot would appear as straight bands of elements from the flank through to the core.

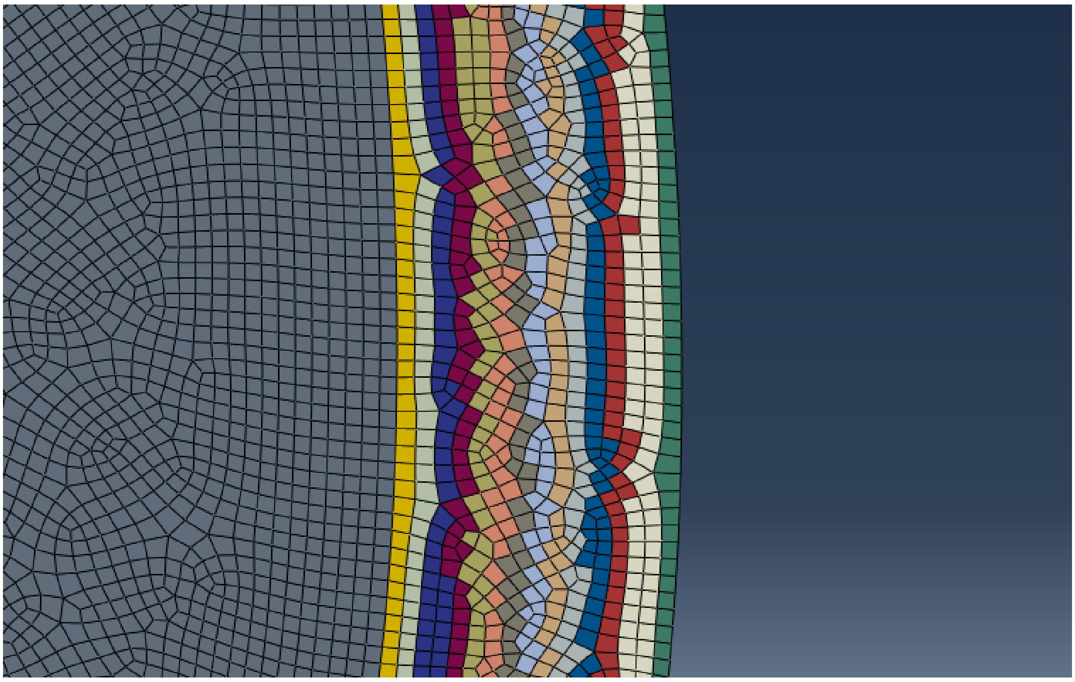

***Figure 8-16**: Influence of poor mesh refinement on FGM*

Following the running of the *MATLAB* algorithm a .txt file is produced that includes sets of element based on their depth from the surface. Following the output of the sets of elements, there is a requirement of the user to manually manipulate the input file to include the desired material properties and sections. Although it was desirable to automate this process and include it within the *MATLAB* algorithm, as this research is a proof of concept it was deemed acceptable to manually re-write the input file. Were this research being continued by the Author, it would be a priority to automate the re-writing of the input file to reduce time to apply a FGM and to further streamline the implementation of this work within the simulation team of the sponsor. Additionally, the inclusion of the Johnson Cook parameters from Chapter 4 would be brought into the algorithm such that material properties could be generated and applied for any depth from the surface, not grouped into layers as they have been within this Thesis. In the further work section later in this chapter, further suggestions for developing the FGM algorithm are explained in durther detail.

8.3. Validation Discussion

Through the use of a VSG non-contact measurement system, a validation process was outlined the testing of a gear tooth to provide sufficient data to validate an FE model. Using a quasi-static approach to gear testing, it was possible to ensure that the FOV of the non-contact measurement system included the whole area of interest on the gear root.

All instrumentation specified for this test was successful in producing data in the correct order of magnitude to make direct comparison to the values calculated from FE. It was noted in Chapter 6 that compliance within the system contributed to the loaded gear and the fixture slipping against ne another. Were the test to be repeated it is recommended that additional LVDTs are mounted in the x and y plane to confirm deflection in these axis and to quantify it. For further testing and increased number of data sets would be desirable. When averaging loads and deflections over multiple gear tests greater confidence can be had in the data.

8.4. Finite Element Analysis Discussion

The main difference between the methods used by the Author and the industrial sponsor at the modelling stage is in the software used. The sponsor creates FE models within Altair's Hypermesh software where geometry clean-up, meshing, boundary conditions, loads and material properties are applied. It is then exported as an *ABAQUS* input file and run in the *ABAQUS* solver. The reason for the mixing of software is due to the preference of the engineers who create and run the simulations and the superior mesh control available within the Altair software. Despite the crossover of software, results will not be affected as the analysis is implicit. Once the solver has run the model, the results are then imported to Altair HyperView software where results are analysed. For the Author all of the aforementioned pre and post-processing work on the models was completed within *ABAQUS*.

In the comparison between FE and experimental data for the tensile coupons from Figure 7-2 and Figure 7-6, correlation was satisfactory up to the value of 0.5% therefore satisfying the criteria from the industrial sponsor. In analysing the curves, it is apparent that specifying more integration points in the FE analysis would provide a better comparison between the two data sets.

The FE simulation of the tensile coupons in Chapter 7 was limited to the 3mm and 6mm variants. As there is existing experimental data for tensile coupons at 0.25mm increments from 3mm to 6mm, further simulation would provide greater confidence in the FE material models. This additional simulation would provide an understanding of how accurate how representative the case layer is being simulated at increments through the case. Following this additional simulation and the resulting data analysis, the equations derived at the end of Chapter 4 can be revisited and modified such that the most representative simulation of the case is achieved.

8.5. Conclusion

This Thesis has provided a literature review, outlining the current approaches to gear modelling used in both industry and research. This included a review of the current standards that outline gear design parameters based on historical physical test data. A review was conducted of computational methods that outlines the important parameters for simulation in general and more specifically for gears. Topics such as computational methods of gear analysis, the modelling software, modelling philosophy, element type, meshing, simplification and computational power were all discussed with firm conclusions regarding the most suitable means of modelling gears.

A test method was provided which, through the testing of case hardened tensile coupons with specific amounts of the case layer removed, generated material data which was analysed with a new approach. Using this data and a new approach, the elastic-plastic behaviour at any depth through a case hardened layer was established.

So that an FE model has the most representative material properties applied for a case hardened layer, an FGM was discussed, developed and produced. The FGM uses data from an FE input file from *ABAQUS CAE* that is manipulated using a *MATLAB* algorithm which extracts node and element coordinates and uses them to assign a material property for each element, based on a user defined depth variable.

Representative material data for a case layer was applied to FE tensile coupon models and validated using experimental data. These material properties were then applied to a gear model, using the FGM. These results were then compared to experimental data with the behaviour also compared using a VSG camera system.

8.6. Future Work

8.6.1. Characterising material properties by Hardness

To characterise the heat treatment further, it is suggested that the relationship between material hardness and the elastic-plastic material parameters be generated. Were a relationship established it would then be possible to investigate the effect of varying parameters within the heat treatment process and estimate its influence on overall gear performance. As the simplest, quickest, cheapest and more established method of quality control within metallurgy is to section components and perform micro-hardness measurements along the case depth, this would perhaps be the most elegant means of measuring the mechanical properties through a case layer, particularly if force-sensing equipment could be used to directly measure the stress-strain curves and their variation across the case depth.

8.6.2. Further modelling of tensile coupon with intermediate sections of case

The simulation of tensile coupons in Chapter 7 was limited to the 3mm and 6mm variations. Additional simulation of intermediate layers would increase confidence in the material data and confirm provide a further correlated model throughout the case layer. As the experimental data for 0.25mm increments of case removal exists, five more coupon models can be investigated.

8.6.3. FGM depth criterion

The depth criterion used in the FGM algorithm of Chapter 5 uses the distance between the element centroid and each of the surface nodes. An alternative approach where the shallowest nodes are compared to the surface nodes would ensure that the elements on the surface of the component are allocated the hardest/most representative material property.

8.6.4. Application for alternative heat treatments

As previously mentioned, the method outlines in Chapter 4 has the possibility to be applied to alternative materials and heat treatments. Induction hardening, plasma nitride and tempering are all examples of heat treatments commonly used within industry.

A literature review investigating the inclusion of these alternative heat treatments in industry and how they are simulated would benefit in understanding the scope of the future work. Hardness testing of sectioned components for each of the heat treatments would provide an understanding of how the properties change through the heat affected zone. This data can be analysed to find the variation in properties and depth, which in turn can inform further coupon testing.

8.6.5. Improvement of strain correlation above 0.5%

Figure 7-2 demonstrates good correlation between experimental data and simulation for strain values of up to 0.7%. This satisfies the initial criteria from the industrial sponsor to have a good understanding for strain of up to 0.5%. For any strain above this point, an investigation into the "B" value of the Johnson Cook equation from Chapter 4 would lead to increased correlation at these higher values of strain.

As the industrial sponsor for this research requested that strain measurement and simulation have accurate correlation up to 0.5%, Figure 7-2 shows that this be characterised with well replicated within simulation was monitored, understood and characterised. specification of the industrial sponsor of this Figure 7-2

8.6.6. Automating re-writing of FE input files

Following the running of the *MATLAB* algorithm in Chapter 5, there is substantial manipulation required by the user to re-write the FE input file prior to re-importing to the *ABAQUS* GUI. There are several sections of additional code that would reduce the time to apply the FGM and to streamline the process for the industrial sponsor.

Modifying the code at the point that the node and element sets are generated from the *MATLAB* algorithm would allow the correct naming convention to be included in the .txt that is generated. This can also include the correct format for the input file and also define the sections, where the sets and the material properties are linked.

The material properties could also be generated within the algorithm. Were the eleastic modulus and Johnson Cook parameter equations from the end of Chapter 4 included in the algorithm, then the A, B and n values can be generated for any depth through the case. Therefore, it would be possible to write a stress v plastic strain curve for any given depth through the case, and output it into the correct format for the input file.

9. References

Abudaia, F. B., Evans, J. T. and Shaw, B. A. (2005) 'Spherical indentation fatigue cracking', *Materials Science and Engineering A*, 391(1–2), pp. 181–187. doi: 10.1016/j.msea.2004.08.068.

Ahamed, N., Pandya, Y. and Parey, A. (2014) 'Spur gear tooth root crack detection using time synchronous averaging under fluctuating speed', *Measurement*. Elsevier Ltd, 52, pp. 1–11. doi: 10.1016/j.measurement.2014.02.029.

American Gear Manufactures Association (2004) 'ANSI/AGMA 2001-D04 Fundamental Rating Factors and Calculation Metrhods for Involute Spur and Helical Gear Teeth', 4, p. 66. Available at: ANSI/AGMA 2001-D04.

Andrews, J. D. (1991) 'a Finite Element Analysis of Bending Stresses Induced in External and Internal', 26(3).

Antunes, J. M. *et al.* (2007) 'A new approach for reverse analyses in depth-sensing indentation using numerical simulation', *Acta Materialia*, 55(1), pp. 69–81. doi: 10.1016/j.actamat.2006.08.019.

Baragetti, S. (2007) 'Fatigue resistance of steel and titanium PVD coated spur gears', *International Journal of Fatigue*, 29(9–11), pp. 1893–1903. doi: 10.1016/j.ijfatigue.2006.11.005.

Barbieri, M., Zippo, A. and Pellicano, F. (2014) 'Adaptive grid-size finite element modeling of helical gear pairs', *Mechanism and Machine Theory*. Elsevier Ltd, 82, pp. 17–32. doi: 10.1016/j.mechmachtheory.2014.07.009.

Barsoum, I., Khan, F. and Barsoum, Z. (2014) 'Analysis of the torsional strength of hardened splined shafts', *Materials & Design*. Elsevier Ltd, 54, pp. 130–136. doi: 10.1016/j.matdes.2013.08.020.

Bepari, M. M. A., Haque, M. N. and Md. Shorowordi, K. (2010) 'The structure and properties of carburized and hardened vanadium microalloyed steels', 83–86, pp. 1270–1281. doi: 10.4028/www.scientific.net/AMR.83-86.1270.

Branch, N. A. *et al.* (2010) 'Material-dependent representative plastic strain for the prediction of indentation hardness', *Acta Materialia*. Acta Materialia Inc., 58(19), pp. 6487–6494. doi: 10.1016/j.actamat.2010.08.010.

Branch, N. A. *et al.* (2011) 'A new reverse analysis to determine the constitutive response of plastically graded case hardened bearing steels', *International Journal of Solids and Structures*, 48(3–4), pp. 584–591. doi: 10.1016/j.ijsolstr.2010.10.023.

Brauer, J. (2004) 'A general ÿnite element model of involute gears', 40, pp. 1857–1872. doi: 10.1016/j.

Brauer, J. (2005) 'Transmission error in anti-backlash conical involute gear transmissions: a global–local FE approach', *Finite Elements in Analysis and Design*, 41(5), pp. 431–457. doi: 10.1016/j.finel.2004.04.007.

Bray, A. *et al.* (1998) 'An Automatic Procedure for Evaluation of Young's Modulus of Metallic Materials', *Journal of Testing and Evaluation*, 26(1), pp. 64–69. Available at: http://www.scopus.com/inward/record.url?eid=2-s2.0-0031653194&partnerID=40&md5=dc5d0c44ebed8e26de6f467e12de6aa3.

Bryant, M. (2013) 'Running-in and residual stress : finite element contact analysis of as measured rough surfaces and comparison with experiment', (July).

Çelik, M. (1999) 'Comparison of three teeth and whole body models in spur gear analysis', *Mechanism and Machine Theory*, 34(8), pp. 1227–1235. doi: 10.1016/S0094-114X(98)00058-5.

Chaouch, D., Guessasma, S. and Sadok, a. (2012) 'Finite Element simulation coupled to optimisation stochastic process to assess the effect of heat treatment on the mechanical properties of 42CrMo4 steel', *Materials & Design*. Elsevier Ltd, 34, pp. 679–684. doi: 10.1016/j.matdes.2011.05.026.

Chen, C. F. and Tsay, C. B. (2005) 'Tooth profile design for the manufacture of helical gear sets with small numbers of teeth', *International Journal of Machine Tools and Manufacture*, 45(12–13), pp. 1531–1541. doi: 10.1016/j.ijmachtools.2005.01.017.

Chen, X. *et al.* (2018) 'Effect of heat treatment on microstructure, mechanical and corrosion properties of austenitic stainless steel 316L using arc additive manufacturing', *Materials Science and Engineering A*. Elsevier B.V., 715(October 2017), pp. 307–314. doi: 10.1016/j.msea.2017.10.002.

Ciavarella, M. and Demelio, G. (1999) 'Numerical methods for the optimisation of specific sliding , stress concentration and fatigue life of gears', 21, pp. 465–474.

Coy, J. J. and Chao, C. H. C. (1981) 'A method of selecting grid size to account for Hertz deformation in finite element analysis of spur gears', 104(October 1982), pp. 759–764. doi: 10.1115/1.3256429.

Dabnichki, P. and Crocombe, A. (1999) 'Finite element modelling of local contact conditions in gear teeth', *Analysis*, 34(2), pp. 129–142. doi: 10.1243/0309324991513957.

Ding, Y., Jones, R. and Kuhnell, B. (1995) 'Numerical analysis of subsurface crack failure beneath the pitch line of a gear tooth during engagement', *Wear*, 185(1–2), pp. 141–149. doi: 10.1016/0043-1648(95)06592-X.

von Eiff, H., Hirschmann, K. H. and Lechner, G. (1990) 'Influence of Gear Tooth Geometry on Tooth Stress of External and Internal Gears', *Journal of Mechanical Design*, 112(4), p. 575. doi: 10.1115/1.2912649.

Elghazal, H. *et al.* (2001) 'Microplasticity characteristics obtained through nano-indentation measurements: application to surface hardened steels', *Materials Science and Engineering: A*, 303(1–2), pp. 110–119. doi: 10.1016/S0921-5093(00)01852-9.

Filiz, H. I. and Eyercioglu, O. (1995) 'Evaluation of Gear Tooth Stresses by Finite Element Method', *Transactions of the American Society of Mechanical Engineers*, 117(May), pp. 232–239. doi: 10.1115/1.2803299.

Fuentes, A., Ruiz-Orzaez, R. and Gonzalez-Perez, I. (2014) 'Computerized design, simulation of meshing, and finite element analysis of two types of geometry of curvilinear cylindrical gears', *Computer Methods in Applied Mechanics and Engineering*. Elsevier B.V., 272, pp. 321–339. doi: 10.1016/j.cma.2013.12.017.

Handschuh, F. and Lev, N. (no date) 'Crowned Spur â€™ Gears : Optimal Geometry and Generation'.

Iso 6336-5:2003(E) (2003) 'Calculation of load capacity of spur and helical gears - Part 5: Strength and quality of materials', 2003, p. 50.

Jing, S. *et al.* (2015) 'Optimum weight design of functionally graded material gears', *Chinese Journal of Mechanical Engineering*, 28(6), pp. 1186–1193. doi: 10.3901/CJME.2015.0930.118.

Jyothirmai, S. *et al.* (2014) 'A Finite Element Approach to Bending, Contact and Fatigue Stress Distribution in Helical Gear Systems', *Procedia Materials Science*, 6, pp. 907–918. doi: 10.1016/j.mspro.2014.07.159.

Kawalec, A. and Wiktor, J. (2004) ‘Tooth-root stress calculation of internal spur gears’, *Proceedings of the Institution of Mechanical Engineers, Part B: Journal of Engineering Manufacture*, 218(9), pp. 1153–1166. doi: 10.1243/0954405041897185.

Kawalec, A. and Wiktor, J. (2008) ‘Simulation of generation and tooth contact analysis of helical gears with crowned flanks’, *Proceedings of the Institution of Mechanical Engineers, Part B: Journal of Engineering Manufacture*, 222(9), pp. 1147–1160. doi: 10.1243/09544054JEM1104.

Kawalec, A., Wiktor, J. and Ceglarek, D. (2006) ‘Comparative Analysis of Tooth-Root Strength Using ISO and AGMA Standards in Spur and Helical Gears With FEM-based Verification’, *Journal of Mechanical Design*, 128(5), p. 1141. doi: 10.1115/1.2214735.

Kirov, B. V (no date) ‘Comparison of the AGMA and FEA Calculations of Gears and Gearbox Components Applied in the Environment of Small Gear Company Comparison of the AGMA and FEA Calculations of Gears and Gearbox Components Applied in the Environment of Small’.

Kramberger, J. *et al.* (2004) ‘Computational model for the analysis of bending fatigue in gears’, *Computers & Structures*, 82(23–26), pp. 2261–2269. doi: 10.1016/j.compstruc.2003.10.028.

Krantz, T. L. and Krantz, T. L. (1992) ‘Gear tooth stress measurments of two helicopter planetary stages', 6th International Power Transmission and Gearing Conference. Phoenix, AZ, United States, September 13th-16th.

Kunc, R., Zerovnik, a and Prebil, I. (2007) ‘Verification of numerical determination of carrying capacity of large rolling bearings with hardened raceway’, *International Journal of Fatigue*, 29(9–11), pp. 1913–1919. doi: 10.1016/j.ijfatigue.2007.02.003.

Lai, J. *et al.* (2009) ‘Case Depth and Static Capacity of Surface Induction-Hardened Rings’, *Journal of ASTM International*, 6(10), p. 102630. doi: 10.1520/JAI102630.

Lewis, W. (1892) ‘Investigation of the Strength of GearTeeth’, *Proceedings of Engineer’s Club ’of Philadelphia*, pp. 16–23.

Li, S. (2007) ‘Finite element analyses for contact strength and bending strength of a pair of spur gears with machining errors, assembly errors and tooth modifications’, *Mechanism and Machine Theory*, 42(1), pp. 88–114. doi: 10.1016/j.mechmachtheory.2006.01.009.

Liao, B. *et al.* (2008) ‘Numerical simulation of the stress–strain curve of duplex weathering steel', *Materials & Design*, 29(2), pp. 562–567. doi: 10.1016/j.matdes.2006.12.021.

Lisle, T. J., Shaw, B. A. and Frazer, R. C. (2017) 'External spur gear root bending stress: A comparison of ISO 6336:2006, AGMA 2101-D04, ANSYS finite element analysis and strain gauge techniques', *Mechanism and Machine Theory*. Elsevier B.V., 111, pp. 1–9. doi: 10.1016/j.mechmachtheory.2017.01.006.

Luo, J. and Lin, J. (2007) 'A study on the determination of plastic properties of metals by instrumented indentation using two sharp indenters', *International Journal of Solids and Structures*, 44(18–19), pp. 5803–5817. doi: 10.1016/j.ijsolstr.2007.01.029.

Ma, H. *et al.* (2015) 'Fault features analysis of cracked gear considering the effects of the extended tooth contact', *Engineering Failure Analysis*. Elsevier Ltd, 48, pp. 105–120. doi: 10.1016/j.engfailanal.2014.11.018.

McCrory, J (2010) 'Novel Methods for Monitoring Fatigue Crack Growth in Steel Gears'

Nobre, J. P. *et al.* (2010) 'Two experimental methods to determining stress–strain behavior of work-hardened surface layers of metallic components', *Journal of Materials Processing Technology*. Elsevier B.V., 210(15), pp. 2285–2291. doi: 10.1016/j.jmatprotec.2010.08.019.

Park, S.-J. and Yoo, W.-S. (2004) 'Deformation overlap in the design of spur and helical gear pair', *Finite Elements in Analysis and Design*, 40(11), pp. 1361–1378. doi: 10.1016/j.finel.2003.10.003.

Pasta, A. and Mariotti, G. V. (2007) 'Finite element method analysis of a spur gear with a corrected profile', *The Journal of Strain Analysis for Engineering Design*, 42(5), pp. 281–292. doi: 10.1243/03093247JSA284.

Patil, S. *et al.* (2014) 'Frictional Tooth Contact Analysis along Line of Action of a Spur Gear Using Finite Element Method', *Procedia Materials Science*, 5, pp. 1801–1809. doi: 10.1016/j.mspro.2014.07.399.

Pullin, R. et al. (2010) 'Detection of Cracking in Gear Teeth Using Acousitic Emission', Applied Mechanics and Materials vols 24-25, pp 45-50

Senthil Kumar, V., Muni, D. V. and Muthuveerappan, G. (2008) 'Optimization of asymmetric spur gear drives to improve the bending load capacity', *Mechanism and Machine Theory*, 43(7), pp. 829–858. doi: 10.1016/j.mechmachtheory.2007.06.006.

Sfakiotakis, V. G. and Anifantis, N. K. (2002) 'Finite element modeling of spur gearing fractures', *Finite Elements in Analysis and Design*, 39(2), pp. 79–92. doi: 10.1016/S0168-874X(02)00063-X.

Spyrakos, C. C. (1996) 'Finite Element Modelling'.

Tran, T. D. (2015) 'An Evaluation of Stresses and Deflection of Spur Gear Teeth Under Strain', (February 1974), pp. 85–93.

Tsay, C.-B. (1988) 'Helical Gears With Involute Shaped Teeth: Geometry, Computer Simulation, Tooth Contact Analysis, and Stress Analysis', *Journal of Mechanisms Transmissions and Automation in Design*, 110(4), p. 482. doi: 10.1115/1.3258948.

Tseng, R.-T. and Tsay, C.-B. (2001) 'Mathematical model and undercutting of cylindrical gears with curvilinear shaped teeth', *Mechanism and Machine Theory*, 36(11–12), pp. 1189–1202. doi: 10.1016/S0094-114X(01)00049-0.

Woods, J. L., Daniewicz, S. R. and Nellums, R. (1999) 'Increasing the bending fatigue strength of carburized spur gear teeth by presetting', 21, pp. 549–556.

9.1. Personal Communication References

Personal Communiction			
#	**Chapter/Page**	**Description**	**Communicator**
1	Chapter 2 - P42	Mesh size for simulation of micro-pitting in the order of 0.1mm	Senior Structural Engineer - Industrial Sponsor
2	Chapter 2 - P42	Mesh size for simulation of contact stresses in the order of 0.1mm	Senior Structural Engineer - Industrial Sponsor
3	Chapter 2 - P44	Gears manufactured with a tolerance at the tooth tip of no less than 0.25µm. No tooth will enter a grand prix with a tooth bend of more than 10µm	Industrial Supervisor - Industrial Sponsor
4	Chapter 3 - P63	The temperature increase in a part during water jet cutting will not exceed 50°C	Precision Waterjet
5	Chapter 3 - P70	For non-contact measurement systems a rule of thumb of 5 to 8 pixels per speckle was recommended	Support Engineer - Dantec
6	Chapter 4 - P91	An error of < 0.5% was found between results between VSG and a mechanical extensometer	Manager - WMTR
7	Chapter 7 - P137	Comparable material behaviour up to 0.5% strain required	Senior Structural Engineer - Industrial Sponsor
8	Chapter 8 - P153	Mesh size for simulation to produce representative behaviour of bending stresses in the order of 0.2mm	Senior Structural Engineer - Industrial Sponsor

10. Appendix

10.1. MATLAB Script

```
%% Import data from text file.
% Auto-generated by MATLAB on 2017/10/02 16:43:41
Clearvars

%% Initialize variables.
%C:\Users\sce9deg\Desktop\PhD_Documents\09) FGM\2)
FGM_Coding\9_Final
folder='C:\Users\Admin\Desktop\Dewi\Code';
filename = 'Tensile.txt';
delimiter = ',';
formatSpec = '%s%s%s%s%s%s%s%s%s%s%s%s%s%s%s%s%[^\n\r]';

%% Open the text file.
fileID = fopen([folder,'\',filename],'r');

%% Read columns of data according to the format.
dataArray = textscan(fileID, formatSpec, 'Delimiter',
delimiter,'ReturnOnError', false);

%% Close the text file.
fclose(fileID);

%% Create output variable
AInputFile = [dataArray{1:end-1}];

%% Clear temporary variable
clearvars delimiter formatSpec fileID dataArray ans;

%% Start/End lines
NodeListLineStart=10;
NodeListLineEnd=271753;
ElementListLineStart=271755;
ElementListLineEnd=519059;
SurfaceListLineStart=519065;
```

```
SurfaceListLineEnd=520126;

%% Assembling all necessary matricies
NodeList=AInputFile(NodeListLineStart:NodeListLineEnd,1:4);
ElementList=AInputFile(ElementListLineStart:ElementListLineEn
d,1:9);
RawSurfaceNodes=AInputFile(SurfaceListLineStart:SurfaceListLi
neEnd,1:16);

%% Translate all the above strings into matrices
ElementList=str2double(ElementList);
NodeList=str2double(NodeList);
RawSurfaceNodes=(str2double(RawSurfaceNodes))';

%% Getting the Surface Nodes in the correct format
SurfNodeConvert=RawSurfaceNodes(:); %Arranges from 4 x 16
into single column
SurfNodeConvert(find(isnan(SurfNodeConvert)))=[]; %Removed
NaN values

%% Creates a Matrix where Surface Nodes have XYZ assigned to
them
for i=1:length(SurfNodeConvert)
    a=SurfNodeConvert(i); %Picks indecie to look into node
matrix
    b=NodeList(a,:); %Uses the indecy to extract useful node
x y z
    SurfaceNodeList(i,:)=b; %Writes into new matrix
end

%% Element Centroid finding.
NodesInAnElement = zeros(length(ElementList(1,:))-1,3);
%Creates the matrix first. Works out memory hold
CentroidCoordinates = zeros(length(ElementList(:,1)),3);
%Same as above
for   i=1:length(ElementList(:,1))
    for        j=2:length(ElementList(1,:))
```

```
        NodesInAnElement(j-1,:) =
NodeList(ElementList(i,j),2:4);
    end
    CentroidCoordinates(i,1:3) = mean(NodesInAnElement);
end

%% Compares centroid coordinates to all of the surface nodes.
tic
n=length(CentroidCoordinates);
m=length(SurfaceNodeList);
ElementDepthThruCentroid=zeros(n,m);
parfor i=1:n
    for j=1:m

c=[CentroidCoordinates(i,1:3);SurfaceNodeList(j,2:4)];
        ElementDepthThruCentroid(i,j)=sqrt((c(1,1)-
c(2,1)).^2+(c(1,2)-c(2,2)).^2+(c(1,3)-c(2,3)).^2);
    end
end
toc

%% Takes minimum value from each row and forms matrix Length
x 1 row.
CentroidToSUrfDist=min(ElementDepthThruCentroid,[],2);

%% Createst matrix of Row Col (Number of Materials v Number
Elements
HAZDepth=1.5;
HAZMaterials=4;
HAZLayerIncrements=HAZDepth/HAZMaterials;
TotalMaterials=HAZMaterials+1;
i=[];
 for i=1:length(CentroidToSUrfDist)
     for j=1:TotalMaterials
         lower=(j-1)*HAZLayerIncrements;
         upper=j*HAZLayerIncrements;
```

```
        if CentroidToSUrfDist(i) > lower &
CentroidToSUrfDist(i) < upper
            Matproptemp(j,i)=i;
        elseif CentroidToSUrfDist(i)>1.5
                Matproptemp(TotalMaterials,i)=i;
        else
            j=j+1;
        end
    end
end

%% Takes rows, gets rid of zeros. Writes a .txt file with all
sections with element numbers.
ID=fopen([folder,'\MaterialLayersElementNumbers.txt'],'w');
B=cell(TotalMaterials,1);
C=B;
for i=1:TotalMaterials
    A=Matproptemp(i,:);
    B{i}=A(A~=0);
    II=ismember(ElementList(:,1),B{i});
    C{i}=ElementList(II,2:end);
    C{i}=reshape(C{i},[],1);
    C{i}=sort(unique(C{i}));
    fprintf(ID,'Layer %d\n',i);
    fprintf(ID,'Elements\n');
    LB=length(B{i});
    k=1;
    for j=1:LB
        if k==17
        fprintf(ID,'\n');
        fprintf(ID,'%d,',B{i}(j));
        k=1;
        else
        fprintf(ID,'%d,',B{i}(j));
        end
        k=k+1;
    end
```

```
    fprintf(ID,'\n');
    fprintf(ID,'Nodes\n');
    LC=length(C{i});
    k=1;
    for j=1:LC
        if k==17
        fprintf(ID,'\n');
        fprintf(ID,'%d,',C{i}(j));
        k=1;
        else
        fprintf(ID,'%d,',C{i}(j));
        end
        k=k+1;
    end
    fprintf(ID,'\n');
end
```